



**HAL**  
open science

# Fluorinated pickering emulsions for droplet-based microfluidics technology

Laura A. Chacon Orellana

► **To cite this version:**

Laura A. Chacon Orellana. Fluorinated pickering emulsions for droplet-based microfluidics technology. Condensed Matter [cond-mat]. Université de Bordeaux, 2018. English. NNT : 2018BORD0121 . tel-02292544v1

**HAL Id: tel-02292544**

**<https://theses.hal.science/tel-02292544v1>**

Submitted on 20 Sep 2019 (v1), last revised 30 Sep 2019 (v2)

**HAL** is a multi-disciplinary open access archive for the deposit and dissemination of scientific research documents, whether they are published or not. The documents may come from teaching and research institutions in France or abroad, or from public or private research centers.

L'archive ouverte pluridisciplinaire **HAL**, est destinée au dépôt et à la diffusion de documents scientifiques de niveau recherche, publiés ou non, émanant des établissements d'enseignement et de recherche français ou étrangers, des laboratoires publics ou privés.



**École doctorale n°40**

**Sciences chimiques**

**Thèse**

présentée pour l'obtention du grade de docteur

de l'Université de Bordeaux par

**Laura A. Chacon O.**

**Fluorinated Pickering emulsions  
for droplet-based microfluidics  
technology**

Spécialité : Physico-chimie de la matière condensée

Soutenue le 23 Juillet 2018 devant un jury composé de :

---

Rapporteur	<b>Mme Valerie TALY</b>	<i>Directeur de Recherche, Université Paris Descartes</i>
Rapporteur	<b>Mme Esther AMSTAD</b>	<i>Professeur assistant, EPFL Laboratoire de la matière molle</i>
Président du jury	<b>Mme Véronique SCHMITT</b>	<i>Directeur de Recherche, CRPP</i>
Directeur de thèse	<b>M. Jean-Christophe BARET</b>	<i>PR, Université de Bordeaux</i>



Thèse effectuée au sein du **Centre de Recherche Paul Pascal**

115 Avenue Schweitzer

33600 PESSAC

FRANCE



Soutien financier du **Conseil Européen de la Recherche (ERC)**.

*To my parents and to Christopher, thank you for all your love and support . . .*



# Acknowledgements

The completion of this thesis project would have not been possible without the support of great people I was fortunate to meet and to whom I want to express my appreciation.

I would like to extend my deepest gratitude to my thesis adviser Jean-Christophe Baret. Thank you for your constant guidance and brilliant inputs, as well as for valuing my ideas and giving me the freedom and encouragement to pursue them. Overall, thank you for being a wonderful supervisor. I am also grateful to all the members of the SMS team for their active exchange of tips and advices such as how to improve microfabrication techniques and the specific usage of lab equipment. Specially, I would like to thank Birte Riechers, for her practical advice and stimulating discussions that were crucial during the initial stages of my thesis work, as well as Mathias Girault and Deniz Pekin, for providing a great amount of assistance during biological experiments.

I also wish to thank the members of the MaFIC team for sharing some of their materials and equipment. The assistance of Céline Hubert, Pierre-Etienne Rouet and Armand Roucher was particularly helpful. I would also like to thank Véronique Schmitt for accepting to be a member of the jury, her feedback comments were deeply appreciated. I would also like to extend my gratitude to Valerie Taly and Ouriel Caen for hosting me a couple of weeks in their lab, where I got an enriching experience and insights on challenges I needed to address in my work. Additionally, I appreciate that Valerie and Esther Amstad accepted to be part of the jury and to take the time to review my thesis project, both of their feedbacks were thoughtful and of great value to me. Thanks should also go to Martial Balland and Katharina Hennig,

who shared with me the adherent cells used in this project and provided useful advise to culture and preserve them.

Finally, I am extremely grateful to the administration personal in the CRPP, for all their patience and assistance with French paper work and to all my colleagues and friends who filled my PhD experience with fun and meaningful moments that I will always treasure.

# Table of contents

<b>List of figures</b>	<b>xi</b>
<b>List of tables</b>	<b>xv</b>
<b>Symbols</b>	<b>xvii</b>
<b>1 Résumé de projet</b>	<b>1</b>
1.1 Contexte du projet . . . . .	1
1.2 Émulsions fluorées de Pickering . . . . .	3
1.3 Effet de la formulation sur les propriétés de fluidité . . . . .	4
1.4 Stabilisation de l'émulsion de Pickering dans les microfluides . . . . .	4
1.5 Incubation de cellules adhérentes dans les gouttes de Pickering . . . . .	5
1.6 Conclusion . . . . .	6
<b>2 State of the art</b>	<b>9</b>
2.1 Droplet-based microfluidics technology . . . . .	9
2.1.1 Fundamental dynamics of droplets in microchannels . . . . .	10
2.1.2 Droplet formation: Device geometry . . . . .	12
2.1.3 Droplet formation: Breakup modes . . . . .	14
2.1.4 Droplet manipulation in microchannels . . . . .	15
2.2 Cell analysis in droplet microfluidics . . . . .	19

2.2.1	Cell encapsulation . . . . .	19
2.2.2	Cell culture . . . . .	20
2.2.3	Interest on single-cell analysis . . . . .	21
2.3	System formulation and interfacial stabilizers . . . . .	22
2.3.1	Droplet transport . . . . .	24
2.3.2	Alternative stabilizing agents . . . . .	24
<b>3</b>	<b>Fluorinated Pickering emulsions</b>	<b>29</b>
3.1	Silica nanoparticles synthesis . . . . .	29
3.1.1	Seed Synthesis . . . . .	30
3.1.2	Re-growth of silica seeds . . . . .	30
3.2	Si-NPs density and specific surface area . . . . .	31
3.3	Nanoparticles as interfacial stabilizers . . . . .	33
3.4	Si-NPs Surface Fluorination . . . . .	35
3.4.1	Avoiding particle aggregation . . . . .	36
3.4.2	Determining Si-NPs concentration and degree of fluorination . . . . .	38
3.4.3	Final Si-NPs fluorination protocol . . . . .	42
3.5	Stabilizing droplets with fluorinated Si-NPs in microfluidics . . . . .	43
<b>4</b>	<b>Formulation effect on flow properties</b>	<b>47</b>
4.1	Empirical observations of Pickering emulsions "sticky" properties . . . . .	47
4.2	The angle of repose test for granular materials . . . . .	50
4.3	Microfluidic angle of repose test for Pickering emulsions . . . . .	51
4.3.1	Materials and methods . . . . .	51
4.3.2	Angle of repose test versus microfluidic adaptation . . . . .	54
4.3.3	Formulation parameters . . . . .	56
4.3.4	Conclusion . . . . .	60

---

4.4	Appendix: Supplementary experiments . . . . .	60
4.4.1	Bio-compatibility: preliminary assay . . . . .	60
4.4.2	Specific surface area and particle tunability . . . . .	62
<b>5</b>	<b>Pickering emulsions stabilization in microfluidics</b>	<b>67</b>
5.1	Current conditions . . . . .	67
5.1.1	Droplet incubation time . . . . .	69
5.1.2	Particles in excess . . . . .	70
5.2	New droplet production design . . . . .	71
5.3	Dynamics of Pickering droplets stabilization . . . . .	72
5.3.1	Incubation time effect on droplet stability . . . . .	73
5.3.2	Droplet stability independent of $\tau$ . . . . .	76
5.3.3	Local particle concentration effect on droplet stability . . . . .	79
5.4	Conclusion . . . . .	81
5.5	Materials and methods . . . . .	82
5.5.1	Microfluidic device fabrication and experimental design . . . . .	82
<b>6</b>	<b>Adherent cells incubation in Pickering droplets</b>	<b>87</b>
6.1	A microfluidic device for Pickering droplets incubation and monitoring . . . . .	87
6.1.1	Selection of PDMS over glass . . . . .	88
6.1.2	Additional technical challenges . . . . .	90
6.2	Studying cells phenotype heterogeneity in Pickering droplets. . . . .	94
6.2.1	Single-cell incubation of RPE cells reveal its phenotypic heterogeneity . . . . .	97
6.2.2	Illustrative model of a study accounting for RPE cells heterogeneity . . . . .	101
6.2.3	Conclusions . . . . .	108
6.2.4	Materials and methods . . . . .	109
<b>7</b>	<b>General conclusions and outlook</b>	<b>115</b>

<b>References</b>	<b>119</b>
<b>Appendix A Publications</b>	<b>133</b>

# List of figures

2.1	Typical geometries for droplet formation . . . . .	13
2.2	Droplet breakup modes . . . . .	15
2.3	Sorting and coalescence examples . . . . .	16
2.4	Droplet inner flow pattern and mixing . . . . .	17
2.5	Splitting and trapping examples . . . . .	18
2.6	Cell encapsulation . . . . .	20
2.7	Fluorescent code library for droplet identification after off-chip incubation .	21
2.8	Ensembled cells vs single-cell analysis . . . . .	22
2.9	Surfactants role and selection . . . . .	23
2.10	Fluorophore extraction by additive solubilized in continuous phase . . . . .	25
2.11	Retention comparison between surfactant-stabilized emulsions and Pickering emulsions . . . . .	25
3.1	Silica nanoparticles synthesis . . . . .	30
3.2	Silica nanoparticles Sears titration . . . . .	33
3.3	Nanoparticles wettability and adsorption . . . . .	34
3.4	Silica nanoparticles fluorination, initial protocol . . . . .	36
3.5	Fluorinated Si-NPs microscopic aggregates . . . . .	37
3.6	Fluorinated Pickering emulsion stabilization in microchannel . . . . .	39
3.7	OD spectra measurements of fluorinated Si-NPs . . . . .	40

3.8	Volume of PFOTES added vs adsorbed weight . . . . .	41
3.9	Final Si-NPs surface fluorination protocol . . . . .	42
3.10	Satabilization of droplets . . . . .	44
4.1	Sticky Pickering emulsion . . . . .	48
4.2	Granular vs powdered sugar piles . . . . .	50
4.3	Microfluidic angle of repose device fabrication . . . . .	52
4.4	Microfluidic angle of repose measurement set-up . . . . .	53
4.5	Dynamic angle of repose and steady state . . . . .	55
4.6	Angle of repose dependence on fluorinated Si-NPs hydrophobicity . . . . .	57
4.7	Bio-compatibility test . . . . .	61
4.8	Angle or repose test for Aerosil OX-50 . . . . .	64
5.1	Schematic representation of simple droplet production . . . . .	69
5.2	Schematic representation of new droplet production design . . . . .	72
5.3	Incubation time effect on droplet stability . . . . .	74
5.4	Droplet stability for fixed incubation time . . . . .	78
5.5	Effect of droplet production step on droplet stability . . . . .	80
5.6	Microfluidic device design and methods . . . . .	83
6.1	Incubation device fabrication . . . . .	88
6.2	E. coli Rossetta culture in a glass-glass trap . . . . .	89
6.3	Technical challenges during droplet incubation . . . . .	91
6.4	Scheme of Retinal Pigment Epithelium . . . . .	94
6.5	RPE cells heterogeneous phenotype . . . . .	97
6.6	Differentiated RPE cell markers . . . . .	99
6.7	Cell migration in droplets . . . . .	100
6.8	Evaluating effect of fibronectin . . . . .	102

6.9	Aspect-ratio vs Circularity map for cell type determination . . . . .	104
6.10	Effect of Fibronectin on cell phenotypic expresion . . . . .	105
6.11	Cell mean fluorescence intensity and area per phenotypic type . . . . .	107
6.12	Fluorescence image and BF of RPE cell culture with high confluency . . . . .	110
6.13	Cell encapsulation, experimental conditions . . . . .	111
6.14	Image analysis . . . . .	112
7.1	Schematic summary and outlook . . . . .	116



# List of tables

3.1	Sears Si-NPs specific surface . . . . .	33
4.1	$c_p$ and $\phi_{wt}$ comparison for different Si-NPs . . . . .	63



# Symbols

## Roman Symbols

$Bo$  Bond number

$Ca$  Capillary number

$D$  Droplet diameter

$g$  Gravity

$h$  Channel depth

$L$  Characteristic length or incubation channel length

$Q$  Flow rate

$Re$  Reynolds number

$S$  Droplet surface

$u$  Velocity

$V$  Volume or droplet volume

$We$  Weber number

## Greek Symbols

$\delta$	Nanoparticle diameter
$\Delta\rho$	Difference in fluid densities
$\varepsilon$	Particles in excess
$\eta$	Viscosity
$\gamma$	Interfacial tension
$\lambda$	Oil-aqueous phase ratio
$\omega$	width
$\phi_{wt}$	Degree of surface functionalization
$\rho$	Density
$\tau$	Droplet incubation time

### Subscripts

$\alpha_r$	Angle of repose
$\alpha_{ss}$	Steady state angle
$\sigma_r$	Cohesive index of granular material
$\sigma_{ss}$	Steady state cohesiveness
$t_{ss}$	Stabilization time
$c_{cp}$	Concentration needed for hexagonal close-packing at the droplet interface
$c_f$	Fluorinated silica nanoparticles concentration (w/v)
$c_p$	Silica nanoparticles concentration (w/v)

$c_p^*$	Particle concentration of co-flow flow rate in design MII
$MII_{\eta\downarrow}$	MII with HFE-7500 as $Q_o$
$MII_{\eta\uparrow}$	MII with FC-40 as $Q_o$
$n_{cp}$	Number of particles for hexagonal close-packing at the droplet interface
$\omega_o$	Channel width
$Q_t$	Total flow rate
$Q_o$	Particle-free cross-flow oil flow rate
$Q_p$	Si-NPs in HFE-7500 flow rate
$Q_p^*$	Si-Nps in HFE-7500 co-flow flow rate in design MII
$Q_w$	Aqueous flow rate
$\rho_p$	Nanoparticles density
$S_c$	Nanoparticles specific surface
$V_p$	Nanoparticle volume

### **Other Symbols**

$p(1)$  Droplet stability against coalescence

### **Acronyms / Abbreviations**

AR Aspect ratio

BF Bright field

ECM Extra cellular matrix

ELISA Enzyme-linked immunosorbent assay

EMT Epithelial-mesenchymal transition

GFP Green fluorescence protein

LOCs Lab-on-chip platforms

MII New droplet production design

MI Standard droplet production method

PCR Polymerase chain reaction

PDMS Polydimethylsiloxane

PEG Polyethylene glycol

PFOTES 1H,1H,2H,2H-Perfluorooctyltriethoxysilane

PFPE Perfluoropolyether

RPE Retinal pigment epithelium

Si-NPs Silica nanoparticles

TEM Transmission electron microscopy

TEOS Tetraethylorthosilicate

# Chapter 1

## Résumé de projet

### 1.1 Contexte du projet

La microfluidique en gouttes ('droplet-based microfluidics' in English) est la science et la technologie par laquelle on génère et manipule des gouttes d'un liquide contenues dans un fluide porteur immiscible à l'intérieur de microcanaux. Cette technologie permet la génération de gouttelettes hautement monodisperses à des cadences supérieures à 20 kHz (20 000 gouttes par secondes). A ce jour, son émergence est stimulée par deux domaines d'application distincts : Dans le domaine de la science des matériaux, la production de gouttes calibrées de manière contrôlée et reproductible est d'un grand intérêt pour les industries pharmaceutiques, cosmétiques et alimentaires, ainsi que pour la fabrication de matériaux aux échelles nanométrique et micrométriques ; Dans le domaine des sciences biologiques et chimiques, l'encapsulation de réactifs chimiques et biologiques dans des gouttelettes isolées est importante pour les applications en laboratoire sur puce. Chaque gouttelette est alors considérée comme un microréacteur individuel, ce qui permet de réaliser des essais biochimiques à haut débit avec une faible consommation de réactifs.

Pour considérer les gouttelettes comme des microréacteurs isolés, leur stabilité contre la coalescence avec les gouttelettes voisines est nécessaire. La stabilisation des gouttes

est typiquement réalisée en utilisant des tensio-actifs. Les tensio-actifs sont des molécules amphiphiles contenant des groupes hydrophobes et hydrophiles. Ils sont dispersés dans une des deux phases (généralement la phase continue) et, lors de la formation de gouttes, ils diffusent et s'adsorbent à l'interface entre les deux fluides. La présence des tensio-actifs aux interfaces modifient les interactions entre les gouttes et stabilise cinétiquement les gouttelettes dans un état thermodynamique métastable. La sélection des tensioactifs adaptés à la microfluidique en goutte est liée à la nature chimique des phases utilisées et à la surface du microcanal dans lequel elles s'écoulent. Les gouttes aqueuses transportées par des huiles fluorées et stabilisées par des surfactants fluorés sont les systèmes de choix pour les applications de laboratoire sur puce, principalement en raison de leur haute compatibilité avec les applications biochimiques et les dispositifs microfluidiques généralement utilisés.

Les surfactants fluorés présentent cependant certaines limites : ils sont difficiles à synthétiser et coûteux ; ils jouent un rôle fondamental dans l'échange moléculaire entre les gouttes ; et ils ne sont pas compatibles avec l'encapsulation des cellules adhérentes, puisqu'ils doivent se répandre sur un substrat approprié pour survivre. Pour surmonter ces limites, l'utilisation de nanoparticules de silice fluorée a été proposée comme une alternative aux surfactants fluorés. Ils ont suscité un intérêt croissant en raison de leur capacité à limiter les échanges moléculaires entre les gouttes, à accroître la fonctionnalité de l'interface de gouttes. Ils ont aussi un intérêt certain pour des applications utilisant des cellules adhérentes.

Cependant, la combinaison des émulsions de Pickering (i.e. des émulsions stabilisées par des nanoparticules) fluorées avec la technologie de microfluidique en gouttes en est encore à ses débuts, et une meilleure compréhension du système est nécessaire pour définir pleinement leur place dans la boîte à outils de la microfluidique en gouttes.

**L'objet de cette thèse est d'explorer les propriétés des émulsions de Pickering fluorées pour les applications de microfluidique en gouttes, avec l'objectif principal d'obtenir une plate-forme technologique appropriée pour l'étude des cellules adhérentes.**

## 1.2 Émulsions fluorées de Pickering

Dans un premier temps, nous nous intéressons à la préparation des nanoparticules adaptées à la stabilisation des interfaces eau - huiles fluorées. Nous partons d'une suspension de nanoparticules de silice vierge dans l'éthanol. Les nanoparticules de silice brute sont hydrophiles en raison de la densité élevée des groupes hydroxyles sur sa surface. L'adsorption des particules à l'interface eau-huile - pour la stabilisation des gouttes - nécessite une mouillabilité partielle pour les deux phases. La mouillabilité partielle des particules de silice pour l'interface huile fluorée est obtenue par un procédé de silanisation, dans lequel les molécules de perfluorooctyle sont greffées à la surface des nanoparticules.

Nous avons optimisé le protocole de fonctionnalisation de surface de ces particules afin d'éviter des phénomènes d'agrégation des particules et de pouvoir déterminer la concentration finale des particules dans la suspension d'huile fluorée. La concentration de particules ( $c_p$ ) est un paramètre important pour la stabilisation des gouttes, nous l'avons déterminé en utilisant une mesure de masse de nanoparticules par volume de solvant. Nous avons également déterminé le degré de couverture de surface ( $\phi_{wt}$ ) - par la masse de perfluorooctyle par poids de particules - qui est alors directement lié au niveau d'hydrophobicité des nanoparticules de silice.

Finalement, nous avons déterminé les conditions minimales de stabilisation des gouttelettes dans un dispositif microfluidique avec ces nanoparticules. Nous avons utilisé un dispositif de production de gouttes standard et fixé le débit d'eau et d'huile, ensuite nous avons déterminé une longueur d'incubation et une concentration de particules appropriées par un test de coalescence microfluidique, où la stabilité contre la coalescence ( $p(1)$ ) a été utilisée comme référence pour évaluer la stabilité des gouttelettes dans différentes conditions.

### 1.3 Effet de la formulation sur les propriétés de fluidité

Les émulsions Pickering présentent le comportement classique de suspensions adhésives. Nous avons observé empiriquement ce comportement pour les émulsions stabilisées avec des nanoparticules de silice fluorée. Cet aspect est particulièrement problématique pour des opérations classiques de microfluidique en gouttes, comme la réinjection d'émulsion. Il est donc essentiel de caractériser et de comprendre les propriétés d'écoulement des émulsions fluorées de Pickering pour les adapter à la boîte à outils de la microfluidique en gouttes.

Les similitudes observées entre les propriétés des émulsions de Pickering et les matériaux granulaires nous ont conduit à développer une version microfluidique de l'essai d'angle de repos, typiquement utilisée pour la caractérisation du comportement d'écoulement des matériaux granulaires. Grâce à cette méthode, nous avons pu utiliser de petits échantillons (45 à 300  $\mu\text{L}$ ) d'émulsions de Pickering pour comparer quantitativement leur fluidité dans différentes conditions de formulation.

Nous avons observé que la fluidité des émulsions fluorées de Pickering est directement liée à la couverture superficielle des nanoparticules de silice ( $\phi_{wt}$ ) ainsi qu'au pH de la phase aqueuse. Il suggère fortement un lien entre l'hydrophobie des particules et la fluidité de l'émulsion de Pickering. De plus, nous avons relevé les limites de stabilité et de biocompatibilité pour les formulations à très forte couverture de surface et obtenu le meilleur contrôle sur la formulation du système pour les particules de silice à surface spécifique élevée.

### 1.4 Stabilisation de l'émulsion de Pickering dans les microfluides

Du point de vue de l'ingénierie microfluidique, il est difficile d'obtenir des émulsions de Pickering avec un débit de production élevé : l'échelle de temps typique requise pour les stabiliser ( $\sim 600$  ms) est significativement plus élevée que celle nécessaire pour les

émulsions stabilisées par surfactant ( $\sim 35$  ms) dans des conditions similaires. La limitation dans le débit réside dans le temps de stabilisation de l'émulsion, qui est lié à l'incapacité des nanoparticules à diffuser rapidement et efficacement jusqu'à l'interface des gouttes. Par conséquent, les méthodes actuelles de stabilisation des émulsions de Pickering dans les dispositifs microfluidiques impliquent un compromis entre un faible débit de production de gouttelettes et le gaspillage d'un grand nombre de nanoparticules.

Nous avons réalisé une étude multi-paramétrique pour la stabilisation des gouttes avec des nanoparticules dans un dispositif microfluidique, incluant l'effet de la concentration des particules, le volume des gouttes, la méthode de production et le temps d'incubation. Notre analyse a révélé le rôle crucial des profils d'écoulement à la jonction de production du dispositif sur la cinétique de stabilisation et nous a permis de mettre en place des règles de designs adaptés pour la stabilisation efficace des gouttes avec des nanoparticules. Les paramètres critiques sont : la concentration des nanoparticules près de l'interface aqueuse et la contrainte de cisaillement fournie par le flux croisé lors de la formation des gouttes.

Notre méthode de production de gouttelettes permet la stabilisation à haut débit des émulsions fluorées de Pickering –temps de stabilisation réduit d'un ordre de grandeur– avec une réduction significative des déchets de particules.

## **1.5 Incubation de cellules adhérentes dans les gouttes de Pickering**

Après avoir intégré les connaissances acquises sur les émulsions fluorées de Pickering et mis en oeuvre des ajustements techniques pour la conception appropriée d'un dispositif d'incubation, nous avons réussi à produire des gouttes de Pickering stables à haut débit de production, à les collecter dans un réservoir, à les réinjecter dans un dispositif d'incubation et à les observer sous microscope sans interruption pendant plus de 48 heures.

Nous avons ensuite appliqué ce système à l'encapsulation et à l'étude d'un modèle cellulaire adhérent : les cellules de l'épithélium pigmentaire rétinien (RPE). Les cellules RPE sont hautement spécialisées et ne prolifèrent pas dans des conditions normales. Cependant, dans plusieurs pathologies rétiniennes et pour certaines conditions *in vitro*, les cellules RPE se différencient en changeant leur phénotype cellulaire, perdant ainsi les caractéristiques typiques des cellules RPE tout en acquérant des cellules macrophages et mésenchyme. La compréhension de la plasticité des cellules RPE est d'une importance majeure pour la recherche fondamentale et appliquée. Des observations récentes ont montré que les cellules RPE ne sont pas uniformes même *in situ*, formant une mosaïque hétérogène de cellules similaires mais non identiques. Les études unicellulaires des cellules RPE sont donc d'un grand intérêt pour tenir compte de leur hétérogénéité intrinsèque et pourraient permettre de mieux comprendre leur comportement.

Nous avons démontré que les émulsions fluorées de Pickering peuvent constituer des plateformes technologiques appropriées pour l'isolement, l'incubation et l'étude des cellules RPE adhérentes. Nous avons confirmé l'hétérogénéité phénotypique - de cellule à cellule - des cellules RPE en culture et enfin, nous avons démontré la possibilité de prendre en compte le phénotype individuel avec un modèle illustratif où nous avons confirmé l'influence de la glycoprotéine fibronectine sur la stimulation de la transition épithéliale-mésenchyme au sein de la population cellulaire.

## 1.6 Conclusion

Les nanoparticules de silice fluorées sont une alternative intéressante aux tensio-actifs fluorés pour la microfluidique en goutte, ouvrant des possibilités d'applications qui jusqu'à présent n'étaient pas réalisables avec des systèmes stabilisés par tensio-actifs.

Ces possibilités sont une conséquence des propriétés intrinsèques des émulsions de Pickering, telles que : la capacité de dépléter la phase continue des particules tout en

conservant la stabilité des émulsions et le substrat rigide généré par les particules adsorbées à l'interface. Ces différences impliquent toutefois que de nouvelles limitations et de nouveaux problèmes techniques sont introduits lorsque l'on tente de mettre en oeuvre les émulsions de Pickering dans le cadre d'une technologie qui s'est développée depuis des décennies sur la base de gouttes stabilisées par des tensioactifs.

Dans ce projet de thèse, nous avons exploré plusieurs de ces limitations - comme la faible fluidité des émulsions de Pickering et le faible débit de production - et nous avons proposé des solutions techniques qui nous ont permis de développer une plateforme technologique appropriée pour l'étude des cellules adhérentes.

De manière plus générale, plutôt que de remplacer les tensioactifs fluorés, les nanoparticules de silice fluorée offrent un excellent complément à la boîte à outils microfluidique en goutte, augmentant ainsi l'éventail déjà large d'options disponibles pour les applications en laboratoire sur puce et avec un grand potentiel d'expansion pour des applications ciblées.

Cette étude aide ainsi à établir les bases fondamentales pour la compréhension et le contrôle de ces systèmes vers la technologie des laboratoires sur puce.



# Chapter 2

## State of the art

This introductory chapter will explore the fundamental concepts that place this work into context: we start by reviewing the basic elements that compose droplet-based microfluidic technology (section 2.1), including most common methods for droplet production and manipulation; then we explore the application of this technology for bio-chemical assays (section 2.2), focusing on single-cell studies; later we discuss the significance of droplet stabilizing agents (section 2.3), as a fundamental element of this technology; and finally, we present a general scope of the thesis project.

### 2.1 Droplet-based microfluidics technology

Droplet-based microfluidics comprises the science and technology that generates, manipulates and processes droplets contained within an immiscible carrier fluid inside microchannels [1–4]. This technology allows the generation of highly monodisperse droplets at rates exceeding 20 kHz [2, 5, 6], and to date, its emergence is driven by two distinct application fields: Within material science, the generation of well calibrated droplets in a controlled and reproducible manner is of great interest for pharmaceutical, cosmetics and food industries, as well as for the fabrication of nano- and microscale materials [7–13] ; Within biological and

chemical science, the ability to incorporate chemical and/or biological reagents in isolated droplets pertains lab-on-chip (LCOs) applications, where each droplet is regarded as an individual microreactor, allowing for high-throughput bio-chemical assays with low reagent consumption [1, 14, 15].

### 2.1.1 Fundamental dynamics of droplets in microchannels

The precise control of droplets and their interfaces within microchannels, requires an understanding of the fluid dynamics of the system. This knowledge enables the design of operational units specific for the generation and manipulation of droplets with diverse morphologies and behaviors [16, 17]. Microflow dynamics and droplet generation depends on the relative influence of four types of forces: inertial force, viscous force, gravity and capillary force. Their relative importance is characterized by dimensionless numbers [18], which are derived from the ratio of any two of these forces in the form of stress (forces per unit area): considering a volume of fluid flowing at a velocity  $u$ , with characteristic length  $L$ , inertial stress scales as  $f_i \sim \rho u^2$ , viscous stress as  $f_v \sim \eta u/L$ , gravity  $f_g \sim \rho gL$ , and capillary pressure  $f_\gamma \sim \gamma/L$ .

#### Reynolds number

The Reynolds number ( $Re$ ), reflects the relative importance of inertia to viscous force:

$$Re = \frac{\rho u L}{\eta} \quad (2.1)$$

Where  $\rho$ ,  $u$  and  $\eta$  are the density, velocity and viscosity of the fluid respectively; and  $L$  is a characteristic length of the microchannel. Due to the small values of  $L$  for a microfluidic device,  $Re$  usually ranges between  $10^{-6}$  and 10, making the inertial contributions for these dimensions irrelevant with respect to the larger viscous stress, and yielding a laminar flow

behavior. [19, 18]

### **Bond number**

When the system have two different fluid phases –case for droplet-based microfluidics– the relative importance of gravity to capillary pressure describes the droplet deformation due to its weight and is given by the Bond number ( $Bo$ ),

$$Bo = \frac{\Delta\rho g L^2}{\gamma} \quad (2.2)$$

where  $\Delta\rho$  is the difference in fluid densities and  $g$  the acceleration of gravity. Typically,  $\Delta\rho$  and  $L$  are small for liquid-liquid microflows, making the gravity force importance negligible with respect to the capillary pressure ( $Bo \ll 1$ ), which means that the interfacial effects dominates over body force [7, 18].

### **Capillary number**

For two flowing fluid-phases, the relative strength of the viscous forces with respect to the capillary forces describes the droplet deformation due to shear stress and is characterized by the Capillary number ( $Ca$ ),

$$Ca = \frac{\eta u}{\gamma} \quad (2.3)$$

where  $\eta$  is generally the larger viscosity acting in the system [7], and  $\gamma$  is the interfacial tension.  $\gamma$  plays a key role in droplet formation, which is characterized by the extension and deformation of the interface induced by local shear stress in competition with the resistance to deformation achieved through capillary pressure [19].

In microflows,  $Ca$  is usually in the range of  $10^{-7}$  to 10 [7].

## Weber number

Although fluid inertia is negligible for most microfluidic flows, its effect becomes relevant for the transition of discrete droplets into continuous jets [20]. The competition between inertia and capillary pressure is given by the Weber number ( $We$ ),

$$We = \frac{\rho u L}{\gamma} \quad (2.4)$$

For most microfluidic flows,  $We < 1$  [18].

Dimensionless numbers derived from the ratio of relevant properties of the two phases are also useful for the characterization of the two-phase fluid system, these properties include: density ( $\rho$ ), viscosity ( $\eta$ ) and flow-rate ( $Q$ ).

### 2.1.2 Droplet formation: Device geometry

The starting point for a droplet-based LOC platform is the accurate generation of monodisperse droplets. This is usually achieved through passive techniques by taking advantage of the flow field to deform the interface and promote the natural growth of interfacial instabilities.

Three main approaches for droplet formation have emerged based on different physical mechanisms, which are best described by the flow field topology in the vicinity of the drop production zone. The phase to be dispersed is driven into a microchannel, where it encounters the immiscible carrier fluid which is driven independently. The geometry of the junction where the two phases meet, together with the flow rates and the physical properties of the fluids, determine the local flow field, which in turns deforms the interface and eventually leads to drop pinch off. [7].

### Co-flow

The earliest production of monodisperse droplets with a microfluidic system was reported by Weitz and coworkers [20]. Specifically, a coflow of two immiscible phases was used to generate droplets within a tapered cylindrical glass capillary inserted in a rectangular microchannel. In a co-flow geometry the dispersed phase flows into the inner channel, and the continuous phase flows in the outer channel in the same direction (Fig. 2.1a) [19]. Co-flow configurations can be three-dimensional (3D) coaxial (tapered cylindrical capillary for the inner phase) or quasi-two-dimensional (2D) planar, which can be fabricated by standard soft lithographic methods [21].

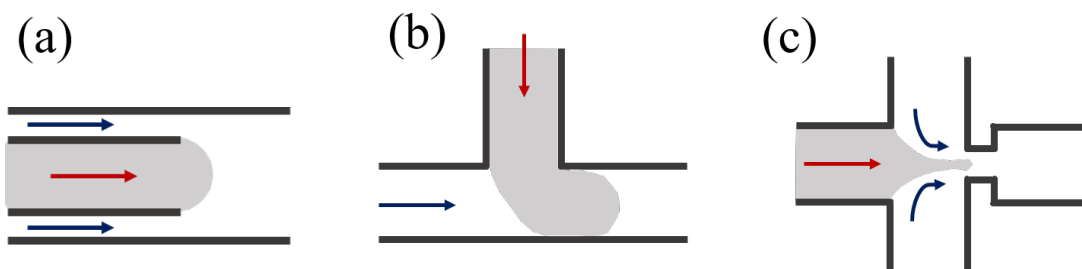


**Fig. 2.1** Schematic representation of junction geometries for droplet formation: (a) Co-flow, (b) Cross-flow and (c) Flow-focusing. The arrows indicate the direction of the continuous (blue) and dispersed (red) flow.

### Cross-flow

Quake and co-workers reported for the first time the generation of droplets in a cross-flow geometry [22]. Here, the immiscible fluids meet at an angle to each other. When this angle is  $90^\circ$ , the configuration is known as T-junction (Fig. 2.1b). This geometry is widely used because of its simplicity and ability to produce monodisperse droplets [18].

### Flow-focusing

The flow-focusing geometry was introduced by Anna *et al.* [23]. Here, the dispersed and continuous phases flow through a contraction region and generate an elongation filament

that eventually breaks into droplets [19]. Before reaching the channel constriction, the two immiscible fluids can flow coaxially or orthogonally, in which case, the dispersed phase is squeezed between two orthogonal entries of the continuous flow (Fig. 2.1c) [24].

### **Step emulsification**

Contrary to the droplet formation methods described above, step emulsification does not rely on shear forces to generate droplets. Instead, variations of channel confinement –due to the presence of an abrupt geometric step– generates a sharp change in capillary pressure which causes droplet pinch-off [25].

Additionally to passive techniques, there are several active methods for droplet formation where droplet production is triggered and droplet volume can be altered on-demand [26], by using an external energy source, such as: electrical, magnetic, thermal, and mechanical [19, 27].

### **2.1.3 Droplet formation: Breakup modes**

Despite the complexity of channel geometry, several modes of droplet breakup have been observed in shear-based droplet generation, the most common ones are: squeezing [28], dripping and jetting [29]. These modes shared similar physical processes and underlying mechanisms, and transition between them occurs with variations on the system dominant forces.

When the capillary number of the continuous phase is low ( $Ca_c < 10^{-2}$ ), droplet production occurs in squeezing mode. Here, the dispersed-fluid obstructs the junction region, restricting the continuous flow and building up a pressure gradient. When the pressure gradient is sufficiently large to overcome the pressure inside the forming droplet, the interface is "squeezed" deforming and necking into a droplet that adopts a plug-like shape confined by the channel walls. (Fig 2.2a)



**Fig. 2.2** Example of different droplet breakup modes for a flow-focusing production junction: (a) Squeezing, (b) Dripping (c) Jetting. Reprinted from Zhu *et al.* [18].

As  $Ca_c$  increases, the production mode transforms from squeezing to dripping [30]. Here, the viscous forces overcome the interfacial tension effects that stabilize the emerging droplet, breaking up the dispersed phase before it obstructs the junction region. (Fig. 2.2b) The produced droplets adopt a spherical shape, which are highly monodisperse for a constant viscous stress. A transition regime has been observed between squeezing and dripping modes, where both shear stress and squeezing pressure play a role in determining the droplet size [31].

By increasing the continuous or the dispersed fluid flow rate independently, a transition between dripping and jetting can occur [20]. Here, an extended liquid jet emits from the dispersed phase, breaking up into droplets at the end of the jet. For co-flowing streams, jetting occurs when the sum of viscous forces exerted by continuous-fluid and dispersed-fluid inertia overcomes interfacial tension forces [32].

#### 2.1.4 Droplet manipulation in microchannels

The ability to manipulate droplets in microchannels is of crucial importance for the scalability of bulk bio-chemical assays into droplet-based microfluidic assays. With this aim, a tool box of unit operations is in continuous development. These components are added to the LOCs and perform a given task which mirrors macroscale operations needed in specific bio-chemical experiments. The most common operations include: droplet sorting, coalescence, mixing, splitting and trapping.

## Sorting

Droplet sorting consist on the selection and segregation of droplets based on particular characteristics. This operation is usually needed to separate droplets intended for further analysis.

When sorting is done by passive methods, droplets are guided along a specific route by hydrodynamic interactions between the channel geometries and droplet properties such as size [33] and viscosity [34] (Fig. 2.3a).

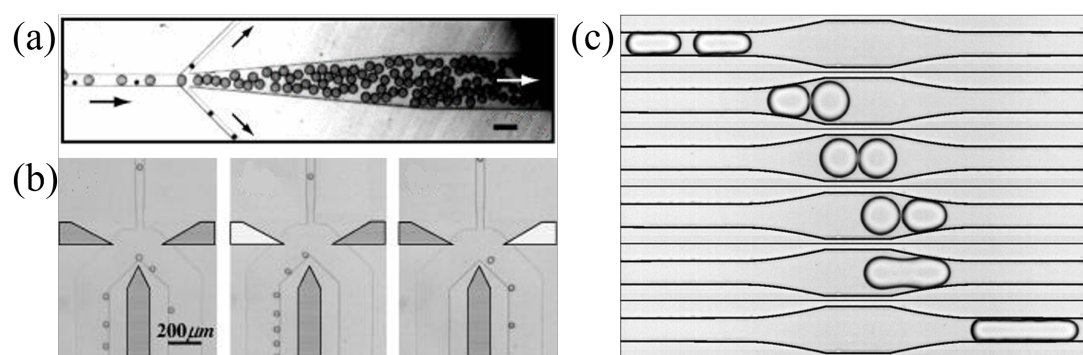


**Fig. 2.3** (a) Size-dependent separation of droplets using hydrodynamics. Reprinted from Mazutis *et al.* [33] (b) Bidirectional manipulation of drops using dielectrophoretic forces; showing grounded electrodes (grey) and energized electrodes (white). Reprinted from Ahn *et al.* [35] (c) Time sequence of droplet pair coalescing in a channel geometrical expansion. Reprinted from Bremond *et al.* [36].

When sorting is done by active methods, it requires the use of an external field [37], such as: electrical (Fig. 2.3b) [35, 38], magnetic [39], thermal [40], and mechanical applied in the form of pneumatic valves [41] or surface acoustic waves [42].

## Coalescence

Chemical and biological analysis commonly need the fusion of droplets with different contents to complete reactions. For this reason, controllable coalescence is of great interest for several applications within LOCs: reactions in droplets can be used for the formation of particles, chemical synthesis, kinetics studies, synthesis of bio-molecules, and the study of

fast organic reactions [26]; Furthermore, coalescence allows to switch back to bulk methods, by recovering the inner phase of selected droplets.

Passive methods for coalescence rely on the precise control over the velocity of individual droplets by specific geometries designs like channel expansions (Fig. 2.3c) and junctions [36, 43]; and by surface modification of the microfluidic device [44].

## Mixing

Mixing of the reagents confined within droplets is essential for reaction control and kinetics studies. In a microchannel, mixing is dominated by slow molecular diffusion typical of low  $Re$  at small dimensions. When a droplet flows on a straight channel, the inside of the droplet presents a symmetric flow pattern, with two equal circulating flows distributed on each half of it (Fig. 2.4a-b) [45]. Therefore, the contents within each half mixes, while keeping a phase boundary between the two adjacent miscible half.

Different channel geometries have been designed to induce chaotic flow and accelerate the homogenization of the droplets content. For example: Liao *et al.* introduced serpentine-like channels with protrusions able to induce mixing of crowded solutions in milliseconds (Fig. 2.4c-d) [46].

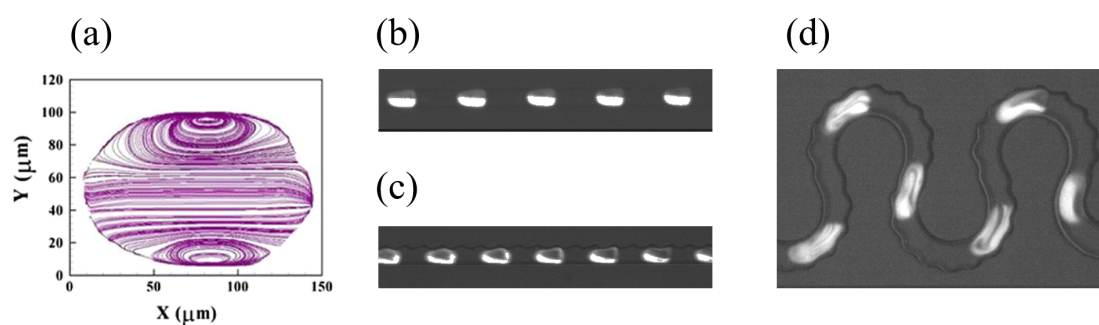


**Fig. 2.4** (a) Flow stream lines inside an aqueous moving droplet. Reprinted from Tung *et al.* [47] (b) Droplet inner mixing of dye for: (b) Straight channel, (c) Straight channel with protrusions, and (d) Serpentine-like channel with protrusions. Reprinted from Liao *et al.* [46].

## Splitting

The division of droplets into two or more daughter droplets, serves applications that require: the reduction of the droplet volume, the control on the concentration of chemicals inside droplets [48], or the production of arrays of droplets for high-throughput screening applications [49].

The most straightforward passive method for droplet splitting is by designing a bifurcated channel with a Y-shaped junction or obstruction (Fig. 2.5a) [50]. Fractal structured channels designed with these junctions, allow the sequential splitting and generation of a series of droplets in high throughput.

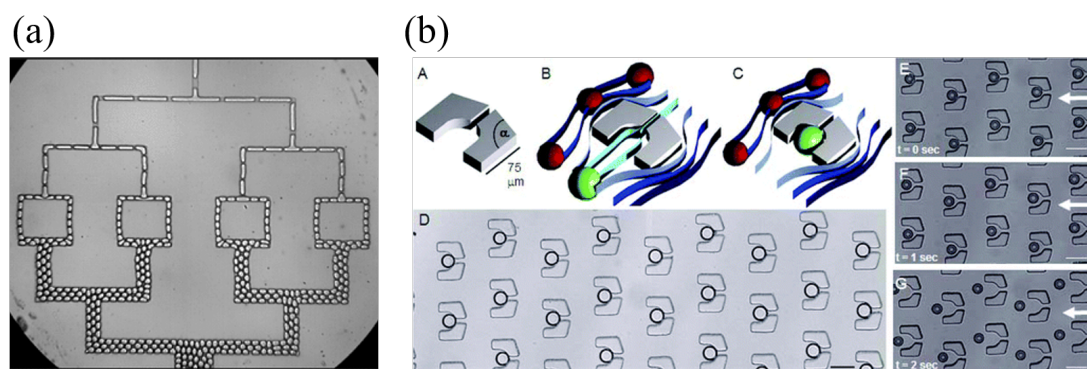


**Fig. 2.5** (a) Sequential application of passive breakup to form small drops. Reprinted from Anna *et al.* [50] (b) Droplet trapping arrays; when the oil flow is inverted, (white arrows) droplets can be recovered. Reprinted from Huebner *et al.* [51].

## Trapping

Due to the fast nature of high throughput screening operations, some applications present difficulties on monitoring the information of interest without the need of trapping the droplet on a specific location.

The most common methods used rely on passive geometric trapping. An example is the design presented by Hollfelder *et al.* (Fig. 2.5b) consisting on a single-layer-structured PDMS device with geometric trap arrays using standard soft lithography techniques [51].

## 2.2 Cell analysis in droplet microfluidics

With the evolution of the technology, and operational units availability, droplet microfluidics has been increasing its reach within different types of bio-chemical assays: Initially, the technology was aimed for molecular analysis, including ions, small molecules and biological macromolecules like nucleic acids and proteins [52, 53]; later, droplet-based microfluidics brought novel platforms for standard molecular techniques, such as polymerase chain reaction (PCR) [54], and enzyme-linked immunosorbent assay (ELISA) [55]; finally, the technology has been used for cell-level analysis [56], and it is of special interest for applications where the isolation of cells within a confined volume is required.

Cell-level analysis within droplet-based microfluidics technology requires the efficient encapsulation of cells and their viability inside droplets for relevant periods of time.

### 2.2.1 Cell encapsulation

When a cell suspension is directly emulsified into droplets, the number of cells in each droplet follows the nonuniform Poisson distribution [57], which is given by:

$$f(\lambda, n) = \frac{\lambda^n e^{-\lambda}}{n!} \quad (2.5)$$

where  $n$  is the number of cells in the drop and  $\lambda$  is the average number of cells per drop. With the aim of ensuring that most droplets contain no more than one cell, cell suspensions are highly diluted before encapsulation (Fig. 2.6a). This method produces a high number of empty droplets, which are commonly separated from occupied ones with a sorting unit [58].

Additional techniques, such as cell ordering prior to encapsulation and through special geometries in the microfluidic chip are also implemented to improve the distribution, and ensure high number of single-cell occupied droplets (Fig. 2.6b) [60].

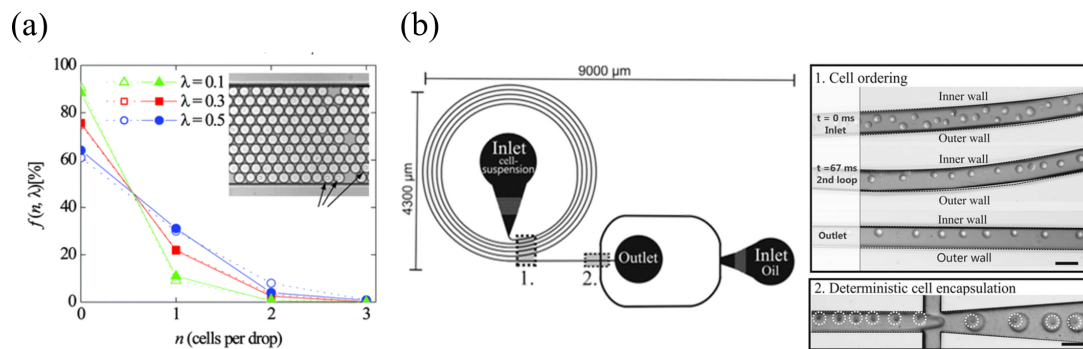


**Fig. 2.6** (a) Poisson distribution for three different cell densities with micrograph showing cells in drops in incubation device. Reprinted from Koster *et al.* [59]. (b) Schematic drawing of a microfluidic chip consisting of a curved microchannel followed by an encapsulation part. The pictures are of inertial cell ordering in the curve microchannel and subsequent encapsulation. Scale bars are 50  $\mu\text{m}$ . Reprinted from Kemna *et al.* [60]

## 2.2.2 Cell culture

A viable cell culture demands a microenvironment suitable for the exchange of substances, including nutrients, gas, and metabolites. Additionally, the components of the microenvironment, such as droplet content, interface and carrier-fluid must be bio-compatible. Different cell types, including prokaryotic and eukaryotic cells, have been successfully cultured in droplet-based microfluidics systems [56], as well as more complex organism like the multicellular “*C. elegans*” [61].

Carrying out cell culture experiments over extended periods of time is usually done by adding trapping units to the LOCs [51, 62]. This approach allows the continuous monitoring of the system, at the cost of limitations on the total throughput. Another approach, consists on droplets incubation off-chip in syringes, or tubings [63], and re-injection into another chip device after incubation for further processing (Fig. 2.7). However, this usually goes with a loss of the droplet order, requiring different strategies for tracing and labeling of the cells or droplets [64].

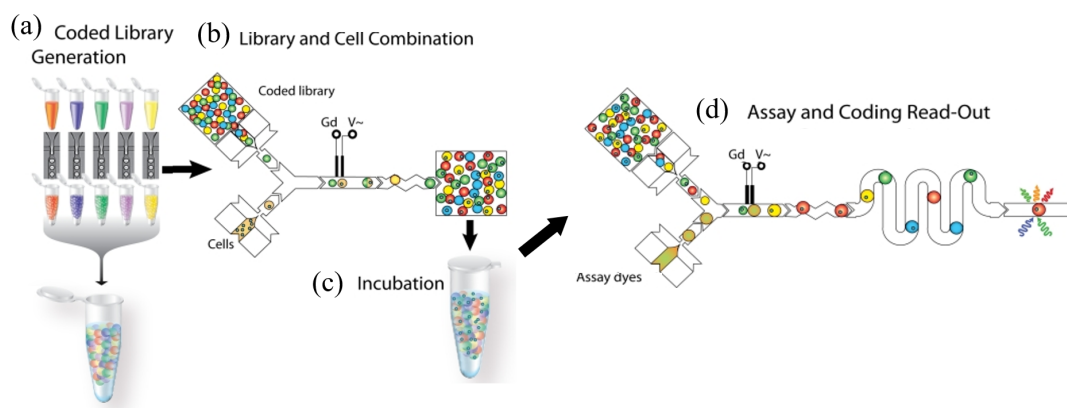


**Fig. 2.7** Workflow scheme for single-cell high-throughput screening. (a) A reformatting step to emulsify compound-code pairs and pool them into a droplet library. (b) Merging each library member with one of the cell-containing droplets that are continuously generated. Hence, each cell droplet has a specific composition defined by the compound droplet it has merged with. (c) Off-chip incubation. (d) Merged droplets are reinjected into an assay chip to identify each compound via their code and assess their specific effect on cells. Reprinted from Boruzes *et al.* [65]

### 2.2.3 Interest on single-cell analysis

Single-cell analysis gained increased interest due to its capacity of revealing cell heterogeneity (Fig. 2.8). In bulk experiments, signal variations between individual cells can be easily masked by cell group signals [66]. Isolated cells in droplets, on the other hand, are blocked from cell-cell communication, eliminating environmental effects arising from neighboring cells. Growth cell conditions are then only affected by the isolated cell itself or daughter cells upon cell division for long-term culture experiments. As a result, conditions are met to reveal differences within isogenic cell populations [67].

Taking advantage of these characteristics, single-cell studies have been done on: gene expression analysis [68]; transcriptome profiling [69] and their effects on protein expression or enzymatic activity; drug and toxicity screening [70]; directed evolution trials [71]; and stem cell research [67]. Moreover, the ability to monitor dynamic events within droplets provides additional competencies. For example, Boedickeretal *et al.* exploited the confinement properties provided by droplets to study the dynamic activation of quorum-sensing pathways in single cells [72]. The authors demonstrated that the mechanism responsible for pathway

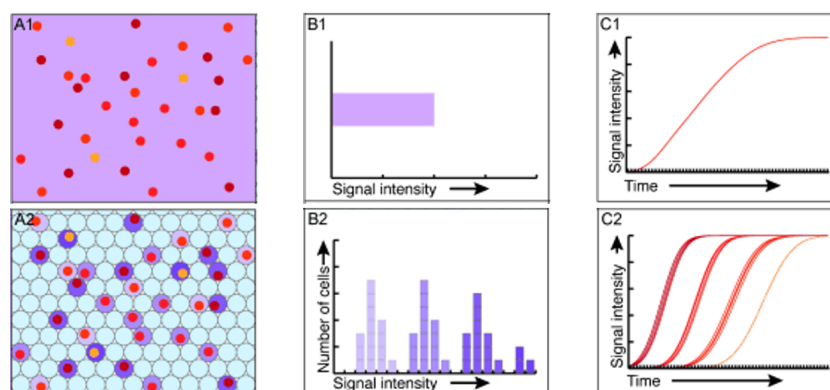


**Fig. 2.8** Schematic illustrations of the differences between ensemble analysis of cells (A1) and single-cell analysis (A2). Single-cell analysis can characterize a bi- or multimodal distribution of a certain trait (B2) or dynamics (C2), while ensemble analysis of the same cells would yield the average of the trait (B1) or dynamics (C1), which in some cases, does not describe the underlying population well. With ensemble cell analysis rare cell types are easily masked by the majority of cells, even though their traits may differ substantially. Reprinted from Joensson *et al.* [56]

activation is mediated by "diffusion sensing" and "efficiency sensing" rather than by cell-cell interactions as previously believed.

Despite the advantages, the main limitation of single-cell studies in droplets originates from the acute sensitivity of cells to their microenvironment. For this reason, a careful selection of the system formulation is of crucial importance. Furthermore, the preservation of the droplet integrity – avoiding unintended coalescence – upon manipulation and static storage, demands the use of interfacial stabilizer agents carefully selected to preserve the biocompatibility of the system.

### 2.3 System formulation and interfacial stabilizers

Stabilization of droplets is typically achieved by using surfactants, these are molecules containing both hydrophobic and hydrophilic groups. They are generally dispersed in the continuous phase, and upon formation of droplets they diffuse and adsorb to the water-oil interface while decreasing the interfacial tension ( $\gamma$ ) between the two immiscible phases

(Fig. 2.9a) [73]. The addition of surfactants kinetically stabilizes droplets in a metastable thermodynamic state. Metastability indicates that the droplets have a limited lifetime before coalescence or coarsening. This lifetime can vary from sub-millisecond to years depending on the stabilizing characteristics of the surfactant in the particular two-phase system and the physical conditions surrounding the emulsion. Therefore, the selection of surfactants for droplet-based microfluidics is intimately linked to the chemical nature of the phases used and the surface of the containing microchannel.

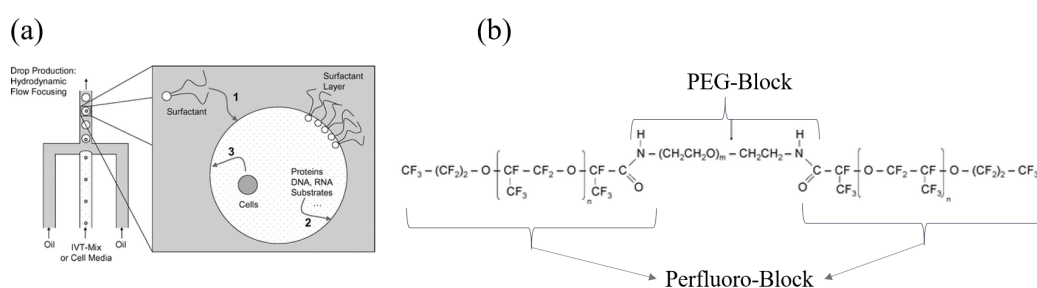


**Fig. 2.9** (a) Left: Drops are generated and biological molecules and/or cells are encapsulated. Right: Surfactants adsorb to the interface (arrow 1), forming an interfacial surfactant layer. The surfactant layer stabilizes the emulsion and prevents the adsorption of biomolecules and cells to the interface (arrows 2 and 3). Tuning the molecular structure and composition of the surfactant is critical for functional drop-based biological assays. Reprinted from Holtze *et al.* [74]. (b) PFPE-PEG block-copolymer surfactant structure

There is a widespread adoption of water-in-fluorinated-oil systems as preferred choice for bio-chemical applications [75]. This derives from the advantages present in fluorinated oils over other possible carriers: their low solubility towards organic molecules, restricts the cross-talk between emulsions droplets [76]; their high permeability to respiratory gases, is a key element for cell survival [77]; their low viscosity and their high compatibility with PDMS [78], allow its used with common microfluidic devices fabricated by conventional soft-lithographic methods.

The PFPE-PEG di- and triblock copolymer surfactants are the most commonly used stabilizing agents (Fig. 2.9b) [74]. The outer block (PFPE) plays a stabilizing role own to its

good solubility in fluorocarbon oils and its large steric repulsion; while the inert inner block (PEG) prevents the non-specific adsorption of biological material to the droplet interface. However the difficulty and cost of synthesizing this type of surfactants, drives the interest for alternative fluoro-stabilizers that could be added to the microfluidics toolbox.

### **2.3.1 Droplet transport**

Apart from stability and biocompatibility, it is necessary to consider the possible molecular exchange between droplets (coarsening). In order for droplets to serve as effective microreactors, they must retain all reaction components during the entire timescale of the experimental assay. Most assays use fluorophore probes as readout, which can be problematic since hydrophobic molecules can partition out of droplets into the continuous phase [79]. Fluorophore exchange not only reduces assay sensitivity, but also increases the false positive rate as probe transfers from positive droplets to negative ones [80].

In fluorinated oils, the transport of small molecules in emulsions has been shown to depend on surfactant concentration (Fig. 2.10) [81]. Surfactants play a fundamental role in driving cross-talk effects by forming micelles and by molecular interactions between their amphiphilic groups and the molecules inside droplets [75]. Additional parameters that has been shown to correlate with molecular transport include inter-droplet distance – of special relevance during off-chip droplet storage – and flow of the continuous phase around stationary droplets [82]. These studies demonstrate that transport is limited by surfactant-mediated transfer of components through the continuous phase, which occurs faster for closely spaced droplets.

### **2.3.2 Alternative stabilizing agents**

Solid particles can replace surfactants as interfacial stabilizers. The so called Pickering emulsions represent an attractive alternative to include in the microfluidic toolbox. They

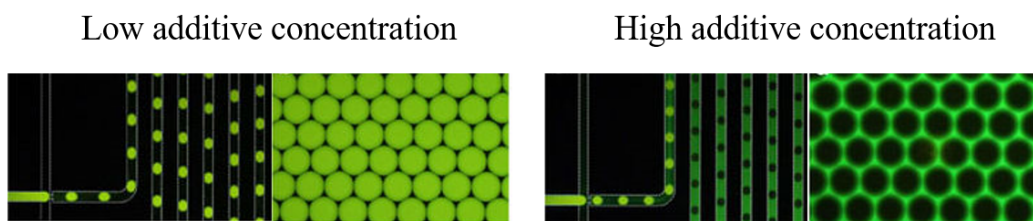


**Fig. 2.10** Fluorescence images of microfluidic droplet production and resulting emulsions in the presence of 0.5 % PFPE–PEG–PFPE surfactant and the additive carboxylic acid surfactant (Krytox-FSH) at low (<1%) and high (30%) mass fractions. This experiment shows a direct control on the process of extraction by the concentration of additives solubilized in the fluoruous phase. Reprinted from Gruner *et al.* [82]

offer new possibilities to overcome limitations of current formulations, for instance: Pan *et al.* demonstrated that by using fluorinated silica nanoparticles as droplets stabilizers, the leakage of resorufin (hydrophobic fluorescent molecule) can be effectively prevented (Fig. 2.11) [83]. Indeed the absence of surfactant in the oil phase reduces drastically the partitioning making this strategy efficient to reduce cross-talk.

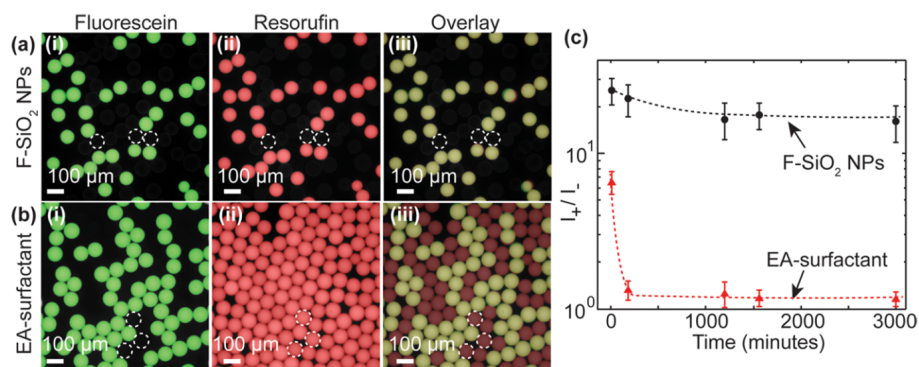


**Fig. 2.11** Two dyes (fluorescein, green and resorufin, red) are (a) encapsulated in nanoparticles stabilized droplets, showing an effective compartmentalization of the dye; and (b) surfactant stabilized droplets, where the resorufin is exchanged (yellow droplets) over time. (c) Quantitative measurement of the exchange process showing how retention is improved using nanoparticles at the interface. Reprinted from Pan *et al.* [83]

Furthermore, the rigid support provided by the particles at the interface, opens the possibility for adherent-cell studies in droplets [84]; the modifiable silica surface, allows the

introduction of additional functional groups [85]; and most recently, Gai *et al.* demonstrated that particle-stabilized droplets suppress unintended splitting in a channel constriction [86].

Nevertheless, the combination of Pickering emulsions with droplet-based microfluidics technology is still in its early stages, and a better understanding of the system – exploring advantages and limitations – is required to fully define its place within the droplet-based microfluidic toolbox.

## PROJECT SCOPE

- In this thesis project we will explore fluorinated Pickering emulsions properties for droplet-based microfluidic applications, with the main goal of obtaining a suitable technological platform for the study of single-adherent-cells.
  - In chapter 3, we will describe the synthesis, characterization and fluorination protocol of fluorinated Si-NPs. We optimize the fluorination protocol and determine the final particle concentration and degree of surface functionalization.
  - In chapter 4, we will explore the flow properties of fluorinated Pickering emulsions, which is of special relevance for emulsions re-injection and manipulation within droplet-based microfluidic platforms. We design a microfluidic device for the quantitative characterization of the emulsion flowability and link their flow properties with the system formulation.
  - In chapter 5, we will study in depth the stabilization of Pickering emulsions within droplet-based microfluidics. From our observations we derived new guidelines that –in comparison to current methods– allow the reduction of the droplet stabilization time by an order of magnitude, and at the same time significantly reduce the particles waste.
  - Finally, in chapter 6, we will apply this engineered system for the study of adherent cells, using as model Retinal Pigment Epithelium (RPE). We demonstrate the suitability of our platform for RPE cells studies, and the open possibilities for new experiments accounting for their inherent phenotypic heterogeneity.



# Chapter 3

## Fluorinated Pickering emulsions

This chapter describes the fabrication and characterization of fluorinated silica nanoparticles. The obtained particles are used for the experimental work presented in the subsequent sections of this project.

### 3.1 Silica nanoparticles synthesis

Pristine silica nanoparticles (Si-NPs) were kindly provided by MaFIC group (CRPP, Bordeaux)<sup>1</sup>. We received them in a suspension of ethanol with their size already characterized by electron microscopy imaging.

In this section we briefly describe the two step protocol followed for the synthesis of Si-NPs: they were synthesized following the Stöber approach for the fabrication of monodispersed spherical silica [87], starting from 25 nm silica seeds generated by the method described by Hartlen *et al.* [88].

---

<sup>1</sup>Synthesis and size determination done by Dr. Céline Hubert and Pierre-Etienne Rouet

### 3.1.1 Seed Synthesis

The seed synthesis was performed in 250 mL flask and involved the addition of 0.1 g of L-arginine to 100 mL of water while mixing the solution with a magnetic stirrer (Fig. 3.1a). Then the solution was heated to 60 °C and the temperature was kept constant and homogeneous with a temperature controller and continuous stirring. Finally, 10 mL of tetraethylorthosilicate (TEOS) was added and the reaction was left stirring at constant temperature for 3 days.

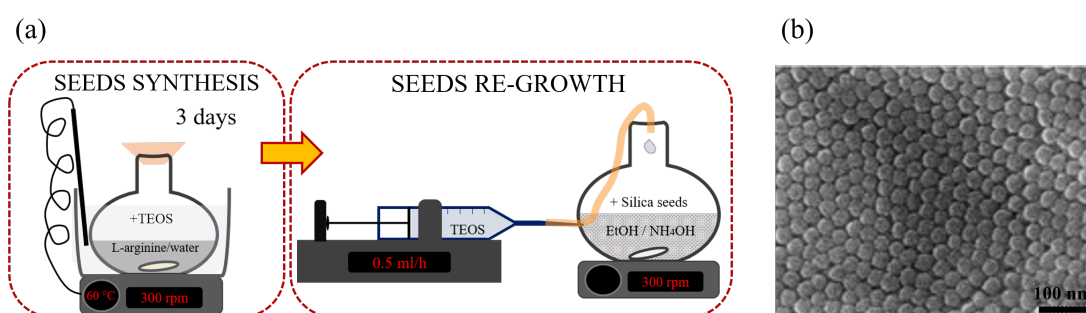


**Fig. 3.1** (a) Schematic representation of silica nanoparticles synthesis: first, silica seeds synthesis with natural protein as catalyzer (L-arginine), then silica seeds re-growth by the Stöber approach. (b) Electron microscopy image of 26 nm silica seeds prepared by Hartlen *et al.* [88].

The obtained silica seeds are highly monodispersed and biocompatible since the dispersion does not contain hazardous chemicals and the particles are stabilized by a natural amino acid [88] (Fig. 3.1b).

### 3.1.2 Re-growth of silica seeds

Re-growing silica seeds was performed following the Stöber approach [87]. In general, the growth of silica particles in the Stöber method is the result of condensation of anionic silanol monomers – derived from TEOS hydrolysis in a mixed ethanol/ammonia solution – into siloxane networks.

The re-growth of the silica seeds was performed in a 1 L flask, containing 455 ml of absolute ethanol, 35 ml of Ammonia (30%) and 10 ml of the silica seeds dispersion obtained

previously (Fig. 3.1a). Then, TEOS was added at a controlled speed of 0.5 ml/h using a syringe pump. The amount of TEOS added determines the final particle size, for example: 8 ml of TEOS for a final particle size of 50 nm.

All the Si-NPs obtained through this method were highly monodisperse and stable in ethanol suspension. Particle sizes used for this thesis project were determined by transmission electron microscopy (TEM) and they were in the range of 49 to 100 nm. Additionally, Si-NPs concentration (weight per volume of solvent w/v) was determined by drying 500  $\mu$ l of sample and weighting the dried Si-NPs.

## 3.2 Si-NPs density and specific surface area

Having the average size of the Si-NPs as well as the concentration ( $c_p$  in w/v) would in principle allow the calculation of the number of Si-NPs ( $n_p$ ) in a given volume of solvent ( $V_s$ ) as:

$$n_p = \frac{c_p V_s}{\rho_p V_p} \quad (3.1)$$

where  $V_p$  is the volume of one particle of size  $\delta$  calculated as a sphere ( $V_p = 4/3\pi(\delta/2)^3$ ), and  $\rho_p$  is the density of the Si-NPs.

The bulk density of silica in its crystal quartz form is of 2.648 g/cm<sup>3</sup> [89]. However, Si-NPs have shown to vary in density. In particular, Si-NPs produced by the Stöber approach present an uniformed spherical shape with a porous structure [90], which in turn affect the density of the Si-NPs.

We determined the density of Si-NPs by estimating first the specific surface area ( $S_c$ ) in m<sup>2</sup>/g. Then, we used the known surface to volume ratio for a sphere –  $6/\delta$  – to calculate the mass of a single nanoparticle of known dimensions as:

$$\rho_p = \frac{6}{\delta S_c} \quad (3.2)$$

Sears introduced a simple method for the calculation of the specific surface area ( $S_c$ ) of colloidal silica by titration with sodium hydroxide [91]. This titration was performed in a medium of 20% aqueous sodium chloride between pH 4 and 9. At pH 9, 1.26 ions of hydroxyl ions are adsorbed per square millimicron of surface. He then obtained an empirical relation between the titer and the  $S_c$  determined by the low-temperature nitrogen adsorption technique [92] as:

$$S_c = 32V_{NaOH} + 25 \quad (3.3)$$

this empirical correlation gives  $S_c$  in  $m^2/g$  and is a function of the needed volume of 0.1 N NaOH (ml) to titer 1.5 grams of colloidal silica in 150 ml of 20% aqueous sodium chloride solution.

We modified this correlation to make it a function of the concentration of NaOH by:

$$V_{NaOH} = \frac{150ml[NaOH]_f}{0.1N} \quad (3.4)$$

finally giving,

$$S_c = 48000[NaOH]_f + 25 \quad (3.5)$$

where,  $[NaOH]_f$  is the concentration needed to titer colloidal silica (10 mg/ml) in a 20% aqueous sodium chloride solution from pH 4 to pH 9.

To verify this correlation the commercial Si-NPs Aerosil<sup>®</sup> OX-50 were used as reference. The titration was performed in a flask at room temperature, with continuous stirring (magnetic stirrer). Change of pH was monitored with a pH meter (Orion Star A121) for: Aerosil<sup>®</sup> OX-50 particles and for three different sizes of synthesized Si-NPs (100, 65 and 49 nm) (Fig. 3.2).

Finally, with the empirical correlation 3.5, we estimated  $S_c$  and with the equation 3.2 we estimated  $\rho_p$  (Table 3.1).

The obtained value of  $S_c$  for the commercial Aerosil<sup>®</sup> OX-50 was clearly within the range reported by the manufacturer (BET-Surface area of  $50 \pm 15 m^2/g$ ). The clear difference

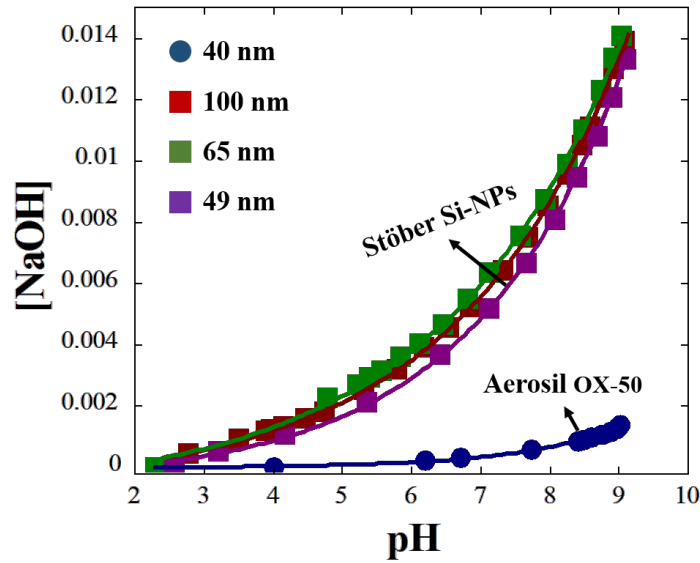


**Fig. 3.2** Concentration of sodium hydroxide required for titration (pH 4 to 9) of Si-NPs dispersion (10 mg/ml) in 20% aqueous sodium chloride solution.

**Table 3.1** Diameter ( $\delta$ ), specific surface ( $S_c$ ), and density ( $\rho$ ) of: Aerosil<sup>®</sup> OX-50 and In-house-synthesized nanoparticles

	Aerosil <sup>®</sup> OX-50	Syn1	Syn2	Syn3
$\delta$ (nm)	40	100	65	49
$S_c$ (m <sup>2</sup> /g)	42	555	560	535
$\rho_p$ (g/cm <sup>3</sup> )	3.6	0.108	0.165	0.229

obtained between the commercial Si-NPs and the synthesized ones are most likely due to a porous structure present in the later ones.

### 3.3 Nanoparticles as interfacial stabilizers

Stabilization of droplets requires an initial adsorption of the particles to the water-oil interface. To adsorb at the interface, particles need to wet both liquids; if the particles are completely wetted by water or oil, they remain dispersed in either phase, and no stable emulsion can be obtained.

Similarly to the hydrophilic-lipophilic balance for surfactants [93]; particle relative wettability determines the emulsion type – oil-in-water (o/w) or water-in-oil (w/o) –, and

for an adsorbed particle it is expressed in terms of the angle ( $\theta$ ), through the water phase, between the tangent to the particle and the interface (Fig. 3.3a) [94]. Hydrophilic particles ( $\theta < 90^\circ$ ), will favor then o/w emulsions, whereas w/o emulsions will be preferentially obtained with hydrophobic ones ( $\theta > 90^\circ$ ).

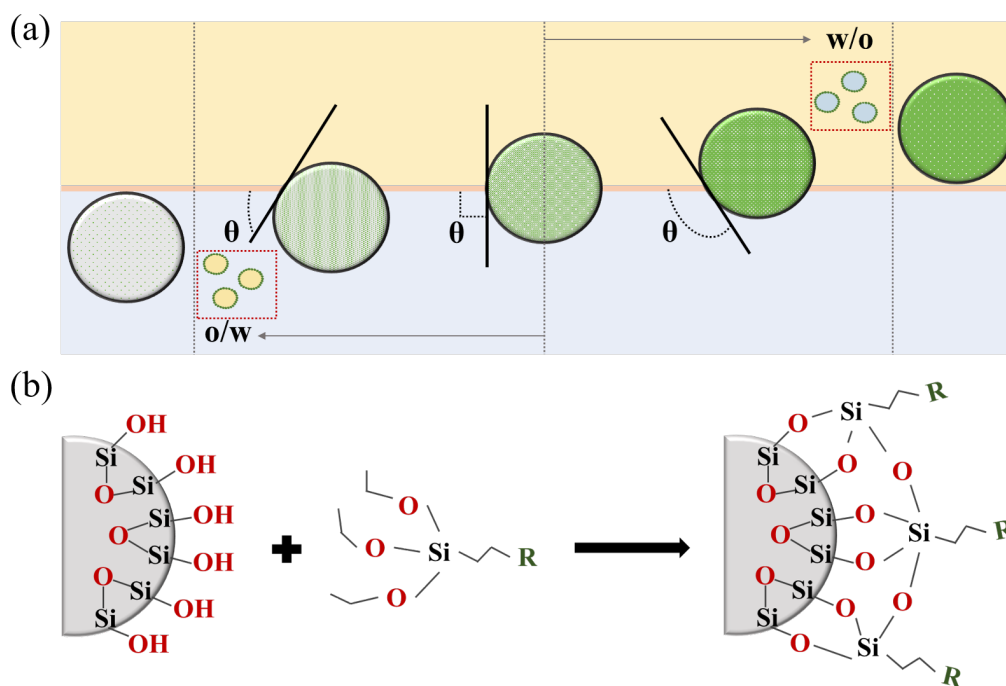


**Fig. 3.3** (a) Particle contact angle  $\theta$  at the w/o interface;  $\theta$  determines the type of emulsion that is preferentially formed (o/w or w/o). Here, the green colored particles represent more hydrophobicity. For  $\theta = 0^\circ$  or  $180^\circ$  no emulsion can be stabilized. (b) Silica nanoparticles wettability can be modified by silanization with organofunctional alkoxy silane molecules. Here "R" represents the organic (hydrophobic) group.

The strength with which a particle is held at an oil-water interface is also related to  $\theta$ . Particles with an angle of  $90^\circ$  at the water-oil interface possess the maximum desorption energy,  $E$ , calculated by equation 3.6 [95]:

$$E = \pi R^2 \gamma (1 - |\cos \theta|)^2 \quad (3.6)$$

where  $\gamma$  is the interfacial tension and  $R$  is the particle radius. This expression shows that

emulsions are better stabilized by large particles. Furthermore, as long as  $30^\circ < \theta < 150^\circ$ , the anchoring energy is large compared to the thermal energy  $k_B T$ , even for nanometric particles.

Particle hydrophobicity/hydrophilicity is therefore a key parameter for the preparation of stable Pickering emulsions. On this thesis project we worked exclusively with silica nanoparticles. Silica is one of the most extensively studied solid particles as Pickering emulsifiers; they are easily obtained and modified, allowing for example, the study of Pickering phase inversion [96].

Bare Si-NPs are hydrophilic owing to the high density of hydroxyl groups on its surface (OH) (Fig. 3.3b). Surface modification is usually made by grafting organofunctional alkoxy silane molecules (silanization); the grafting degree (surface coverage) controls the hydrophobic character of silica and its wetting by water and oils [97].

### 3.4 Si-NPs Surface Fluorination

As discussed in section 2.3, the preferred carrier phase for droplet-based microfluidic applications consists on fluorinated oils [73, 75]. We modified the partial wettability of our pristine Si-NPs for the carrier phase by anchoring on its surface a fluorinated compound. The fluorinated Si-NPs would then be able to adsorb to the water-fluorinated oil interface and stabilize w/o emulsions.

The surface fluorination protocol initially tested was that described by Pan *et al.* [83] (shown schematically in Fig. 3.4): First, 10 ml of Si-NPs dispersion (obtained by method described on section 3.1.2) was centrifuged at 8000 rpm for 30 min; then the supernatant was removed and 5.4 ml of absolute ethanol along with 150  $\mu$ l of ammonia (30%) was added and vortexed; next, the mixed dispersion was transferred to a flask with a magnetic stirrer and 1 ml of 1H,1H,2H,2H-Perfluorooctyltriethoxysilane 98% (PFOTES) was added and let stirring for 30 min; later, the dispersion was centrifuged (8000 rpm, 30 min), and the obtained

particles were dried after removing the supernatant. Finally, 5 ml of HFE-7500 fluorinated oil was added and vortexed.

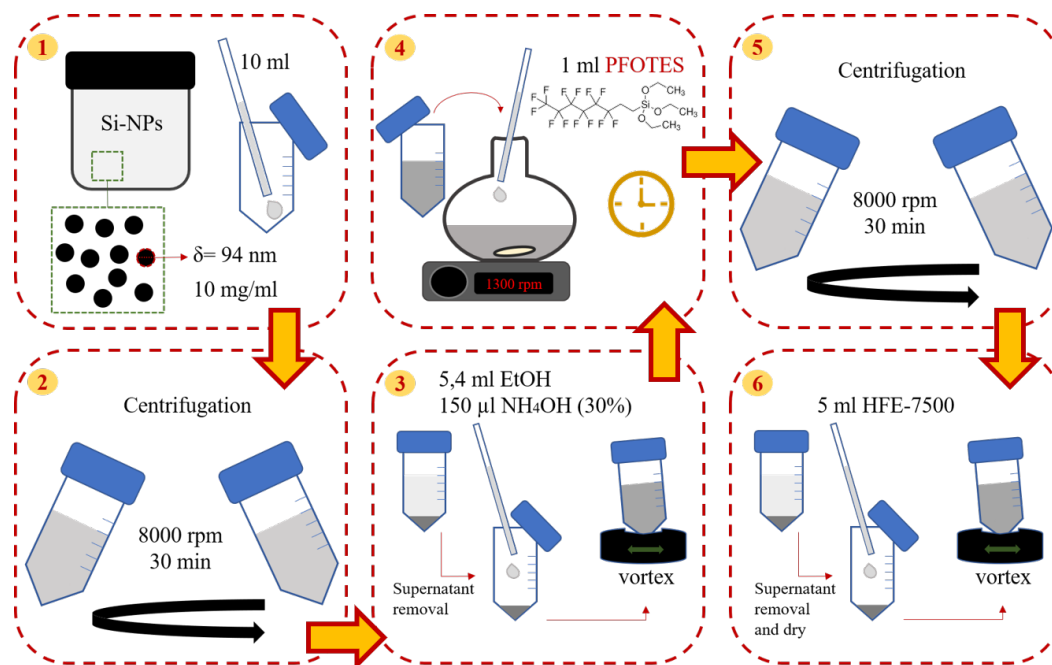


**Fig. 3.4** Schematic representation of Si-NPs fluorination protocol initially tested

Directly applying this protocol with our pristine Si-NPs brought along several drawbacks that prompt us to implement various adjustments to optimize the Si-NPs fluorination protocol.

### 3.4.1 Avoiding particle aggregation

After applying the surface fluorination protocol – as described on Fig. 3.4 – and re-disperse them in HFE-7500, the obtained particles had microscopic size aggregates that couldn't be dissolved with intense vortex mixing and sonication. These samples were not able to effectively stabilize emulsions prepared by bulk or in a microfluidic device.

We determined two critical steps that were contributing on the formation of these aggregates: Poor mixing and complete drying.

After separating the Si-NPs by centrifugation, vortex mixing was not sufficient for a complete re-dispersion of the particles in ethanol and ammonia. Microscopic aggregates

– not noticeable by naked eye – remained, apparently resulting in a non-homogeneous functionalization of Si-NPs. The resulting aggregates could not be dissolved in fluorinated oil by long mixing times and sonication. Separation of these aggregates by filtration, would result in a significant amount of material wasted.

Poor mixing problem was solved by adding 15 min of sonication before and after vortex mixing. This step was added on both: before Si-NPs surface fluorination and during fluorinated particles re-dispersion in HFE-7500 (3rd and 6th step in Fig. 3.4).

The second origin of aggregates was identified as crystal-like clusters formed when the sample was completely desiccated before dispersion in HFE-7500 (6th step in Fig. 3.4). These aggregates grew in size when exposed to 1 h of sonication (Fig. 3.5).

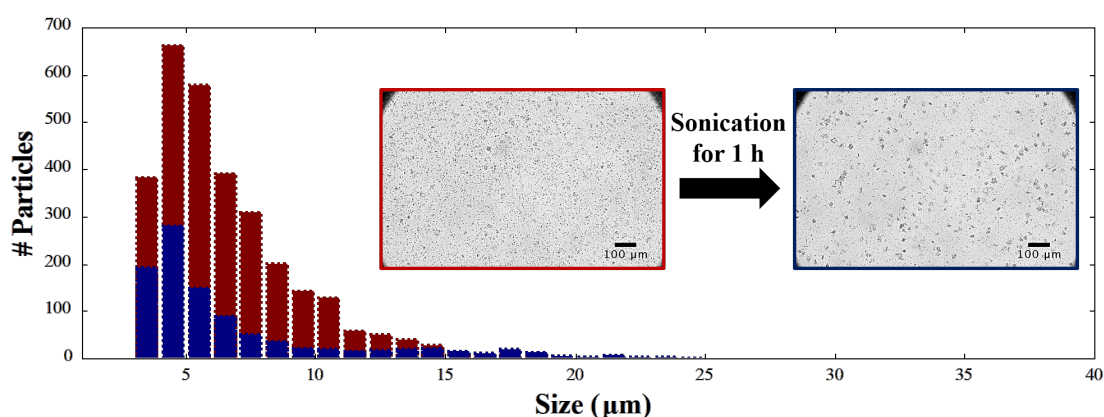


**Fig. 3.5** Microscopic aggregates obtained after lyophilization of fluorinated Si-NPs and redispersion in HFE-7500. Sample is observed *before* and *after* 1 h of sonication. The size distribution is calculated by image analysis as the largest diameter of an ellipsoid approximation for each particle.

Three drying methods were tested: desiccation in an oven at 60°C over night; desiccation by lyophilization (after removing supernatant, adding water, and freezing); and desiccation with a rotary evaporator (without previous centrifugation step). For all three desiccation methods, microscopic aggregates were obtained, and droplets could not be effectively stabilized.

The protocol was modified by avoiding entirely the complete desiccation of the particles. Instead, after supernatant extraction the particles were directly re-dispersed in fluorinated oil

and left 2 h in a vacuum chamber at room temperature to extract traces left of the original solvent.

### 3.4.2 Determining Si-NPs concentration and degree of fluorination

The concentration of fluorinated Si-NPs ( $c_f$ ) was determined by dried weight of an aliquot (300  $\mu$ L) of the particle dispersion in HFE-7500. Knowing the particle concentration is of key importance, since it is a determining factor for the stabilization of Pickering emulsions.

For example, in order to test the ability of our fluorinated Si-NPs to stabilize droplets in microchannels a droplet production test was performed in a PDMS microfluidic device following a method described previously by Baret *et al.* [98]. The device consisted of a simple flow focusing production – where the fluorinated oil met the aqueous phase orthogonally – followed by an incubation channel (2 mm length) and a channel expansion where the droplets experienced stochastic collisions that promoted coalescence.

The fluorinated Si-NPs concentration was varied between 3.2 and 24 mg/ml. Droplet production conditions were kept constant: channel nozzle and device thickness were 120  $\mu$ m and 80  $\mu$ m respectively; the oil and aqueous flow rates were each 5  $\mu$ L/min. The channel expansion was monitored with a high speed camera, and the droplet diameter extracted through image analysis (Fig. 3.6).

As observed in the example on Fig. 3.6; droplet stability against coalescence improves by increasing  $c_f$  on the oil stream. Zero coalescence concentration is obtained for  $c_f \geq 24$  mg/ml. However, this result was not consistent between different batches of fluorinated Si-NPs, which needed different concentrations to reach stability against coalescence for the same conditions; despite the fact that these batches were prepared with the same concentration of Si-NPs before functionalization and the same reaction time (30 min) with PFOTES.

The inconsistencies observed between batches was found to be related with a loss of Si-NPs during the fluorination protocol. An unknown amount of particles lost before and/or

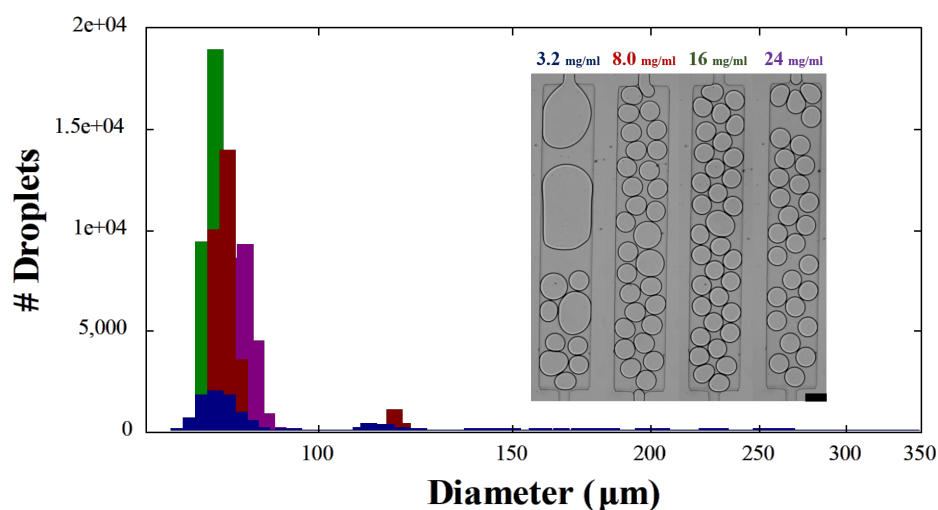


**Fig. 3.6** Example of droplet size distribution in a coalescence chamber for increasing  $c_f$ . (Scale bar 150  $\mu\text{m}$ ).

after the surface fluorination with PFOTES implies that the actual concentration of Si-NPs ( $c_p$ ) in HFE-7500 is also unknown. We identified the steps where that could be the case and modified the fluorination protocol accordingly.

Avoiding particles losses which could be removed along with the supernatant (after centrifugation step), required the increase of the speed and centrifugation time (3rd and 5th step on Fig. 3.4) to 15000 rpm and 1 h respectively. Additionally, transferring the Si-NPs dispersion to a different flask as well as contact stirring was avoided by doing the entire functionalization protocol in 50 ml centrifugation tubes, and using an external tube shaker (instead of magnetic stirrer) to mix during the Si-NPs surface functionalization with PFOTES.

Assuming negligible losses of Si-NPs,  $c_p$  was then calculated by taking the original weight of Si-NPs used and dividing it by the total volume of fluorinated oil used to re-disperse them.

From this dispersion, we took an aliquot (100  $\mu\text{L}$ ) and performed several sample dilutions ( $c_p < 0.5 \text{ mg/ml}$ ) in HFE-7500. The sample dilutions were used to carry out optical density (OD) measurements (incident wavelength 200 to 400 nm) in a quartz crystal cuvette with an UV-Vis spectrophotometer.

For non-adsorbing particles – case of Si-NPs – the OD value is directly related to turbidity; which is the decrease in the intensity of the incident light caused by light scattering of the nanoparticle suspension [99]. For a monodisperse system like ours, the turbidity is proportional to the concentration of nanoparticles.

Using pure HFE-7500 as reference, we found that Si-NPs present a peak in OD for an incident wavelength between 215 and 230 nm (Fig. 3.7). Taking the  $OD_{peak}$  as a function of  $c_p$  a linear relation was obtained. We determined a calibration curve taking dilutions of three different batches of particles, and for two different particle sizes ( $\delta = 96$  and 78 nm).

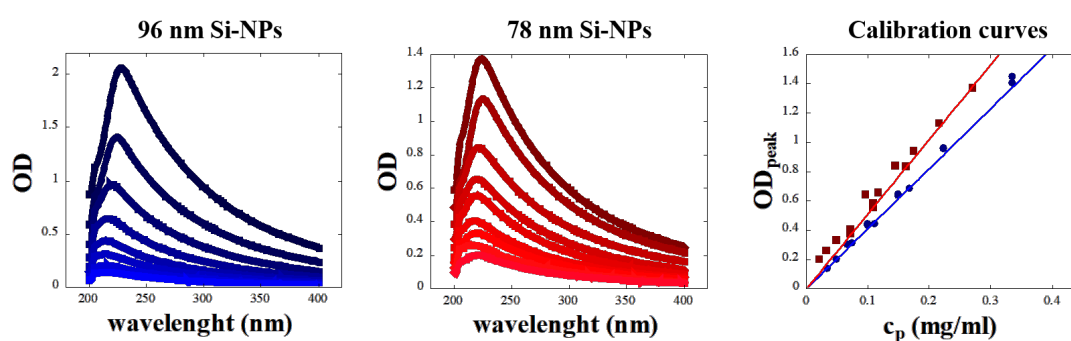


**Fig. 3.7** Two examples of OD spectra measurements (between 200 and 400 nm) shown for dilutions of two samples:  $\delta = 78$  nm in red, and  $\delta = 96$  nm in blue. Calibration curve slope higher for smaller particle size.

The calibration curve was seemingly independent on the content of PFOTES. We corroborated this observation by measuring the OD spectra for a sample of PFOTES (1 mg/ml) in HFE-7500, and obtaining an OD spectra equal to the reference sample of pure HFE-7500.

With these calibration curves a more accurate determination of  $c_p$  in HFE-7500 was done for each batch of particles. Corroborating a very small loss of Si-NPs ( $<0.1\%$ ) with the introduced protocol modifications. It is worth noting that this calibration curves were shown to be highly dependent on the specific quartz crystal cuvette used, so a new calibration curve was needed when the cuvette was replaced for a new one.

In order to have a reference on the amount of PFOTES that reacted with the Si-NPs surface, and consequently a relative reference on the hydrophobicity of the functionalized

Si-NPs; we defined a degree of surface functionalization ( $\phi_{wt}$ ) as:

$$\phi_{wt} = \frac{c_f - c_p}{c_p} \quad (3.7)$$

$\phi_{wt}$  gives then a weight relation between the adsorbed PFOTES and the Si-NPs.

We determined  $\phi_{wt}$  for all different batches of particles and found that the degree of functionalization was highly sensitive to reaction time and PFOTES initial concentration. The reaction time was highly difficult to control, since the reaction continued even during the centrifugation step, and diluting the sample with absolute ethanol as an attempt to stop the reaction proved to be unsuccessful.

In order to achieve a control on the degree of Si-NPs surface functionalization we modified the fluorination protocol by increasing the reaction time to 3 days. We then controlled  $\phi_{wt}$  by modifying solely the total amount of PFOTES added to the reaction (Fig. 3.8).

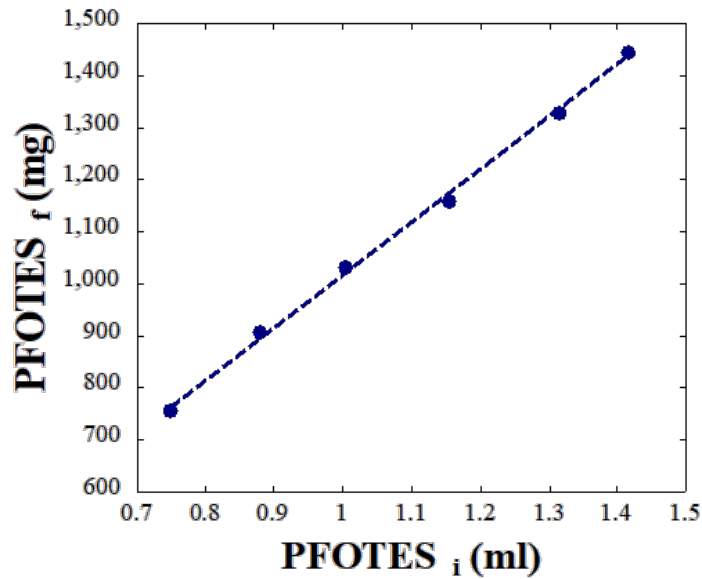


**Fig. 3.8** Weight of PFOTES<sub>f</sub> (mg) adsorbed to Si-NPs ( $\delta = 65$  nm) surface after 3 days of functionalization time, as a function of the volume PFOTES<sub>i</sub> (ml) initially added.

### 3.4.3 Final Si-NPs fluorination protocol

The final surface fluorination protocol is summarized schematically on Fig.3.9: First, the desired sample of Si-NPs was placed in 50 ml centrifugation tubes and centrifuged at 15000 rpm for 1 h; then, the supernatant was careful extracted and replaced with ethanol absolute (0.07% Ammonia), while keeping  $c_p$  between 10 and 20 mg/ml, the particles were thoroughly re-dispersed by combining sonication and vortex mixing.

Depending on the  $\phi_{wt}$  desired, equation 3.7 was used to calculate  $c_f$ , and the final volume of PFOTES to add was calculated using the linear correlation shown on Fig. 3.8. The reaction was left mixing with external tube shaker and after 3 days the dispersion was centrifuged (15000 rpm for 1 h), the supernatant carefully extracted and the particles re-dispersed in 10 ml of HFE-7500 by mixing with a combination of sonication and vortex mixing steps.

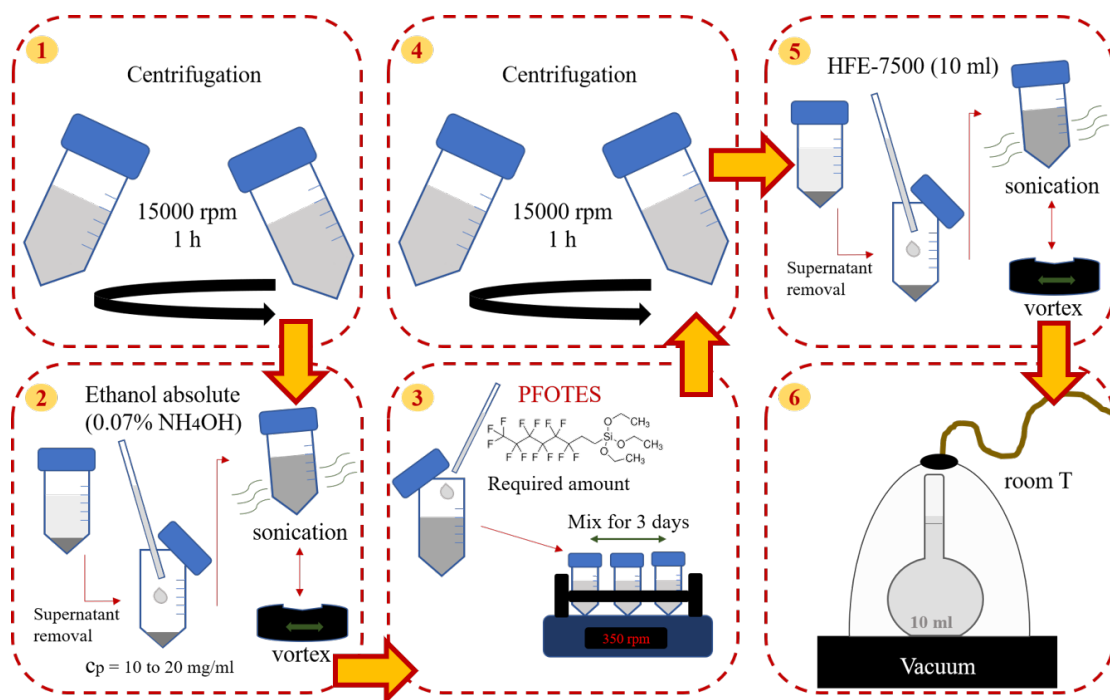


**Fig. 3.9** Schematic representation of final Si-NPs fluorination protocol

Finally, the particles dispersion was transferred to a volumetric flask and the sample was left at room temperature in a vacuum chamber for 2 h, after which time, the volume mark

(10 ml) was completed with HFE-7500 (if required) before taking an aliquot to measure  $c_f$  by dry weight.

### 3.5 Stabilizing droplets with fluorinated Si-NPs in microfluidics

In order to obtain the needed conditions for the stabilization of droplets with fluorinated Si-NPs we performed an additional coalescence test, similar to the one shown in Fig. 3.6. Here,  $c_p$  was varied between 1 and 6 mg/ml and the incubation channel length ( $L$ ) was varied between 0.2 and 16 mm. The flow rates were controlled with syringe pumps and kept constant: the dispersion of fluorinated Si-NPs in HFE-7500 flow rate ( $Q_p$ ) was 10  $\mu\text{L}/\text{min}$  and the aqueous flow rate ( $Q_w$ ) was 5  $\mu\text{L}/\text{min}$ .

The coalescence chamber dimensions were of 0.5 mm width and 3 mm length. The droplet population size was extracted through image analysis from the first and last 0.5 mm segment of coalescence chamber (red and green selected areas in Fig. 3.10a respectively). Then, the average droplet area was calculated from the first segment and the droplet stability against coalescence from the last one.

Droplet stability ( $p(1)$ ) is the total amount of non-coalesced droplets ( $n(1)$ ), divided by the total amount of droplets. This is calculated for the last segment of the coalescence chamber as described before by Baret *et al.* [98].

$$p(1) = \frac{n(1)}{\sum in(i)} \quad (3.8)$$

Here  $i$  indicates the coalescence level: droplet sizes which are  $i$  times the original droplet size. Naturally,  $p(1)$  varies between 0 and 1; for each studied conditions we measured at least 20000 droplets, and we considered a system stable when less than one coalescence event per 1000 droplets occurred ( $p(1) > 0.999$ ).

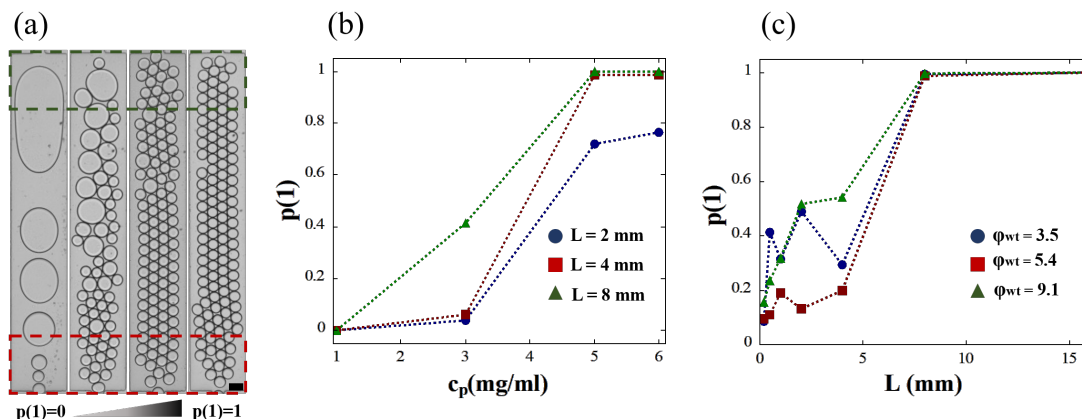


**Fig. 3.10** (a) Coalescence chamber for increasing  $p(1)$ , droplet size extracted from first chamber segment (red), and  $p(1)$  calculated from last segment (green). (b) Droplet stability against coalescence as a function of particle concentration. (c) Droplet stability against coalescence as a function of incubation length.

We inquired the effect of  $c_p$  on droplet stabilization with a sample of  $\phi_{wt} = 5.4$  (Fig. 3.10b). Independently of the investigated  $L$ , we observed that a minimum concentration of 5 mg/ml was necessary to reach a stable system.

We then proceed to study three batches of particles with different degrees of surface functionalization ( $\phi_{wt} = 3.5, 5.4$  and  $9.1$ ) and the same particle concentration,  $c_p = 4.5$  mg/ml (Fig. 3.10c). We observed the three samples reached stability for an incubation length  $L > 8$  mm.

This short test allowed us to determine suitable minimal conditions to stabilize fluorinated Pickering emulsions in microchannels. These conditions are used as reference only and cannot be generalized, since the systems are highly sensitive to variations of flow rates and geometry. We will explore in-depth the effects of these variables on Pickering emulsion stabilization later on (chapter 5). But before we tackle these questions, we will study another property of Pickering emulsions, namely their flowability (chapter 4).

## CHAPTER 3

**Summary**

- Starting from pristine Si-NPs as raw material, we produced fluorinated Si-Nps that effectively stabilized water-in-fluorinated oil droplets.
  - First, we characterized their specific surface ( $S_c$ ) and density ( $\rho_p$ ) which are relevant parameters for the calculation of the total number of particles.
  - We optimized the fluorination protocol of their surface to avoid problems such as particle aggregation.
  - We determined the Si-NPs final concentration ( $c_p$ ) in a fluorinated oil dispersion, as well the degree of surface functionalization ( $\phi_{wt}$ ).
  - Finally, we used a microfluidic method to determine the minimal conditions for the stabilizaion of Pickering emulsions in a standard droplet production device.



# Chapter 4

## Formulation effect on flow properties

In this chapter we will explore the flowability of Pickering emulsions, an important property for applications requiring the collection and re-injection of emulsions in a new microfluidic device for further manipulation.<sup>1</sup>

### 4.1 Empirical observations of Pickering emulsions "sticky" properties

In chapter 3 we described the protocol followed for the fluorination of Si-NPs as well as the minimal conditions required for the stabilization of droplets –with said Si-NPs– in a microfluidic device.

While testing the emulsions stabilized through this method, we encountered a problem that could become a major challenge for the full adaptation of fluorinated Pickering emulsions to droplet-based microfluidic operations.

Differently to emulsions stabilized with fluorinated surfactants; emulsions stabilized with fluorinated Si-NPs presented a sticky-like behavior. Where the droplets seemed to adhere to each other and behave more like a gel than a fluid.

---

<sup>1</sup>Part of this chapter is published in Chacon and Baret 2017 [100]

This behavior was specially a problem when we collected the produced emulsion, and attempted to re-inject it in a new microfluidic device. For example, on Fig. 4.1a<sup>2</sup> we observe a reservoir where most of the emulsion adhered to the walls after a re-injection attempt. This emulsion would not flow even after flipping the reservoir upside-down.

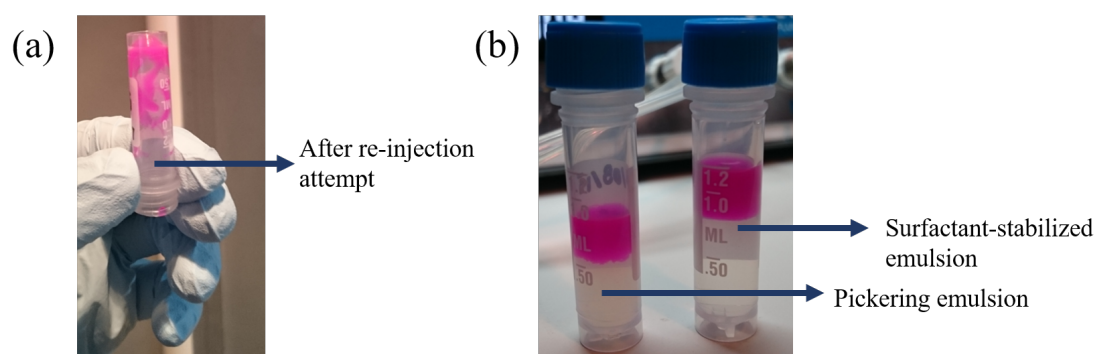


**Fig. 4.1** (a) Reservoir with fluorinated Pickering emulsion adhered to the walls after a re-injection attempt. (b) Difference between the emulsion interface for: Pickering emulsion (left) and emulsion stabilized by surfactant (right).

Furthermore, the droplet-droplet interactions for collected Pickering emulsions is evidenced by the irregular interface formed between the droplets and the continuous phase (Fig. 4.1b); in contrast to the smooth interface present in a system stabilized by fluorinated surfactants.

Pickering emulsions often exhibit the classical behavior of adhesive suspensions. This behavior directly results from strong attractive interactions between the droplets. Such a drop adhesion can result from particles that tend to aggregate, even in the dispersed state or from bridging between the droplets (where different droplets partially share the same particle interface) [101, 102].

Furthermore, both surfactant stabilized emulsions and solid-stabilized emulsions exhibit elastic behaviours over a critical droplet volume fraction, from which its osmotic pressure, and shear modulus, increase as the volume fraction increases over its critical value [103, 104]. However, Arditty *et al* showed that the osmotic pressure and shear modulus values are

<sup>2</sup>Empirical observation and pictures done with Dr. Ouriel Caën

higher for solid-stabilized emulsions due to different droplet deformation processes between these two emulsion types. While surfactant stabilized emulsions are controlled by capillary pressure of the non-deformed droplets, solid-stabilized emulsions are controlled by the 2-D yield stress of the droplet surface [105].

Measuring flow properties of these emulsions and choosing their optimal formulations is essential to demonstrate a full compatibility of these systems with the wide range of modules of droplet-based microfluidics. The most widely used method to characterize the flow behaviour of complex fluids such as Pickering emulsions, is the rheometric measurement of steady shear viscosity. However, macroscale rheometers are typically limited by sample volumes, access to high shear rates, hydrodynamic instabilities, and interfacial artifacts [106].

Lately, a broad range of microfluidic viscometers with various working principles have been developed to overcome typical limitations of macroscale rheometers [107–109]. Since the microstructure of a fluid strongly influence flow behaviour, the capability of microfluidic viscometers to simultaneously characterize rheology and microstructure through microscopic visualization distinguishes them from macroscale rheometric methods[106].

The rheological behaviour of complex fluids can range from viscoelastic fluids to soft solids, and it is strongly dependent on shear rates. Similarly, flowing properties of granular materials exhibit non-trivial transitions between static, quasi-static and dynamical states, behaving like a solid or a fluid according to the applied stress [110]. Additionally, the apparent link between droplet-droplet interactions with the bulk flow behavior (evidenced on the irregular droplet-continuous phase interface), further resembles granular materials systems.

We believe well-known techniques used to characterized flowing properties of granular materials could potentially bring an additional insight to complex fluids flow behaviour. Where the droplets would be treated as equivalent to particles in granular material systems.

## 4.2 The angle of repose test for granular materials

The angle of repose of a granular material is the steepest angle that the surface of a granular pile makes with the horizontal under gravity. Over this angle, avalanches spontaneously flow down the slope. This avalanche flow occurs in a relatively narrow boundary layer, so that granular flow is strongly non-Newtonian [110].

Granular materials can be split in two categories, cohesive and non-cohesive granular materials (Fig. 4.2): Non-cohesive granular materials, present interactions between grains mainly related to steric repulsion and friction forces, this means that the macroscopic properties of the assembly are governed by the geometry and surface properties of the grains; cohesive granular materials on the other hand, present forces between grains greater than the weight of one grain, this means that the macroscopic properties are strongly influenced by the cohesion inside the packing [111].

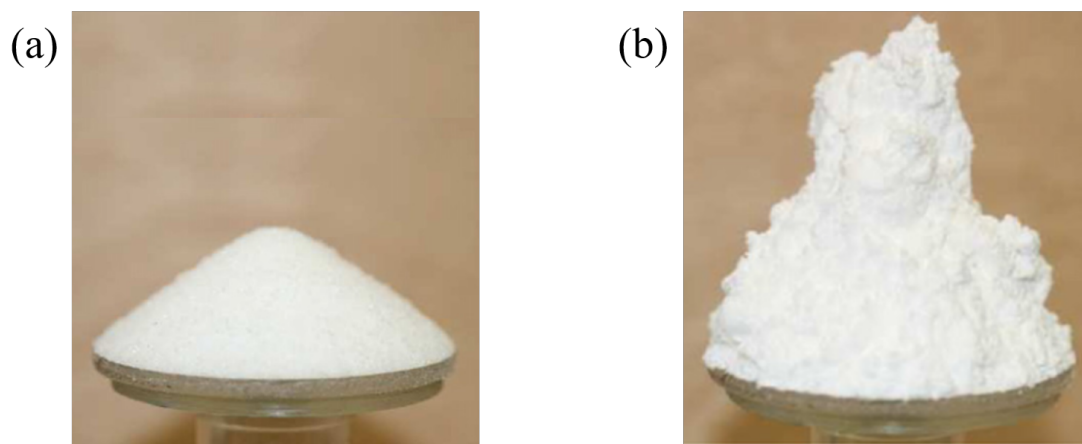


**Fig. 4.2** Two typical heap shapes. (a) Conical heap shape obtained with a non-cohesive granular sugar. (b) Irregular heap of powdered sugar which is a cohesive granular material. Reprinted from Lumay *et al.* [112].

Lumay *et al.* described a simple method to measure the angle of repose for granular materials: it consisted of placing the studied granular material on top of a circular support until a conical heap naturally develops. The angle of repose  $\alpha_r$  is the angle of the isosceles triangle which has the same surface area as the heap formed. Typically,  $\alpha_r \leq 36^\circ$  indicates

good to excellent flow properties, whereas  $\alpha_r \geq 57^\circ$  indicates very poor flowability [112].

They also characterized a cohesive index of the material ( $\sigma_r$ ) as the deviation between the heap interface and the ideal isosceles triangle shape. For a non-cohesive powder,  $\sigma_r$  would be close to zero [112].

## 4.3 Microfluidic angle of repose test for Pickering emulsions

Inspired on the angle of repose test presented by Lumay *et al* [112]; we developed a microfluidic adaptation of the angle of repose test to characterize the flow behavior of emulsions. Our method provides a quantitative reference on the flow properties of fluorinated Pickering emulsions, and aides in the selection of their optimal formulations for droplet-based microfluidics applications. In this section, we present the methods and results section as published in Chacon and Baret 2017 [100].

### 4.3.1 Materials and methods

#### Fluorinated silica nanoparticles

Fluorinated Si-NPs ( $\delta = 94$  nm) were synthesized and functionalized with PFOTES as described on chapter 3. All the experiments were done with a fixed concentration of Si-NPs ( $c_p = 6$  mg/ml) and degree of surface functionalization  $\phi_{wt}$  values ranging from 3.6 to 10.5 (equation 3.7).

#### Angle of repose microfluidic device design and fabrication

A standard microfluidic droplet maker device with a flow-focusing junction and a stabilization length of 8 mm was designed and moulded in polydimethylsiloxane (PDMS) using soft-

lithography techniques of replica moulding of a SU-8 master [73, 113]. A 0.5 cm PDMS stamp was obtained and its inlet ports were pierced with a 0.75 mm-diameter biopsy. Then it was bounded to a 0.5 cm patternless PDMS substrate through oxygen plasma activation. Afterwards, an area of the bounded PDMS was cut and removed as shown in the Fig. 4.3a, where the edge of the removed area coincides with the ending of the micropattern outlets that are between the two PDMS substrates. A 5 mm-diameter biopsy needle was used to obtain PDMS circular bases, that were fixed 1.5 cm away from the microfluidic device outlets (Fig. 4.3b) and finally, a glass slide was bounded on each side of the PDMS device through oxygen plasma activation (Fig. 4.3c), the remaining PDMS was cut and removed (Fig. 4.3d). The microfluidic channels were hydrophobized using a commercial coating agent (Aquapel, PPG industries).

It is important to remark that due to the density differences between the aqueous phase (droplets) and the heavier fluorinated solvent ( $\rho=1.614 \text{ g/cm}^{-3}$ ) used as continuous phase, the droplets deposition in our device occurred upwards and the cylindrical PDMS support worked as an upper limit for the droplets.

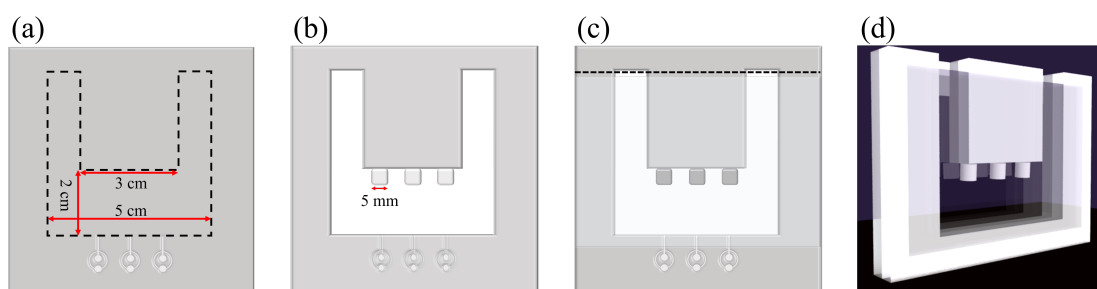


**Fig. 4.3** Schematic representation of the angle of repose measurement device fabrication: (a) indicated area of PDMS-PDMS microfluidic device was cut and retrieved; (b) 5 mm cylindrical PDMS supports were fixed and aligned with microfluidic outlet; (c) glass slides were plasma bounded on both sides of the microfluidic device and extra PDMS was cut. (d) 3D projection of the finished device.

### Angle of repose measurement set-up

In Fig. 4.4b, the set-up used for all the angle of repose measurements is shown. A phantom 4.2 high speed digital camera was mounted on a horizontal rail and connected to a Canon

macro photo lens (MP-E 65 mm) as shown in Fig. 4.4(a.3).

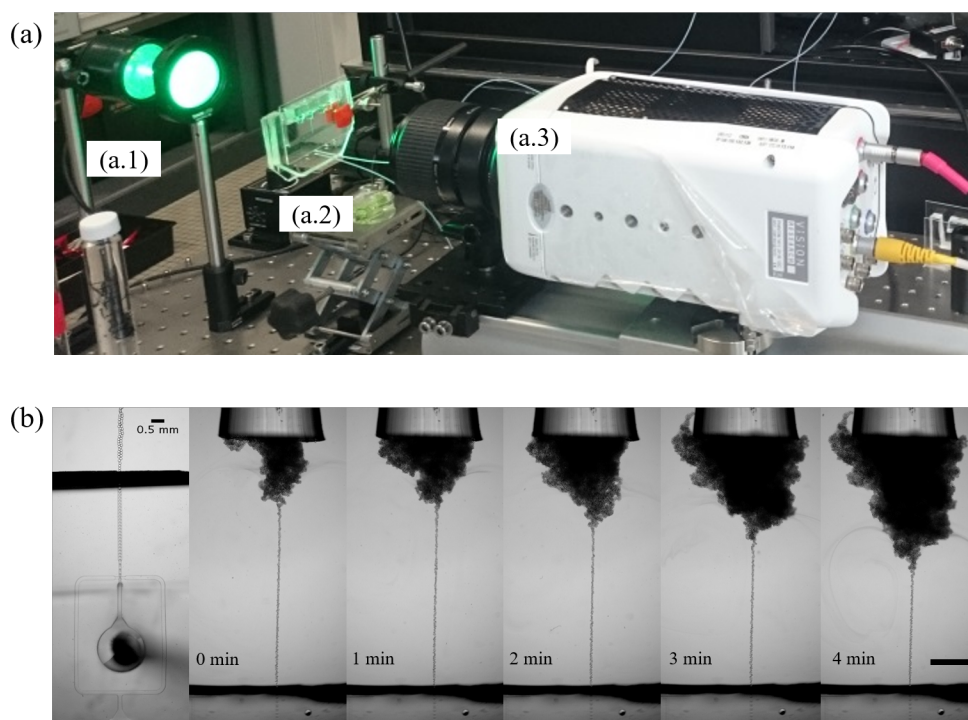


**Fig. 4.4** Microfluidic angle of repose measurement set-up: (a.1) back-light; (a.2) angle of repose microfluidic device held in place by a clamp on a support; (a.3) high speed camera with photo lens. (b) Pickering emulsion production and heap formation recorded at 24 fps

The angle of repose device was fixed on a support and filled with clean fluorinated solvent (Fig. 4.4(a.2)). Before each trial, the correct alignment of the device was verified using air bubbles injected from the microfluidic device. For illumination, a flash light and filter were placed behind the device as shown in Fig. 4.4(a.1).

The microfluidic inlets were connected to syringes through Peek tubing of 0.75 mm inner diameter and the fluids flow rates were controlled using syringe pumps (Nemesys, Cetoni). For all the trials, unless stated otherwise, the flow rates were fixed as  $10 \mu\text{L}/\text{min}$  for the fluorinated phase, and  $5 \mu\text{L}/\text{min}$  for the aqueous phase. Obtaining monodispersed droplets of  $\sim 80 \mu\text{m}$  diameter. Droplet production is shown in Fig. 4.4b as well as the particle-stabilized droplets deposition on the cylindrical base which was monitored and recorded at a frame rate of 24 images per second. Droplet size variations were not observed with the controlled

parameters studied (pH of aqueous phase and particle wettability).

### **Image processing and data analysis**

Image processing was performed with ImageJ software [114]. All the images were flipped 180° before processing. The contour of the pile formed on the PDMS base was extracted as coordinates (x-y) per each frame. This data was processed with a homemade script using Matlab, obtaining an angle of repose value as a function of deposition time.

Time zero was set as the moment the entire surface of the base was completely covered by droplets. The total monitored time was between 3 and 20 minutes, depending on the time required for the specific system to reach a steady state.

### **4.3.2 Angle of repose test versus microfluidic adaptation for complex fluids**

Our microfluidic adaptation of the angle of repose test brings along inherent differences with the method described by Lumay *et al* [112]. Rather than a fixed amount of material left on the support to reach a static equilibrium, in our system, the continuous deposition of droplets on the cylindrical support builds up a heap that eventually reaches a dynamic equilibrium, where the amount of droplets that falls off the base is equivalent to the amount that comes on it.

The droplets are regarded as individual grains –since their interface is stabilized against coalescence through the use of surfactants or NPs– and monodisperse droplets are obtained by keeping the same flow rate conditions in the droplet maker microfluidic device.

In figure 4.5, the evolution over time of the angle of repose is shown for droplets stabilized by a fluorinated surfactant (Fig. 4.5a) and droplets stabilized by fluorinated Si-NPs (Fig. 4.5b).

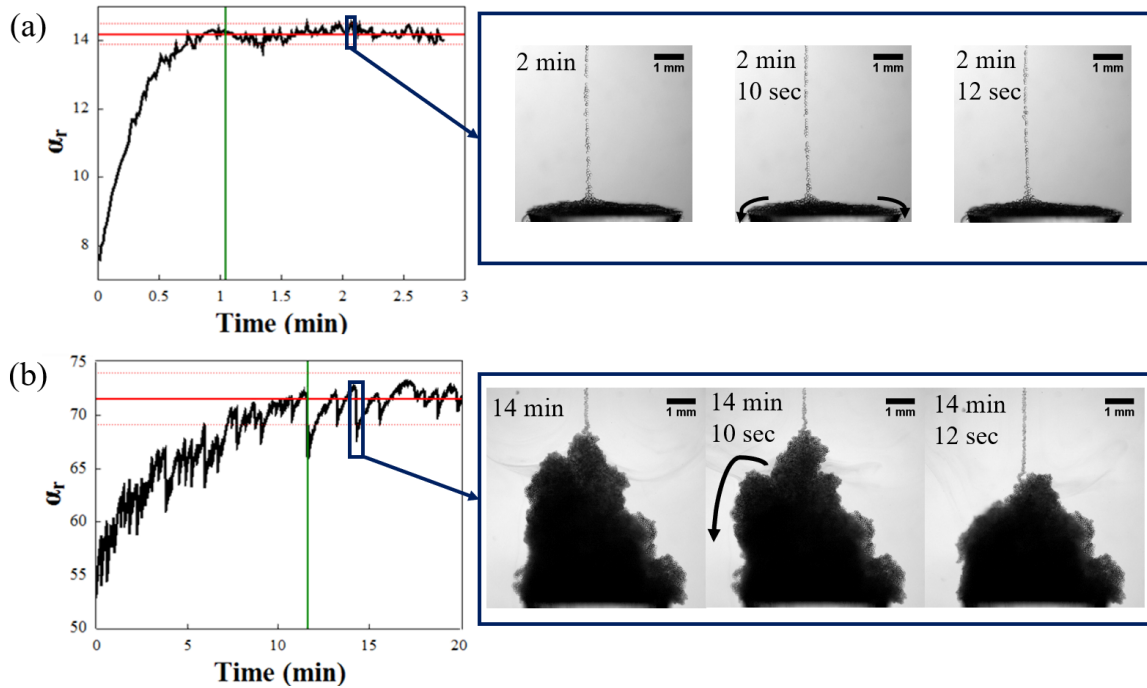


**Fig. 4.5** Angle of repose evolution over time, with indicated stabilization time  $t_{ss}$  ( $\mid$ ), steady state angle  $\alpha_{ss}$  ( $\text{---}$ ) and cohesiveness  $\sigma_{ss}$  ( $\cdots$ ). (a) Emulsion stabilized by Krytox (2% wt) where droplets slide off the edge of the support. (b) Fluorinated Pickering emulsion with consecutive avalanche events. (All pile images are tilted  $180^\circ$ )

There are clear differences between both systems: the stabilization time ( $t_{ss}$  green vertical line in Fig. 4.5) required to reach a steady state is ten times smaller for a flowable emulsion stabilized by surfactant, since the final steady state angle reached ( $\alpha_{ss}$  red horizontal line in Fig. 4.5) is significantly smaller. Additionally, instead of droplets sliding off the edge of the support with the continuous feeding stream in the middle, in the poorly flowable Pickering emulsion, droplets aggregate with each other until the weight difference is enough to promote an avalanche event, which consists of chunks of aggregated droplets falling from the top of the pile, as shown in figure 4.5b.

We consider the system reaches a steady state after the consecutive cycles of aggregating droplets, followed by an avalanche event has a mean angle variation smaller than 1% between cycles. Then, an additional parameter can be extracted by taking four times the standard deviation ( $\sigma_{ss}$  pointed red horizontal lines in Fig. 4.5) of the mean angle of repose after

reaching a steady state ( $\alpha_{ss}$ ).  $\sigma_{ss}$  will be directly related to the aggregation level of droplets, since the stronger the aggregation, the less disrupted the pile is by gravitational stress [105]. Consequently, the stronger the aggregation, the bigger the maximum angle reached before each fall and the bigger the aggregated chunks falling per cycle.

Lumay *et al* quantified a similar parameter by relating cohesiveness between grains –originated from interactions, such as liquid bridges, electric charges and van der Waals forces– with the deviation of the irregular contour of the pile in repose formed from the ideal isosceles triangle shape expected for non-cohesive materials [112].

### 4.3.3 Formulation parameters

The wettability of the particles is a key element in the formulation of Pickering emulsions, similar to how the hydrophilic-lipophilic balance (HLB) is for emulsions stabilized by surfactants. In both cases, these parameters directly influence the emulsion type and stability [97]. In our system, we monitor this variable by changing the Si-NPs surface coverage,  $\phi_{wt}$ , which is the weight ratio of PFOTES on the Si-NPs surface and the Si-NPs weight (equation 3.7). When we increase  $\phi_{wt}$ , the wettability of the particles for the continuous fluorinated phase increases.

In Fig. 4.6a, we show how by increasing  $\phi_{wt}$ , we can effectively improve the flowability of the Pickering emulsion obtained. In particular, going from  $\phi_{wt} = 7.3$  to  $\phi_{wt} = 8.0$  dramatically decreases  $\alpha_{ss}$  from  $70^\circ$  to  $30^\circ$ , going from an empirically very poor flow behaviour to a good one. This effect is also apparent in Fig. 4.6b, where the interface line of the collected Pickering emulsions with the organic phase becomes more irregular the smaller the  $\phi_{wt}$  value is.

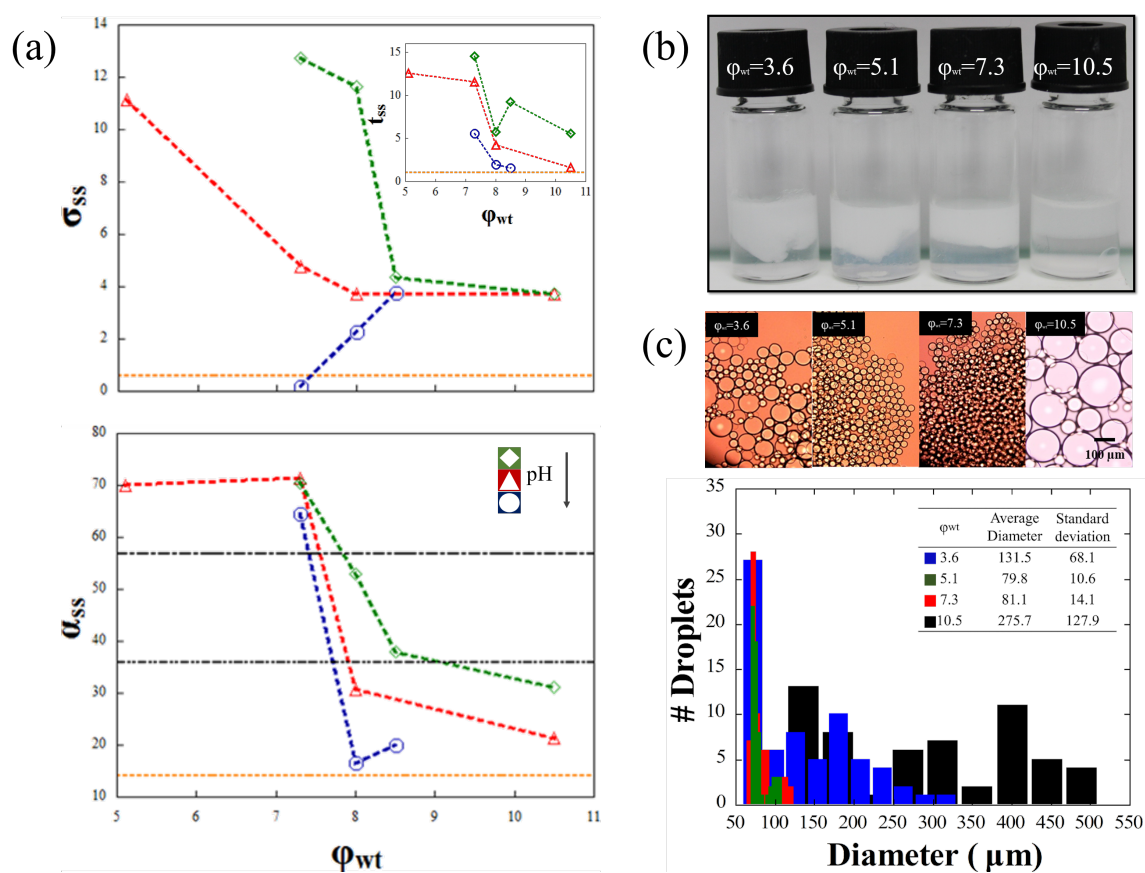


**Fig. 4.6** (a) Degree of surface functionalization  $\phi_{wt}$  effect on steady state angle ( $\alpha_{ss}$ , aggregation level ( $\sigma_{ss}$  and stabilization time ( $t_{ss}$ ): pH=3 ( $\dots \circ \dots$ ), pH=6.8 ( $\dots \triangle \dots$ ) and pH=9.5 ( $\dots \diamond \dots$ ). Emulsion stabilized by surfactant is also indicated ( $\dots$ ), as well as empirical upper  $\alpha_r$  limit for a good flowability ( $---$ ), and lower limit  $\alpha_r$  for very poor flow behaviour ( $---$ ). (b) Pickering emulsions collected in vials for different  $\phi_{wt}$ . (c) Droplet size distribution for collected Pickering emulsions after one week of production (original droplet size 80  $\mu\text{m}$ ). Images correspond to emulsions observed on a glass slide.

The ability to improve the flow behaviour by increasing the degree of Si-NPs coverage,  $\phi_{wt}$ , provides a very useful parameter to control when selecting the optimal formulation of Pickering emulsions for droplet-based microfluidics applications. However, increasing  $\phi_{wt}$  to extreme values, renders the particles too hydrophobic and limits their ability to stabilize collected emulsions, as shown in Fig. 4.6c, where microfluidic made emulsions with the same droplet size (80  $\mu\text{m}$  diameter) were observed after one week of collection, showing significant coalescence for small and high values of  $\phi_{wt}$ .

pH is another commonly studied variable affecting Pickering emulsions behaviour, par-

ticulary when the particles involved are pH responsive, meaning that its surface chemistry undergoes some type of modification in response to changes in proton concentration [115]. We used hydrochloric acid or sodium hydroxide to vary the pH of the aqueous phase. In Fig. 4.6a, we show how this parameter affects the flow behaviour of our system more significantly for intermediate values of  $\phi_{wt}$ . When  $\phi_{wt} = 8.0$ , we can effectively vary  $\alpha_{ss}$  to empirically flowable or non-flowable emulsions by decreasing or increasing the pH of the aqueous phase, respectively. For  $\phi_{wt} = 7.3$ ,  $\alpha_{ss}$  is not affected by the change of pH; however, a significant effect can be observed on the aggregation level of droplets reflected on the magnitude of the avalanche events ( $\sigma_{ss}$ ).

The aggregating nature of fluorinated Pickering emulsions –evidenced in the irregular interface line (4.6b) and the heap formation during the angle of repose test–suggest the presence of adhesive interactions between the droplets. These interactions, as shown previously by Arditty *et al*, dominate the bulk elasticity of these emulsions for droplet volume fractions below the random close packing and give remarkably high shear modulus for strongly flocculated emulsions [105].

Observing the droplets in our system (4.6c), we can discard the droplets-bridging effect as a possible origin of the adhesive interactions between droplets. As described by Lee *et al*, when droplet bridging is present, a deviation from the clear circular geometry of the droplets is observed [101].

A more likely origin of the observed droplet adhesion could be from the natural tendency of the more hydrophilic Si-NPs to aggregate. When dispersed in the fluorinated phase, this aggregation is not evident, probably because the density of particles is sufficiently low and because Brownian motions helps to prevent the Si-NPs from forming aggregates. The aggregation might, however, be favored at the interface through an increase of local density of the particles. When the Si-NPs hydrophobicity is raised by increasing  $\phi_{wt}$ , the aggregation should be decreased leading to a decrease in droplet adhesion. It is surprising nonetheless to

observe a dependence of the droplet adhesive properties on the pH of the dispersed aqueous phase.

When the pH is increased, the dissociation of silanol groups on the surface on to negatively charged silanolate ions renders the surface charge in contact with the aqueous phase more negative, resulting in more hydrophilic NPs and smaller contact angles. This effect is usually employed to destabilize the Pickering emulsion [115] and it has also been used to prevent droplet agglomeration in o/w emulsions [116]. However, it is not obvious why it would cause an effect on particle mediated interactions between droplets for w/o emulsions. One interpretation for such a pH dependence could originate from electrostatic interactions between particles at the oil-water interface [117].

Another effect of special significance above the random close packing volume fraction is droplet deformability. Arditty *et al* showed a solid-stabilized emulsion is dependent on the tension generated by 2D plasticity in the particle layer. They identified three different contributions to the lateral interparticle attractions: van der Waals forces, capillary forces and the attractive interactions arising from the interpenetration of the hydrophobic chains grafted on the solid particles [105].

In our case, we cannot provide a definitive answer to the origin of the modulation of the mechanical properties of the interface. However, the deformation of the interface involves the deformation of the capillary menisci between nanoparticles. The force required to deform these menisci is presumably a function of the particle wettability and considering the length scale of the menisci –typically the size of the particles– it seems reasonable to consider that the first-order effect in the modulation of the interfacial properties of the droplet comes from capillary effects.

### 4.3.4 Conclusion

In summary, our angle of repose microfluidic adaptation provides a quantitative reference on the flow behaviour of emulsions, combining the advantages that microfluidic rheometers have over macroscopic ones, such as low amounts of samples required (between 45 and 300  $\mu\text{L}$  of emulsion) and the visual monitoring of the fluid behaviour. Additionally, it is possible to study samples that present a very strong gel-like behaviour; a task that could be challenging for microfluidic rheometers previously proposed. With our method, we were able to determine the optimal formulation of fluorinated Pickering emulsions as a function of the degree of surface functionalization ( $\phi_{wt}$ ), as well as flow behaviour changes, due to pH variations in the aqueous phase. Further analysis will be of interest to determine a quantitative link between this method and classical rheological characterization parameters, as well as the effect of additional formulation variables, such as Si-NPs size, droplet size and salt content, to further improve fluorinated Pickering emulsions and implement them into the droplet-based microfluidics toolbox.

## 4.4 Appendix: Supplementary experiments

In this section we describe some short additional tests –not included in the publication– directly linked to the Si-NPs degree of fluorination and the angle of repose test.

### 4.4.1 Bio-compatibility: preliminary assay

As shown on Fig. 4.6c, one limitation at the moment of selecting a suitable Si-NP degree of surface fluorination ( $\phi_{wt}$ ) is related to the emulsion stability: Increasing  $\phi_{wt}$ , even though improves the flowability of the emulsion, also destabilizes it (for  $\phi_{wt}= 10.5$ ).

For several droplet-based microfluidic applications, the bio-compatibility of the droplet micro-environment is also of great concern, and it could become a limiting factor for the

selection of  $\phi_{wt}$ . Consequently, we design a simple experiment to verify the bio-compatibility of our system for different particle  $\phi_{wt}$  values (Fig. 4.7)<sup>3</sup>.

*Escherichia coli* Rosetta (transfected by pET15-EGFP plasmid, expressing GFP) was encapsulated in fluorinated Pickering droplets with a standard flow-focusing microfluidic device. The flow rates were fixed as 10  $\mu\text{L}/\text{min}$  (fluorinated particles in HFE-7500) for the oil phase and 5  $\mu\text{L}/\text{min}$  for aqueous phase (bacteria in Lysogeny broth medium).

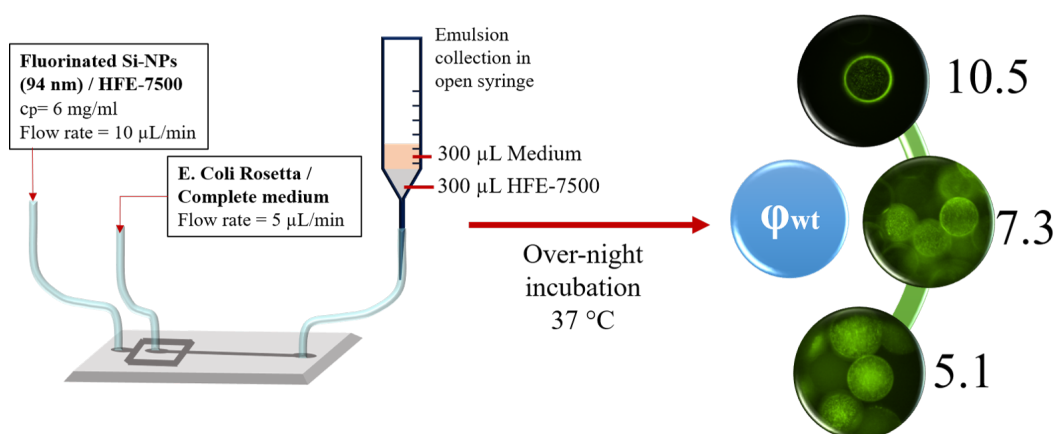


**Fig. 4.7** Schematic representation of bio-compatibility test with *E. coli* Rosetta. The system bio-compatibility is apparently independent on the Si-NP  $\phi_{wt}$  value.

The emulsion collection was done inside an open syringe. The syringe was connected to the outlet of the microfluidic device, fixed in a vertical position and pre-loaded with 300  $\mu\text{L}$  of HFE-7500 and 300  $\mu\text{L}$  of medium.

The encapsulation was done for three batches of particles (96 nm) with  $\phi_{wt} = 5.1$ , 7.3 and 10.5. After collection, the syringes were placed in an incubator at 37  $^{\circ}\text{C}$  and left over night. Finally, an aliquot of the emulsion was placed on a glass slide for observation in an epifluorescence microscope.

*E. coli* Rosetta proliferated over night for droplets stabilized with low ( $\phi_{wt}=5.1$ ) and intermediate ( $\phi_{wt}=7.3$ ) degrees of surface fluorination, showing an overall good bio-biocompatibility of the droplet microenvironment, apparently not affected by  $\phi_{wt}$ .

<sup>3</sup>Bacteria growth tests and pictures taken with Dr. Deniz Pekin

For high values of surface fluorination ( $\phi_{wt}=10.5$ ), most of the emulsion coalesced. We found some droplets preserving their original size and with clear living bacteria inside, this could be an indication of bio-compatibility even for high levels of particle fluorination. However, apparent lower proliferation (when comparing with  $\phi_{wt}=5.1$  and 7.3) and what it seems like adsorption of part of the bacteria to the droplet interface; indicates that for high values of  $\phi_{wt}$  the system might lose some bio-compatibility.

#### 4.4.2 Specific surface area and particle tunability

All the flowability tests presented so far were performed with the same type of pristine Si-NPs. They were synthesized by (MaFIC, CRPP) the two step protocol described on section 3.1 [88].

On section 3.2 we calculated the specific surface ( $S_c$ ) of these Si-NPs and compared them with commercial Si-NPs Aerosil OX-50. We found that the in-house synthesized particles had  $S_c$  larger than Aerosil OX-50 for more than an order of magnitude. We wondered if fluorinated Pickering emulsions stabilized with Aerosil OX-50 would differ on its flow behavior as well.

With this aim, we functionalized Aerosil OX-50 particles with PFOTES, following the same protocol as the one described for in-house synthesized particles (section 3.4). We also determined the concentration required to stabilize droplets for the same production conditions (section 3.5).

We observed that the concentration of PFOTES required to stabilize droplets with fluorinated OX-50 particles was notably less than the required for in-house synthesized ones. While we were able to stabilize droplets for  $\phi_{wt}$  values between 5 and 10 with 94 nm in-house synthesized particles, with Aerosil OX-50 seemingly stable emulsions were only possible for values between 1.6 and 1.8 (Table 4.1).

This difference is not surprising: smaller  $S_c$  for OX-50 particles implies, less amount

**Table 4.1** Concentration ( $c_p$ ) and degree of surface fluorination ( $\phi_{wt}$ ) needed to stabilize Aerosil® OX-50 and In-house-synthesized 94 nm particles.

	<b>Aerosil® OX-50</b>	<b>Syn(94nm)</b>
$c_p$ (mg/ml)	25	6
$\phi_{wt}$	1.6-1.8	5-10

of functional silanol groups at the particles surface, and hence, less quantity of PFOTES is needed to reach a suitable partial wettability of the particles and consequent favorable adsorption to the interface.

Additionally, we observed that the concentration of particles ( $c_p$ ) needed to stabilize the emulsion under the same production conditions was also larger for the OX-50 particles (25 mg/ml in contrast to 5 mg/ml). This is a direct consequence of the particle density ( $\rho$ ), which is also larger for the case of Aerosil OX-50 particles.

Finally, we measured the angle of repose for emulsions stabilized with fluorinated OX-50 particles and we observed a similar behavior as that obtained for the in-house synthesized ones: The emulsion flowability increases with particle hydrophobicity, and this is evidenced by the effect of the pH of the aqueous phase and  $\phi_{wt}$ .

It is worth noting that due to the intrinsic characteristics of the OX-50 particles, the ability to finetune the system formulation is limited in comparison to the less dense and more porous in-house synthesized ones. For this reason, we did not considered these particles for the subsequent experiments presented in this work.

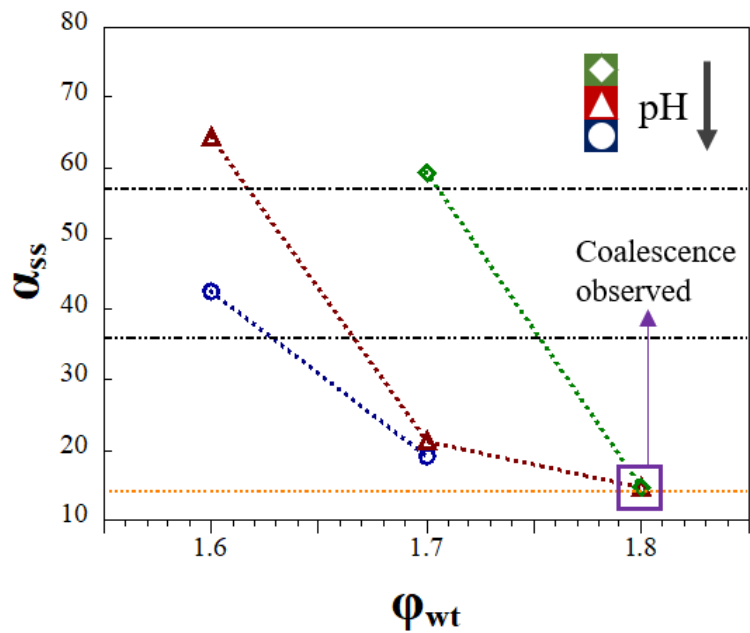


**Fig. 4.8** Degree of surface functionalization  $\phi_{wt}$  effect on steady state angle ( $\alpha_{ss}$ ) for fluorinated OX-50 particles: pH=3 ( $\cdots\circ\cdots$ ), pH=6.8 ( $\cdots\triangle\cdots$ ) and pH=9.5 ( $\cdots\diamond\cdots$ ). Emulsion stabilized by surfactant is also indicated ( $\cdots$ ), as well as empirical upper  $\alpha_r$  limit for a good flowability ( $-\cdots-$ ), and lower limit  $\alpha_r$  for very poor flow behaviour ( $---$ ).

## CHAPTER 4

**Summary**

- We developed a microfluidic version of the angle of repose test –commonly used for granular materials– for the comparative study of flowability properties of fluorinated Pickering emulsions.
  - The angle of repose test serves as a quantitative reference to scan the effect of formulation conditions on emulsion flow properties while requiring small sample volumes (between 45 and 300  $\mu\text{L}$ ).
  - The flowability of fluorinated (w/o) Pickering emulsions is directly related to the Si-NPs surface coverage by PFOTES, as well as the pH of the aqueous phase. Strongly suggesting a link between the Si-NPs partial wettability for both phases and the Pickering emulsion flow behavior (flow behavior would improve the more hydrophobic the Si-NPs surface is).
  - A practical consequence of our results is the ability to qualitatively assess the difference in flowability between two –substantially different– samples by the simple observation of the irregularities of the emulsion-oil interface.
- Increasing  $\phi_{wt}$  in order to improve fluorinated Pickering emulsions flowability should be done with caution: high levels of fluorination produce less stable emulsions and it potentially has a negative effect on bio-compatibility.
- Si-NPs with high surface area give a better flexibility and control of the system formulation.



# Chapter 5

## Pickering emulsions stabilization in microfluidics

In this chapter we will explore the different variables involved on the stabilization of droplets by nanoparticles in a microfluidic device. Our aim is to gain a better understanding of droplet stabilization by solid particles, with the objective of reducing the particle waste while increasing the production yield.

### 5.1 Current conditions

On section 3.5 we determined minimal conditions for the stabilization of droplets with nanoparticles in microfluidics. We used a standard flow-focusing production device with both phases meeting orthogonally at the droplet production junction and fixed flowrates for both: dispersed ( $Q_w$ ) and continuous phase ( $Q_p$ ). Under these specific conditions we determined a suitable Si-NPs concentration ( $c_p$ ) and incubation length ( $L$ ) to produce stable emulsions ( $\sim 80 \mu\text{m}$  size droplets).

We applied these conditions for the microfluidic angle of repose study presented on chapter 3. However, a better understanding of the variables involved on Pickering droplets

stabilization in microchannels would be of great benefit to gain control and flexibility over droplet production conditions such as: droplet volume ( $V$ ),  $c_p$  needed and production throughput.

From an engineering perspective, Pickering emulsions have a limited throughput of production: the typical timescale required to stabilize them ( $\sim 600$  ms) [118] is significantly higher than the needed for surfactant stabilized emulsions ( $\sim 35$  ms or less) [98]. The low throughput of production is a fundamental flaw for large-scale material production and the overall production yield of colloidal capsules through droplet-based microfluidics is significantly smaller than that obtained with other emulsification methods [119].

The bottleneck in the throughput lies in the stabilization time of the emulsion, which relates to the inability of the nanoparticles to quickly and efficiently reach the interface. A method typically used to reduce the droplet stabilization time scale consists in increasing the concentration of particles in the continuous phase to a large excess. With this method, the production of colloidal shells at a rate of 10 droplets per second was demonstrated [120]. However, the excess of particles leads to their undesired loss, and it also affects the flow properties of the Pickering emulsion and of the material derived from it [121].

An alternative is to introduce the particles in the droplets phase to minimize their waste [121]. However, such an “Inside-Out” approach for the fabrication of Pickering emulsions is not suitable for most of “lab-on-chip” applications where the biochemical material inside droplets needs to be similar to the one use in bulk experiments. Furthermore, when particles can not be effectively dispersed in the inner phase (as it is the case for fluorinated particles in the aqueous phase) the usability of this method is limited.

Consequently, current methods for fluorinated Pickering droplets stabilization in microfluidic devices involve a trade-off between low droplet production throughput and waste of large amount of nanoparticles.

### 5.1.1 Droplet incubation time

Until now we had controlled the droplet incubation time ( $\tau$ ) by varying  $L$ :  $\tau$  is the time a droplet spends in a microchannel before it is exposed to collisions with other droplets either by a channel expansion (coalescence chamber) or collection of the emulsion at the device outlet.

We define  $\tau$  as

$$\tau = \frac{Lh\omega_o}{Q_t} \quad (5.1)$$

here  $h$  and  $\omega_o$  are the channel depth and width respectively (as shown on Fig. 5.1) and  $Q_t$  is the total flow rate ( $Q_t = Q_p + Q_w$ ).

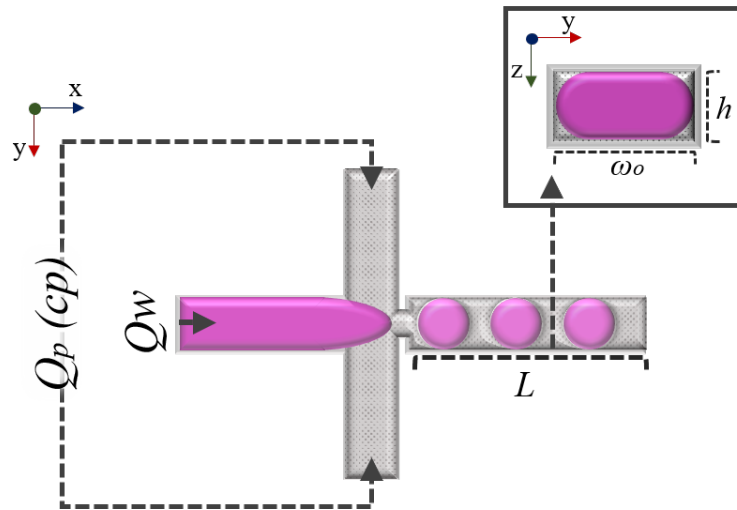


**Fig. 5.1** Schematic representation of simple droplet production with indicated channel dimensions ( $L$ ,  $\omega_o$  and  $h$ ) and flow rates ( $Q_p$  and  $Q_w$ ).

When we use Eq. 5.1 to calculate  $\tau$  with the conditions we fixed for our previous experiments, we obtain  $\tau = 160$  ms. This result is almost four times faster than the typical timescale used for the stabilization of Pickering emulsions in microchannels [118]. However, we are most likely using a large amount of particles –from which great part remain in the continuous phase and do not absorb to the droplet interface– than the one required to fully cover the droplet interface.

### 5.1.2 Particles in excess

In order to estimate how many particles in excess ( $\varepsilon$ ) we are using with respect to the particles needed to cover the droplet interface we define

$$\varepsilon = \frac{c_p}{c_{cp}} \quad (5.2)$$

here  $c_{cp}$  is the amount of particles needed to hexagonally close-pack a monolayer of particles at the droplet interface.

To estimate  $c_{cp}$ , we calculate first the number of particles ( $n_{cp}$ ) at the droplet interface assuming a  $90^\circ$  particle contact angle at the aqueous-oil interface and an hexagonal packing density of 0.9069. Hence,  $n_{cp}$  is the covered droplet surface ( $S$ ) divided by the area covered by one particle

$$n_{cp} = \frac{0.9069 S}{\pi(\delta/2)^2} \quad (5.3)$$

then,  $c_{cp}$  is calculated as,

$$c_{cp} = \frac{\pi \delta^3 \rho_p n_{cp}}{3 \cdot 2 \lambda V} \quad (5.4)$$

where  $\delta$  and  $\rho_p$  are the nanoparticle diameter and density respectively,  $V$  is the droplet volume and  $\lambda$  corresponds to

$$\lambda = Q_p/Q_w \quad (5.5)$$

the ratio between the oil and the aqueous phase.

When we use Eq. 5.3 and 5.4 to estimate  $c_{cp}$  with the conditions fixed for the previous experiments. We obtain  $c_{cp} = 0.24$  mg/ml, this means that we have been stabilizing emulsions with an amount of particles in the continuous phase equivalent to around 25 times the required to cover the droplet interface (Eq. 5.2).

Self-evidently this amount of particles implies a considerable waste of material, and it would be of great benefit to come up with a different approach –for Pickering droplets stabilization in microchannels– that could potentially reduce the amount of particles wasted without the need to trade-off with longer stabilization times.

## 5.2 New droplet production design

The adsorption dynamics of particles to the oil-water interface is broadly controlled by two distinct processes: diffusion controlled transport to a thin sublayer, and the adsorption from the sublayer to the interface [122].

In a microfluidic device, mixing is dominated by molecular diffusion, due to the laminar flow conditions imposed by the small dimensions of the system [123]. Hence, the adsorption dynamics of particles in a microfluidic device is most likely limited by diffusion controlled transport, which leads to long stabilization times to stabilize droplets.

In light of this, we propose a new design for droplet production, where we aim to promote the adsorption of particles to the oil-water interface by increasing the confinement of particles near it (Fig. 5.2).

This design consist on separating the continuous phase –by function– in two streams: one stream will be solely dedicated to the delivery of particles ( $Q_p^*$ ) to the interface, and it will co-flow with the aqueous phase right before droplet formation; the second stream will contain no particles and will be mainly used for the production of droplets ( $Q_o$ ) while also helping to promote particle confinement near the interface.

In the following sections of this chapter, we evaluate this new design –which we name MII– by comparing it systematically with a standard droplet production method –which we name MI– (Fig. 5.1). We divide MII in two cases according to the type of oil used for  $Q_o$ : MII $_{\eta\downarrow}$  for HFE-7500 (viscosity  $\eta= 0.77$  cSt) and MII $_{\eta\uparrow}$  for FC-40 (viscosity  $\eta= 2.2$  cSt).

For all the comparison experiments between MI and MII the relations:

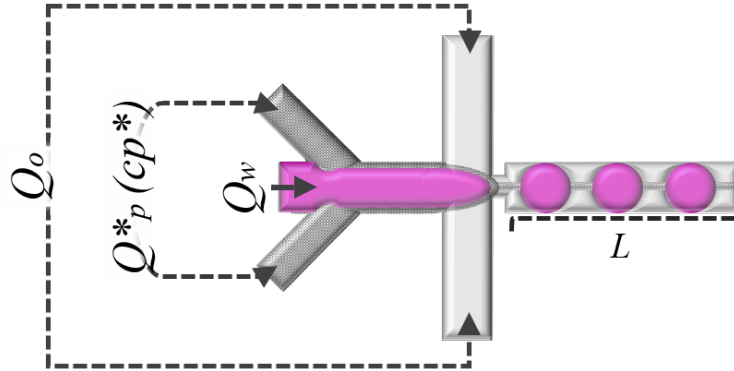


**Fig. 5.2** Schematic representation of new droplet production design with indicated flow rates: aqueous phase flow rate ( $Q_w$ ) and continuous phase flow rate ( $Q_o + Q_p^*$ ).

$$Q_p = Q_o + Q_p^* \quad (5.6)$$

and

$$c_p = \frac{c_p^* Q_p^*}{Q_p} \quad (5.7)$$

are always fixed. Here,  $c_p^*$  is the particle concentration of the oil stream  $Q_p^*$ , and it reaches a concentration equal to  $c_p$  after dilution with  $Q_o$ .

### 5.3 Dynamics of Pickering droplets stabilization in microfluidics

In this section we present the results obtained when comparing droplet stability against coalescence for two droplet production methods: a standard flow-focusing production (MI, Fig. 5.1) and a new design (MII, Fig. 5.2).

### 5.3.1 Effect of $\tau$ on droplet stability

We investigate the effect of  $\tau$  on droplet stability against coalescence. For this, we use a similar platform as the one presented in section 3.5, then droplet stability against coalescence is in the form of  $p(1)$  (Eq. 3.8). Similarly to section 3.5, we consider an emulsion stable when  $p(1) \geq 0.999$ : It corresponds to less than one coalescence event for one thousand droplets. As shown on 3.5, the behavior of  $p(1)$  depends on the amount of particles available in the continuous phase and on the time  $\tau$  (varied by  $L$  on section 3.5) these particles have to adsorb to the interface of the droplets before exposure to collisions. This would also be the expected behavior by analogy with the surfactant stabilization case [98].

First, we fix some parameters:  $\lambda$  (Eq. 5.5) to a value of 2.5;  $c_p$  and  $c_p^*$  to a value of 2 mg/ml and 12 mg/ml respectively; and the incubation length ( $L = 2$  mm). By keeping  $L$  fixed, we vary  $\tau$  (Eq. 5.1) through the total flow rate ( $Q_t$ ):  $Q_t$  is varied from 70  $\mu\text{L}/\text{min}$  ( $\tau = 8.6$  ms) to 20  $\mu\text{L}/\text{min}$  ( $\tau = 30$  ms).

We observe an increase of  $V$  and  $\varepsilon$  with increasing  $\tau$  for both MI and MII methods (Fig. 5.3 left panel). The droplet size is a function of the capillary number  $Ca$  (Eq. 2.3) which is independent of  $c_p$  [19], and since the viscosity ( $\eta$ ), surface tension ( $\gamma$ ) and channel cross-section ( $\omega_o \cdot h$ ) are constant:  $Ca$  depends on  $Q_t$ . As a consequence,  $V$  decreases for larger  $Q_t$ . On the other hand,  $\varepsilon$  increases as a consequence of increasing  $V$ : when  $V$  increases at fixed  $\lambda$ , the surface per unit volume of the droplets decreases; then for fixed  $c_p$ ,  $\varepsilon$  increases (Eq. 5.2 to Eq. 5.4).

Our measurements show an interesting behavior of  $p(1)$  with respect to  $\tau$  (Fig. 5.3 left panel): for MI,  $p(1)$  progressively decreases with increasing  $\tau$ , for MII  $p(1)$  remains stable with increasing  $\tau$  but it reaches an unstable region for  $\tau > 30$  ms. This result is surprising –since we would expect that longer incubation times in addition to more particles in excess would yield more stable emulsions– and indicates that additional processes are dominating the dynamic stabilization of the Pickering emulsions against coalescence.

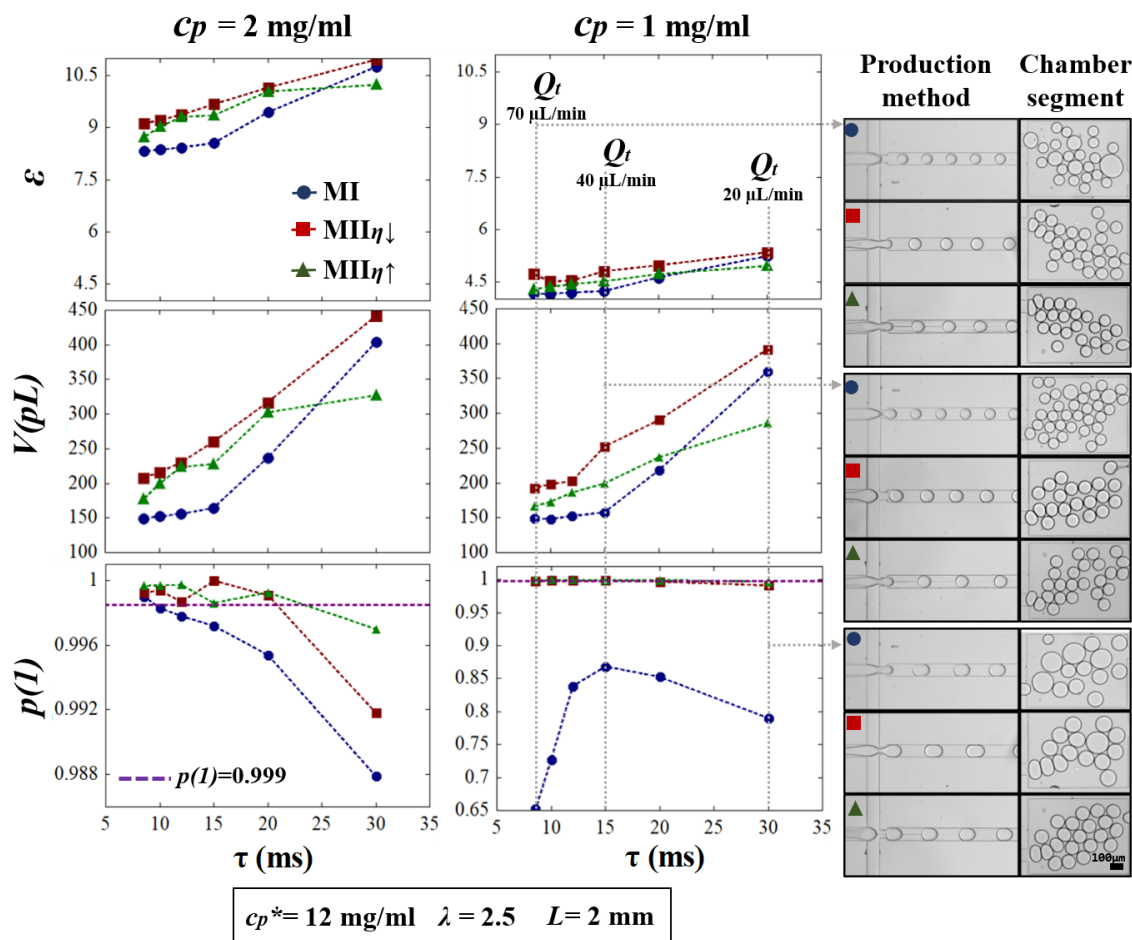


**Fig. 5.3** Comparison of methods MI and MII ( $Q_o$  being ( $\eta^\downarrow$ ) HFE7500 and ( $\eta^\uparrow$ ) FC40) on the effect of  $\tau$  (Eq. 5.1 by varying  $Q_t$ ) on  $p(1)$  (Eq. 3.8),  $V$  (droplet volume) and  $\varepsilon$  (Eq. 5.2).  $\lambda$  (Eq. 5.5),  $L$  and  $c_p^*$  are kept constant,  $c_p$  is also kept constant at: 2 mg/ml (left panel) and 1 mg/ml (central panel), where we show snapshots of droplet production and the last segment of coalescence chambers for three data points ( $Q_t = 70, 40$  and  $20 \mu\text{L}/\text{min}$ )

However, under these conditions  $p(1)$  is always larger than 0.98, which corresponds to an emulsion with less than 2% of coalescence events. An excess of particles between 8 to 11 times the needed to cover the droplet interface prevents coalescence even for short incubation times (between 8 to 30 ms).

Next we tested the system under more stringent conditions by measuring the stability for lower particles concentration. We reduce  $c_p$  to 1 mg/ml and measure  $p(1)$  as a function of  $\tau$  while monitoring  $V$  and  $\varepsilon$  as previously.

The general trends are similar to the high particle concentration case: for both MI and MII,  $V$  and  $\varepsilon$  increase with increasing  $\tau$  (Fig. 5.3 central panel), as a result of the droplet size control by the flow conditions. It is worth noting the differences –on droplet size– between the two droplet production methods. MI produce consistently smaller droplets than MII, this is a direct consequence of the working principle of MII: contrary to MI, in MII the continuous phase stream ( $Q_p$ ) is divided between  $Q_p^*$  and  $Q_o$ , from which only  $Q_o$  is providing shear-stress at the cross-flow junction for droplet formation. Furthermore, this shear stress would be larger for a larger oil viscosity; hence, the consistently smaller  $V$  observed for case MII $_{\eta\uparrow}$  with respect of MII $_{\eta\downarrow}$ .

The emulsion stability in MI for  $c_p = 1$  mg/ml presents a significantly lower value than the one found for  $c_p = 2$  mg/ml case, as well as different behavior with respect to  $\tau$ : for low  $\tau$  values,  $p(1)$  increases with increasing  $\tau$ , it reaches a maximum at 15 ms ( $Q_t = 40$   $\mu\text{L}/\text{min}$ ) and then it decreases with higher  $\tau$  values. This behavior coincides with a notable change in  $V$ : before  $p(1)$  reaches its maximum at  $\tau = 15$  ms,  $V$  remains approximately constant at 150 pL then it increases abruptly up to 350 pL for higher values of  $\tau$ .

This abrupt increase of  $V$  happens for both methods, MI and MII, and it seems to be related to a transformation of the droplet production mode from dripping to squeezing when  $Q_t < 40$   $\mu\text{L}/\text{min}$ . This is observable on the production snapshots shown on Fig. 5.3 (right panel), where the droplets produced transition from circular shape ( $Q_t > 40$   $\mu\text{L}/\text{min}$ ) to plug-like shape ( $Q_t < 40$   $\mu\text{L}/\text{min}$ ) inside the incubation channel [30].

Nevertheless, the behavior of  $p(1)$  in MI suggests the competition between two processes affecting droplet coalescence: for low  $c_p$  and constant  $V$ , longer  $\tau$  yield more stable Pickering emulsions; while for higher  $V$  values, an additional process dominates droplet coalescence.

The stability of Pickering emulsions against coalescence relies on the adsorbed particles at the interface preventing the dispersed fluids from contacting each other [124]. When the droplet surface is not fully covered by absorbed particles, the drainage of the liquid films of

the continuous phase between two approaching droplets becomes the rate-determining step for droplet contact and fusion [125].

An increase in droplet size increases the level of droplet confinement in the microfluidic device (constant channel depth  $h = 50 \mu\text{m}$ ). Previous studies have found that geometrical droplet confinement results in additional hydrodynamic wall forces, which promotes coalescence due to an increased rate of film drainage between approaching droplets [126, 127]. Additionally, smaller  $Q_t$  increases the residence time of droplets in the coalescence chambers, giving more time for film drainage to occur [128].

On the other hand,  $p(1)$  in MII presents the same behavior observed for the higher particle concentration case: the emulsion remains stable with increasing  $\tau$  ( $p(1) \geq 0.999$ ), with a slight decrease of  $p(1)$  down to 0.99 at  $\tau = 30$  ms. However, it is unclear if this small loss of stability is a consequence of a confinement effect of larger droplets.

Overall we deduced: for a fixed particle concentration, Pickering emulsions stability against coalescence in a microfluidic device is not necessarily improved by increasing the droplet incubation time; additional processes –apparently related to droplet volume– are able to dominate the dynamic stabilization of Pickering droplets.

Additionally, the droplet production design MII bears a clear advantage for Pickering stabilization over the standard method of production MI: for a concentration of particles in the continuous phase of around five times the needed to cover the droplet surface, the stability criteria cannot be reached by MI (maximum  $p(1)$  value below 0.9); for the same  $\varepsilon$  value, droplets produced by method MII remain stable even for  $\tau$  as low as 8 ms.

### 5.3.2 Droplet stability independent of $\tau$

To further study the differences between MI and MII independently of  $\tau$ , we examined the data point where MI experiences maximum stability:  $\tau$  is 15 ms ( $L = 2$  mm,  $Q_t = 40 \mu\text{L}/\text{min}$ ), and  $c_p$  is 1 mg/ml (Fig. 5.4 left panel) or 2 mg/ml (Fig. 5.4 right panel);  $\lambda$  is increased

from 0.8 to 3. Since  $Q_t$  is constant, an increase of  $\lambda$  implies a decrease of the aqueous flow ( $Q_w$ ) with respect to the particle dispersion flow ( $Q_p$ ), which favors an increase of  $\varepsilon$  (more particles available per volume of water). We then monitor  $p(1)$  and  $V$  as a function of  $\varepsilon$ .

For both  $c_p$  values and methods,  $V$  decreases and  $p(1)$  increases with increasing  $\varepsilon$  (Fig. 5.4). The production of smaller droplets is a direct result of the decrease of  $Q_w$ . Additionally,  $V(MII_{\eta\downarrow}) > V(MII_{\eta\uparrow}) > V(MI)$  remains as a result of the inherent differences between the droplet production conditions highlighted in the previous section. The increase of  $p(1)$  is consistent with an increase of particles in excess, as well as a decrease of the droplet volume (less confined droplets).

Interestingly, for  $\varepsilon$  values between 4 and 5, we obtain a range for which the two  $c_p$  cases overlap presenting significantly different droplet size: for  $c_p = 1$  mg/ml (Fig. 5.4 left panel),  $V$  varies between 150 and 280 pL; for  $c_p = 2$  mg/ml (Fig. 5.4 right panel),  $V$  varies between 330 and 400 pL. We then compare the effect of droplet confinement on  $p(1)$  for the same amount of particles in excess.

For all cases, we obtained  $V$  and  $p(1)$  for  $\varepsilon = 4$  by interpolating our data points using an exponential fit: for MI, the emulsion does not reach stability for the two droplet sizes compared, the smaller droplet (167 pL) presents a smaller  $p(1)$  value (0.899) in comparison to the significantly more confined case ( $V = 332$  pL,  $p(1) = 0.982$ ); for MII, in all cases the emulsion presents a value of  $p(1)$  above 0.99, and we observe a minor decrease on stability when the droplet size increases. Because these two observations are at odds, we can not explain them from the same physical origin, e.g. the effect of confinement: additional effects control the stabilization of the system.

The higher stability for larger droplets could be a result of the initial emulsification step: the dilution of particles in MI from  $c_p^*$  to  $c_p$  occurs off-chip. For  $\lambda_1 = 2.5$  and  $c_{p1} = 1$  mg/ml (Fig. 5.4 central panel), the oil stream ( $Q_{p1} = 28.6$   $\mu$ L/min) has a smaller local concentration of particles, than the similar data point at  $\lambda_2 = 1$  and  $c_{p2} = 2$  mg/ml ( $Q_{p2} = 20$   $\mu$ L/min). We

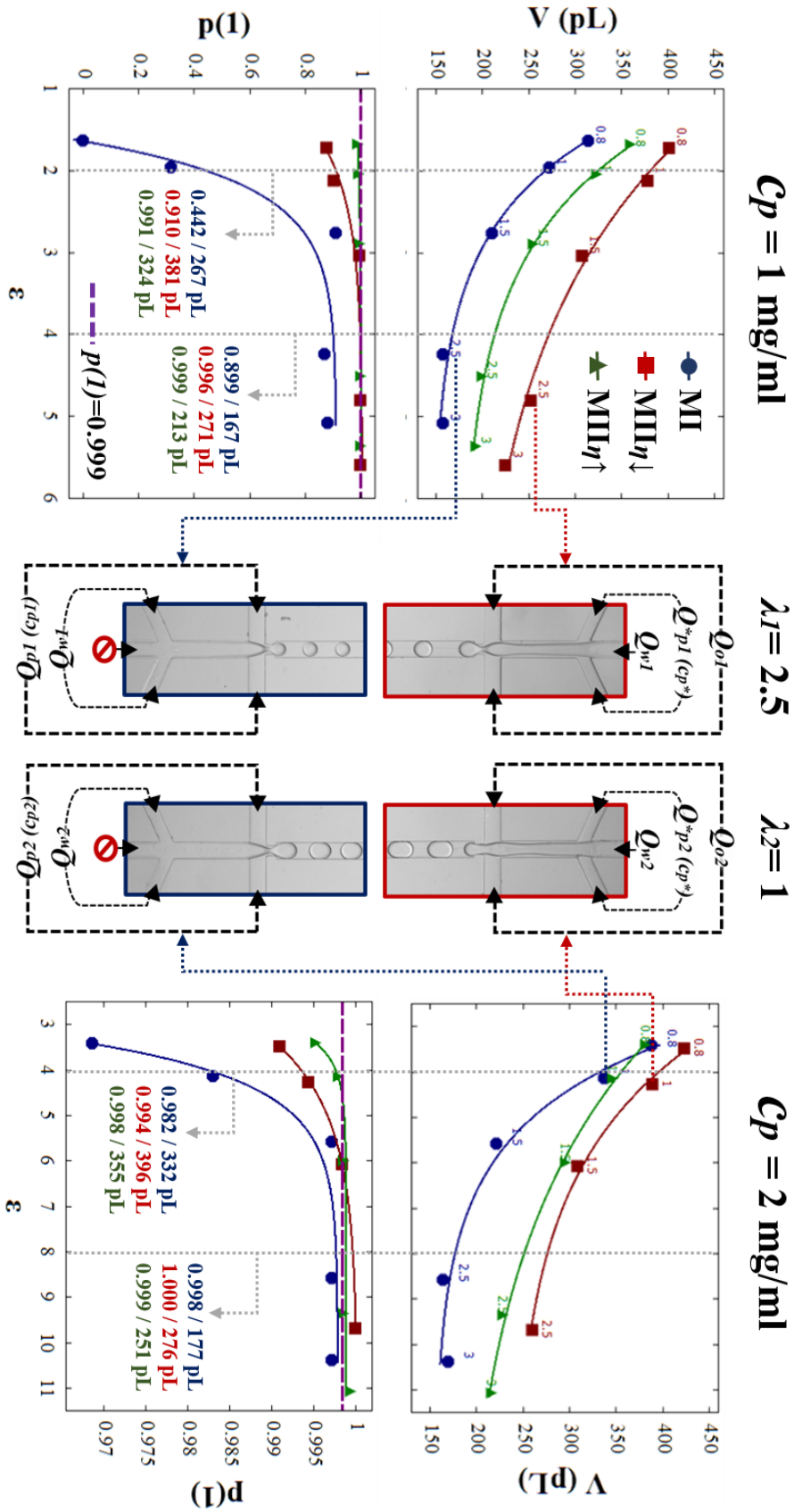


**Fig. 5.4** Comparison of methods MI and MII ( $Q_o$  being ( $\eta^+$ )HFE7500 and ( $\eta^-$ )FC40), for a fixed incubation time ( $\tau = 15 \text{ ms}$ ). Stability ( $p(1)$ ) is monitored as a function of  $\epsilon$ , which is varied along with  $V$  by increasing  $\lambda$  from 0.8 to 3.  $p(1) / V(\text{pL})$  values are calculated for  $\epsilon = 2, 4$  and 8 (an exponential decay fit is used to interpolate the data).  $c_p$  is kept constant at: 1 mg/ml (left, production snapshot for MI and MII  $\eta^-$  at  $\lambda = 2.5$ ) and 2 mg/ml (right, production snapshot for MI and MII  $\eta^-$  at  $\lambda = 1$ ).

hypothesize that a higher local concentration of particles at the droplet formation junction is favoring particle adsorption, and consequently improving the emulsion stability.

This hypothesis is consistent with our data. Indeed, the higher local concentration of particles at the production explains the difference found so far between our new method MII and the standard method MI. For MII, the dilution from  $c_p^* = 12$  mg/ml to  $c_{p1} = 1$  mg/ml (or  $c_{p2} = 2$  mg/ml) occurs inside the chip at the flow-focusing point.  $Q_{p1}^*$  (or  $Q_{p2}^*$ ) co-flows with the aqueous phase when it reaches the flow-focusing point, where the stream of particle-free oil  $Q_{o1} = 26.2$   $\mu$ L/min (or  $Q_{o2} = 16$   $\mu$ L/min) generates sufficient stress to break the aqueous stream into droplets. The local particle concentration during droplet formation is 12 mg/ml (significantly more than method MI), increasing the adsorption of particles to water-oil interface. Furthermore, particle adsorption at the droplet-formation step would be aided by the shear-stress provided by the cross-flow –which also controls the droplet size– hinting at this effect –rather than droplet confinement– as the one dominating the dynamic stabilization of Pickering droplets when the local particle concentration is constant.

Overall we deduce that droplet formation is a critical step on Pickering emulsion stabilization (in a microfluidic chip): the adsorption of particles to the interface –aided by high local particle concentration and shear stress provided by the cross-flow– during droplet formation have a greater impact on stability than the bulk particle concentration and incubation time given to droplets downstream the microchannel.

### 5.3.3 Local particle concentration effect on droplet stability

We further test the influence of the local particle concentration and of the two production methods by designing a new set of experimental conditions: Here we aim to reduce the droplet size variations between production methods while keeping a substantial difference of the local particle concentration at the moment of droplet formation.

We use the co-flow/flow-focusing combination for method MI (fig. 5.5a), with  $c_p$  in both

oil streams:  $Q_p^*$  (co-flow) and  $Q_p$  (cross-flow). We fix the oil-aqueous ratio ( $\lambda = 2.7$ ) as well as  $Q_w/Q_p^*$  (4.28).

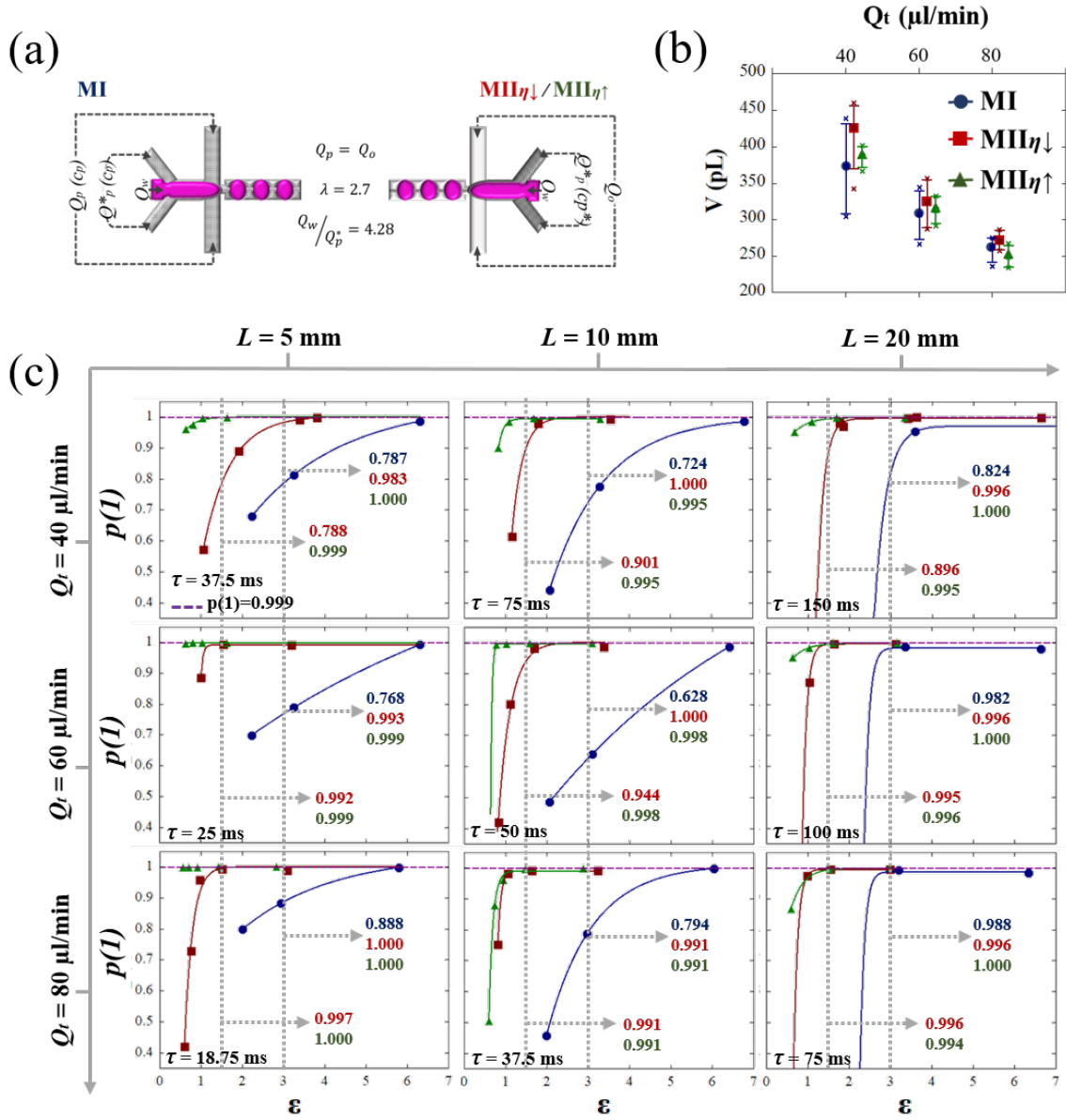


**Fig. 5.5** (a) Schematic representation of experimental conditions for method MI and MII ( $Q_o$  is ( $\eta^\downarrow$ ) HFE7500, ( $\eta^\uparrow$ ) FC40). (b)  $V$  variation as a function of  $Q_t$  for MI and MII, the error bars represent the standard deviation and the crosses the maximum and minimum values. (c)  $p(1)$  variation as a function of  $\varepsilon$  for  $L$  between 5 and 20 mm and  $Q_t$  between 40 and 80  $\mu\text{L}/\text{min}$ .

We vary  $c_p^*$  (off-chip) between 1.3 and 6.5 mg/ml, obtaining  $c_p$  values between 0.11 and 0.55 mg/ml. We monitor  $p(1)$  as a function of  $\varepsilon$  for different incubation times ( $\tau$ ) by

changing both  $L$  (from 5 to 20 mm) and  $Q_t$  (from 40 to 80  $\mu\text{l}/\text{min}$ ).

The droplet volume (fig. 5.5b) remains similar for both methods (MI and MII) and decreases with increasing  $Q_t$ , likewise our previous observations.

For all cases,  $p(1)$  increases with increasing  $\varepsilon$  (fig. 5.5c). The increase of incubation length ( $L$ ) does not affect the stability of the systems significantly. Only a minor increase on the stability is observed for the standard production method (MI) when  $L$  reaches 20 mm.

When the total flow rate ( $Q_t$ ) increases, an increase of  $p(1)$  is observed for MI and MII $_{\eta\downarrow}$ , when  $L = 5$  mm.

For the studied range of  $\varepsilon$  (from 1 to 6), MI could not reach the stability criteria ( $p(1) > 0.999$ ) with incubation times as large as 150 ms; while MII reached it even for  $\tau$  values as small as 1.5 and 18.75 ms.

These results confirm the importance of the droplet formation step over final droplet stability. During this step most of the particles adsorb to the water-oil interface. This adsorption strongly depends on the local concentration of particles, as well as the viscous stress provided by the oil stream at the flow-focusing point (which would be stronger for the more viscous oil (FC40) used in MII $_{\eta\uparrow}$ ).

When insufficient amount of particles are adsorbed during the formation step, very large incubation times are needed to obtain a stable system. In practice, our results bring a new design rule for droplet production in the presence of particles: maximizing the local particle concentration at the moment of droplet production, in addition to the viscous stress provided by the cross-flowed oil, is the most efficient mean to stabilize a Pickering emulsion in microfluidics.

## 5.4 Conclusion

In summary, we analyzed quantitatively the dynamics of stabilization of interfaces by nanoparticles in microfluidics. Our analysis revealed the crucial role of the flow profiles at the pro-

duction junction on the stabilization kinetics. From our measurements, we determined design rules for the effective stabilization of Pickering emulsions in microfluidics. The critical parameters for an efficient stabilization are the nanoparticle concentration near the aqueous interface and the shear stress provided by the cross-flow at the moment of droplet formation. We control the former by adding a co-flow of particles dispersion with the aqueous phase, and the later by increasing the velocity or the viscosity of the cross-flow oil. These design rules allow us to significantly increase the droplet production throughput with a minimal amount of particle waste. Taking these guidelines, new designs could be implemented and adapted to the particular requirements of each technological application.

## 5.5 Materials and methods

### Fluorinated silica nanoparticles

Fluorinated Si-NPs ( $\delta = 65$  nm) were synthesized and functionalized with PFOTES as described on chapter 3. The Si-NPs specific surface ( $S_c = 560$  m<sup>2</sup>/g) and density ( $\rho_p = 0.165$  g/cm<sup>3</sup>) was determined as described on section 3.2. All the experiments were done with the same batch of particles with a fixed degree of surface fluorination ( $\phi_{wt} = 7$ , Eq. 3.7).

#### 5.5.1 Microfluidic device fabrication and experimental design

The microfluidic device was designed and moulded in PDMS using soft-litography techniques of replica moulding of a SU-8 master [73, 113] with a pattern depth of  $h = 50$   $\mu$ m (Fig. 5.6a). The PDMS was treated under oxygen plasma and bounded to a glass slide. The device channels were made hydrophobic by surface treatment with a commercial coating agent (Aquapel, PPG Industries). The microfluidic inlets were connected to syringes through Peek tubing of 0.75 mm inner diameter and the flow rates were controlled using syringe pumps (Nemesys, Cetoni).

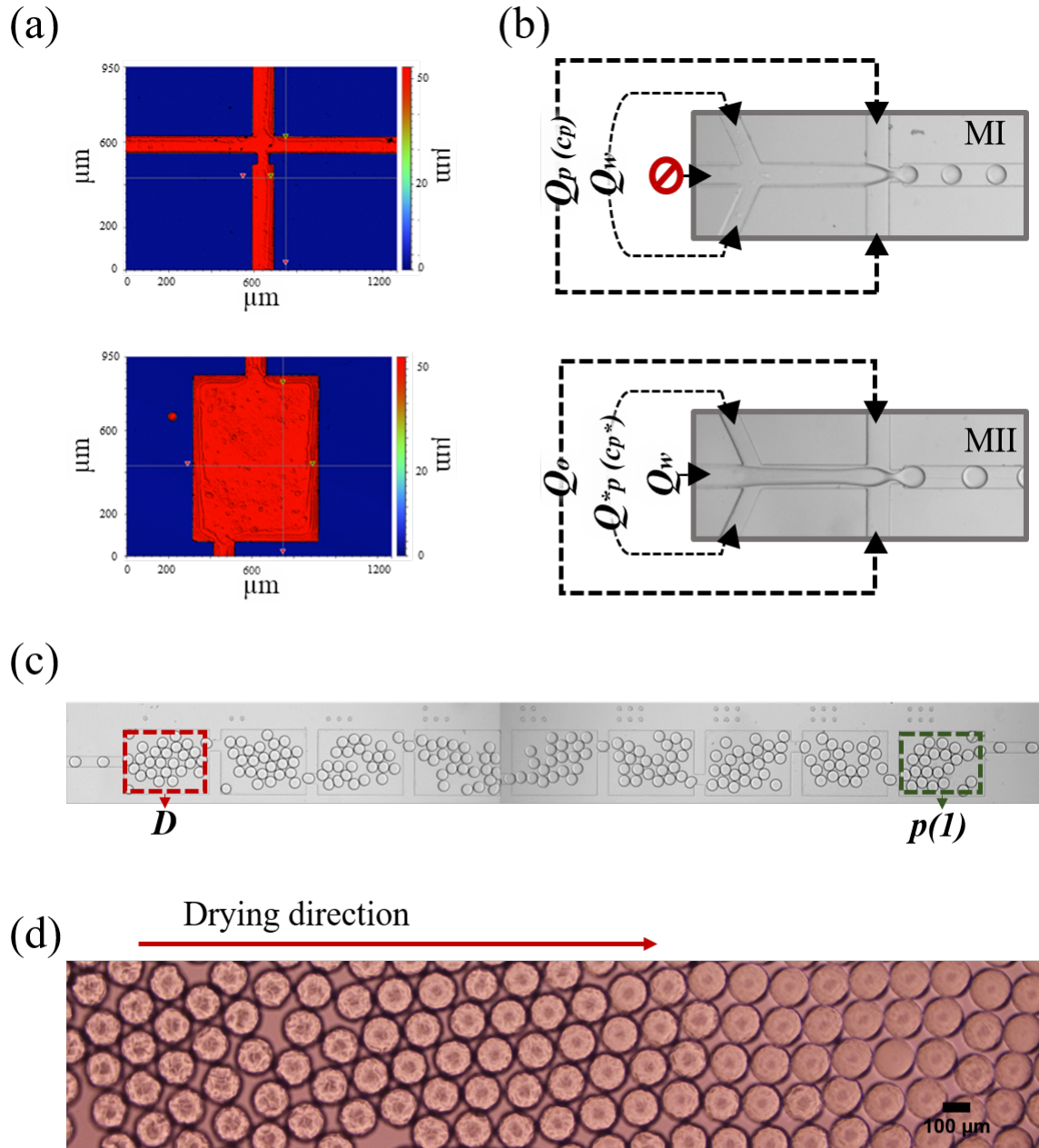


**Fig. 5.6** (a) Profilometer measurements for the determination of the SU-8 master pattern depth. (b) Operation modes for droplet production with the same microfluidic pattern: for method MI, the central inlet is not pierced. (c) Coalescence chamber design divided into nine segments, droplet size is extracted from the first chamber,  $p(1)$  value is extracted from the last chamber. (d) Empirical observation of buckling pattern at the collected droplets interface upon drying.

The device was designed to test stability against droplet coalescence for two different production methods, which are achieved by selective puncture of the device inlets (Fig. 5.6b):

The first method (MI) consists in a standard flow-focusing production, where the particles are dispersed in the continuous phase (HFE-7500) and pre-diluted at the required concentration ( $c_p$ ); the second method (MII) is the system presented on section 5.2, the aqueous phase (deionized water) co-flows with a concentrated dispersion of particles ( $c_p^*$ ) right before the droplet production junction where it meets (cross-flow) a stream of particle-free oil that dilutes  $c_p^*$  down to  $c_p$ . Additionally, two different oils are tested for the cross-flow in MII: HFE-7500 (MII $_{\eta\downarrow}$ ), which has a viscosity of 0.77 cSt and FC-40 (MII $_{\eta\uparrow}$ ) which has a viscosity of 2.2 cSt.

After production, the droplets are “incubated” in a channel of fixed width ( $\omega = 100 \mu\text{m}$ ) which keeps them separated for a time proportional to a length (L). The incubation channel ends with an abrupt expansion of  $600 \mu\text{m}$  that leads to a set of nine consecutive coalescence chambers of  $800 \mu\text{m}$  length each (Fig. 5.6c). This coalescence chamber has a different design than the one used on section 3.5: instead of a straight chamber (0.5 mm width, 3 mm length), a larger coalescence area (0.6 mm width, 7.2 mm length) was divided into nine equal sections with the aim of introducing larger random collisions between droplets. This helped to identify small differences on stability between emulsion conditions that previously seemed equally stable. However, even though effective as a reference to compare different systems stability against coalescence, reaching the set stability criteria ( $p(1) > 0.999$ , Eq. 3.8) does not guarantee full coverage of the droplets interface by particles. We empirically verified droplet coverage after emulsion collection by an optical readout (Fig. 5.6d): upon drying, the volume of the droplet decreases. As the particles do not desorb from the surface, a buckling pattern is observed at the interface, characteristic of a layer of irreversibly adsorbed particles [129, 130].

For all the experiments, at least 1500 frames were recorded at a frame rate of 20 fps. The images were processed with Image-J software [114] where the area of each droplet was extracted for the first coalescence chamber (Fig. 5.6c (red)), and the apparent diameter ( $D$ )

calculated as the median value of the droplet population distribution. The droplet volume ( $V$ ) and surface ( $S$ ) was calculated using a nodoid shape approximation, which it has been shown to accurately describe a droplet confined in a microchannel [131]. The stability against coalescence ( $p(1)$ ) was calculated (Eq. 3.8) with data extracted from the last coalescence chamber (Fig. 5.6c (green)).

## CHAPTER 5

**Summary**

- We present a multi-parametric study for the stabilization of droplets with nanoparticles in a microfluidic device, including the effect of particle concentration, droplet volume, production mode and incubation time.
  - Our analysis revealed the crucial role of the flow profiles at the production junction on the stabilization kinetics: the adsorption of particles to the interface during droplet formation have a greater impact on stability than the bulk particle concentration and incubation time given to droplets downstream the microchannel.
  - The critical parameters for an efficient stabilization are the nanoparticle concentration near the aqueous interface and the shear stress provided by the cross-flow at the moment of droplet formation.
  - Our droplet production design allows the high throughput stabilization of fluorinated Pickering emulsions –in a microfluidic device– with a significant reduction of particles waste.

## **Chapter 6**

# **Adherent cells incubation in Pickering droplets**

In this chapter we explore the application of fluorinated Pickering emulsions for the study of adherent cells. We first make a description of the set-up utilized for droplet monitoring and of the various technical challenges that led us to our final incubation model (section 6.1). Then we applied this incubation model to a system of Retinal Pigment Epithelium cells (RPE-1), and present the results obtained (section 6.2).

### **6.1 A microfluidic device for Pickering droplets incubation and monitoring**

We built our microfluidic incubation device as shown schematically in Fig 6.1: First, by standard soft lithographic methods [113] we obtained a PDMS thin layer (thickness  $\sim 1$  mm), with a pattern (depth  $\sim 75$   $\mu\text{m}$ ) consisting of six parallel chambers of 16 mm x 2.6 mm each (Fig. 6.1a). Two patternless thicker ( $\sim 5$  mm) blocks of PDMS were plasma bonded on top of our patterned thin layer covering the extremes of the chambers (inlet/outlet) on its patternless

side.

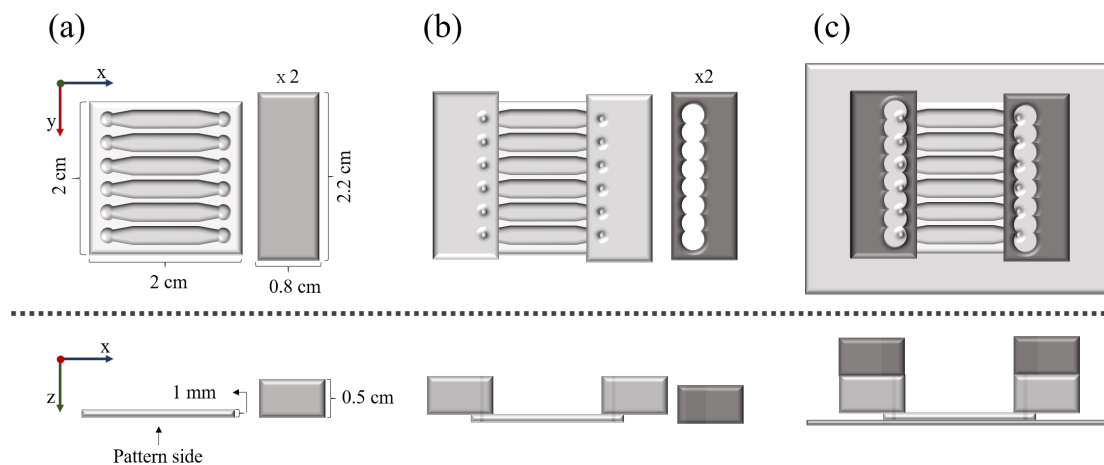


**Fig. 6.1** Schematic representation (top-view and side-view) of the fabrication steps for an incubation device.

Afterwards, we used a 0.75 mm biopsy puncher to pierce holes on the inlets and outlets of each one of the parallel chambers (Fig. 6.1b). Two additional patternless and thick ( $\sim 5$  mm) PDMS blocks were plasma bonded on top of the previous two. This PDMS pieces had a continuous chamber made earlier with a 3.5 mm biopsy puncher, the chamber was placed in a position that allowed the visibility of the inlet/outlet holes.

Finally, the patterned side of the thin PDMS layer was plasma bonded to a glass slide previously coated with a very thin PDMS layer ( $\sim 30 \mu\text{m}$ ) (Fig. 6.1c), and the chamber channels were made hydrophobic – right before use – by surface treatment with Aquapel.

This design was the result of adjustments made after several failed incubation tests where monitoring droplets over night presented various technical inconveniences.

### 6.1.1 Selection of PDMS over glass

Droplets incubation and monitoring inside a microfluidic device require their preservation during times ranging from hours to days. Due to the permeability of PDMS to water and oil,

glass is usually the chosen material for long incubation times, avoiding the need to control humidity to prevent evaporation [132].

During biocompatibility experiments performed in chapter 3, we presented the overnight culture of *E. coli* Rosetta for droplets stabilized by particles with different degrees of surface functionalization ( $\phi_{wt}$ ). Said culture was performed in bulk (culture flask) and verified with an epifluorescence microscope after overnight incubation (Fig. 6.2a)<sup>1</sup>, where a viable bacterial population was observed.

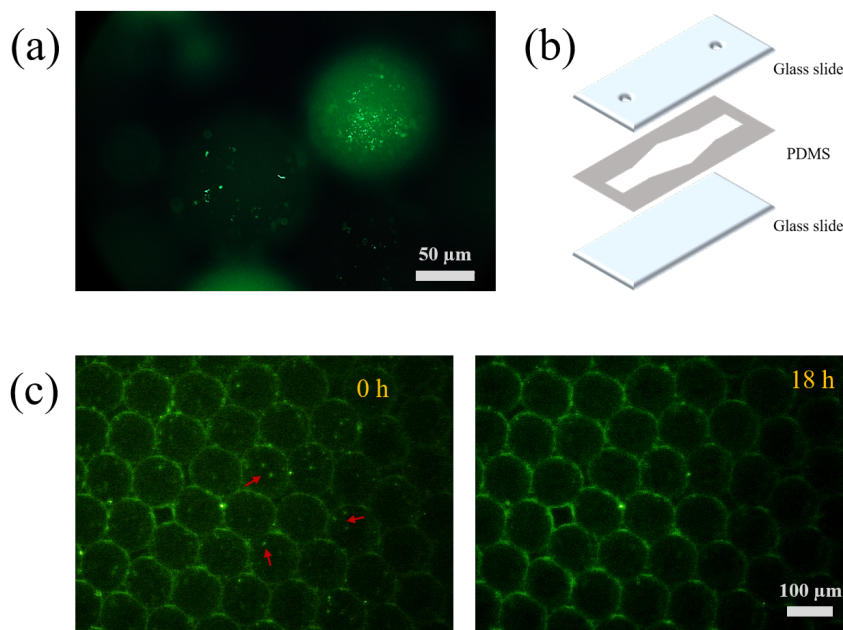


**Fig. 6.2** (a) *E. coli* proliferation inside Pickering droplets after overnight culture in a petri-dish. (b) Schematic representation of sandwich-like glass device before plasma bonding. (c) Trapped Pickering droplets in sandwich-like glass device showing initial bacteria population dramatic decrease after 18 hours.

Several attempts were made to monitor bacteria growth inside a sandwich-like glass device, where two glass slides were bonded together using a thin layer of PDMS (thickness  $\sim 50 \mu\text{m}$ ). The PDMS layer delimited the droplet incubation area and chamber height (Fig. 6.2b).

The glass chamber was effective for monitoring bacteria growth within droplets stabi-

<sup>1</sup>Bacteria growth experiments and pictures taken with Dr. Deniz Pekin

lized by fluorinated surfactants. However, every attempt made with droplets stabilized by fluorinated nanoparticles resulted on a decrease of the bacteria population and death after several hours (Fig. 6.2c).

We lack the understanding of why the bacteria did not proliferate under the described conditions. We speculate that the Pickering emulsion –in contrast to a surfactant stabilized emulsion– under said sealed device, was not able to exchange the needed oxygen to keep the bacteria alive.

Additional tests were performed with various PDMS trap devices. For these cases, we were able to observe bacteria proliferation inside droplets, however, technical problems were introduced due to the permeability of PDMS to water and oil.

Additional problems encountered while working with our fluorinated Pickering emulsions inside devices with a glass support came from wetting of the droplets on the glass surface. To avoid this problem, surface hydrophobic treatment – either for production, manipulation or incubation – was applied right before using a microfluidic device, showing to be an effective solution in most cases. Furthermore, a more reliable solution consisted on making the production and incubation devices fully out of PDMS. The device support (glass slide, coverslip, plastic or glass petri-dish) was then covered by a very thin PDMS layer ( $\sim 30 \mu\text{m}$ ) before bonding the microfluidic PDMS chip.

### **6.1.2 Additional technical challenges**

Monitoring Pickering droplets over extended periods of time in a PDMS chamber proved to be difficult due to various disrupting events. The first issue considered was the evaporation of the aqueous phase through the PDMS device.

The permeability of PDMS to water and oil permits the rapid evaporation of the aqueous phase and droplet shrinkage and wrinkling (characteristic of particle-covered droplets) is

observed in less than one hour (Fig. 6.3a)<sup>2</sup>.

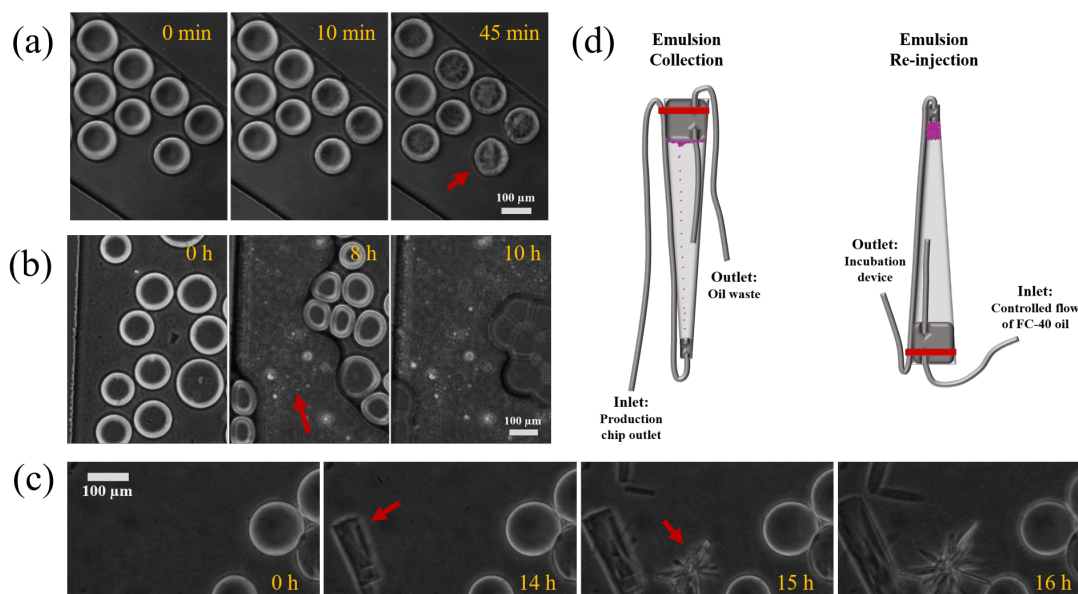


**Fig. 6.3** (a) Droplet shrinkage due to aqueous phase evaporation through PDMS layer. (b) Air bubble entering observation device. (c) Crystals forming in oil phase. (d) Schematic representation of reservoir made for emulsion collection and re-injection.

Placing the incubation chamber inside a humid environment (Petri-dish with wet filter paper or directly covered with water) was not sufficient to solve this problem. Apparently, the PDMS layer was not only serving as a permeable membrane for the evaporation of the aqueous phase, but it was also adsorbing water into its inner layer, causing the shrinkage of droplets.

An approach considered to solve this problem consisted on the pre-incubation of the PDMS device in a wet environment for two days before the droplet monitoring experiment. Even though effective on the prevention of droplet shrinkage, this approach introduced additional problems of wettability and ineffective hydrophobic treatment of our incubation chamber.

The final solution taken consisted on reducing the thickness of our PDMS device from 5 mm to 1 mm or less (Fig. 6.1a). This solution in combination with a humid environment

<sup>2</sup>Evaporation, bubbles and crystallization problems observed with Dr. Mathias Girault and Dr. Deniz Pekin

–device placed in humid chamber– was sufficient to prevent droplet shrinkage for extended monitoring times (>48 h).

The reduction of the device thickness however, did not allowed the connection of tubing in the inlet of the chamber (needed for droplets injection). For this reason, a thicker block of PDMS was bonded to the inlet and outlet areas of the incubation device through which the inlet and outlet holes were pierced (Fig. 6.1b).

The second disruptive event experienced consistently during over night incubation was the entrance of air bubbles inside the incubation chamber (Fig. 6.3b). Even though we carefully prevented any air bubble from being trapped initially in our observation chamber (for which case the bubble would expand inside the chamber displacing and/or destroying the Pickering drops), air bubbles would enter from the inlet/outlet holes of the device after several hours of monitoring.

Even though we do not fully understand the mechanism by which the air gets pulled into the device, we speculated that a pressure gradient between the inlet and outlet of the chamber was causing this effect. Consequently, we added a third layer to our incubation device. It consisted of a thick block of PDMS (~ 5 mm) with an open chamber placed right on top of the inlet and outlet holes of the device (Fig. 6.1c). These open chambers were filled with fluorinated oil right after the emulsion injection, effectively preventing the incursion of air inside the observation chamber during the monitored times tested (> 48 h).

The final disruptive effect observed during our droplet monitoring time consisted on the formation of crystals in the oil phase (Fig. 6.3c). These crystals appeared during overnight incubation, sometimes between the droplets while displacing and/or deforming them.

We speculated that this problem was related to a combination between high particle concentration and some minor oil evaporation. Similar to the crystals observed when a suspension of fluorinated Si-NPs in HFE-7500 was fully dried and re-suspended on section 3.4.1.

Crystallization effect was observed only for tests done with a standard flow-focusing droplet production device, which required high particle concentration to avoid droplet coalescence. All our tests were then done with the droplet production method described on chapter 5, where a stream of particles co-flows with the aqueous phase right before droplet production by a cross-flow of clean fluorinated oil.

This droplet production method is particularly sensitive to pressure variations downstream of production. Any pressure build-up at the outlet destabilizes the production stream, causing the highly concentrated particle stream to retract (stream with smallest flow rate) and resulting on the production of insufficiently particle-covered droplets which are unstable to coalescence.

Consequently, the outlet of the production device cannot be directly linked through tubing to the incubation device, and the emulsion must be carefully collected for posterior re-injection in the incubation chambers.

The emulsion collection was done in a reservoir shown schematically in figure 6.3d. This reservoir was made with 1 ml plastic pipette tip sealed with PDMS at the bottom and the top. The PDMS at both ends was pierced and connected through tubing to the device of interest: for emulsion collection, the thinner bottom was connected to the production device outlet; for emulsion re-injection, the reservoir was turned up-side down and connected to the incubation device.

The collection of droplets from the bottom towards the upper part of the reservoir was important to keep the production device outlet at a stable atmospheric pressure: If the emulsion collection was performed directly at the upper part of the reservoir, the accumulated layers of drops right at the tubing outlet (inside the reservoir) were sufficient to build-up pressure and make the droplet production unstable.

Taking into account the described considerations, we were able to produce stable droplets, collect them in a reservoir, re-inject them in an incubation device and observe them without

disruptions for more than 48 hours. This technical achievement is an important milestone as no equivalent result could be found in the literature with Pickering emulsions.

We then used this set-up for the study of adherent cells. Specifically, we used as a model retinal pigment epithelium (RPE) cells.

## 6.2 Studying cells phenotype heterogeneity in Pickering droplets.

The retinal pigment epithelium (RPE) is a monolayer of cuboidal epithelial cells found in the eye between the photoreceptors and the choriocapillaries. The RPE cells are bound together with tight junctions and they are polarized into a basal half, facing the choroid and containing the nucleus and mitochondriae; and an apical half, facing the neural retina and containing numerous pigment granule. These pigments give the epithelium its macroscopic black appearance for which it derives its name (Fig. 6.4) [133].

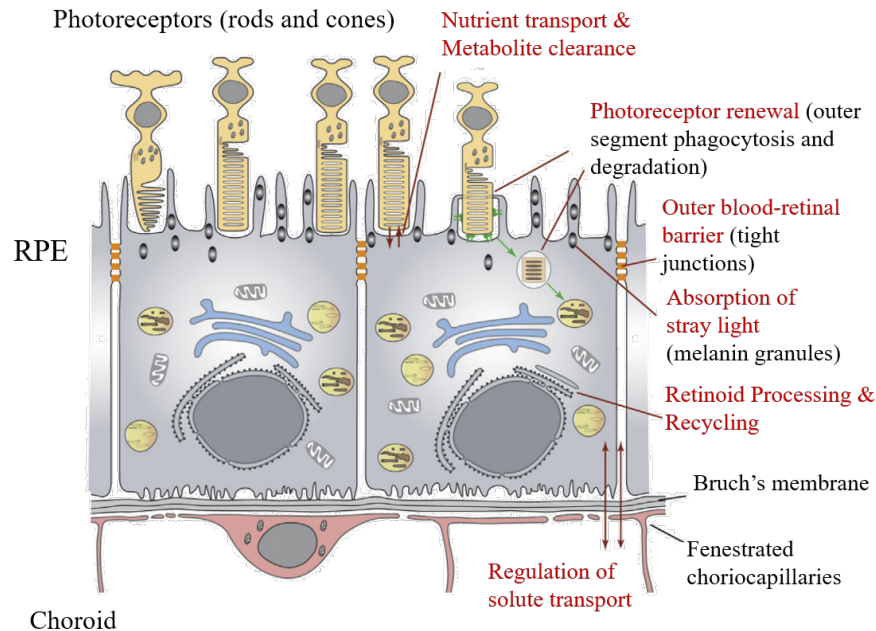


**Fig. 6.4** . Schematic representation of the outer retina and the support functions of RPE. Reprinted from [134]

The RPE cells serve a variety of functions that support and protect the retina. These

include: phagocytosis of photoreceptor outer segments [135], essential for their renewal; adsorption of free radicals by pigment granules [136], which helps to maintain retinal homeostasis; and maintenance of ocular immune privilege by forming the outer blood-retina barrier [137]. Additionally, RPE cells control the exchange of nutrients and metabolites between the choroid and the subretinal space [133].

The RPE cells are highly specialized and do not proliferate under normal conditions, but unlike the photoreceptor cell their differentiation is not terminal. In several retinal pathologies including inflammation and vascular disease RPE cells change from being differentiated, stationary and nondividing cells into undifferentiated, migratory and proliferating ones [138]. This dedifferentiation or transdifferentiation is accompanied by changes in cellular phenotype, acquiring macrophage and mesenchyme-like characteristics, distortion of intercellular contacts, and loss of pigmentation [139]. Altered RPE cells damage the retina and other eye structures, often impairing vision or leading to blindness [140].

RPE cells plasticity in adult humans besides being responsible for a variety of ocular pathologies, provides a limited capacity to heal acquired in situ defects resulting from aging, inflammation, surgery, or trauma [141]. In contrast, certain amphibian species –such as the frog and the newt– exhibit RPE-mediated retinal regeneration after metamorphosis [140].

For example, when the neural retina of the African clawed frog is carefully removed from the eye by a surgical operation, some populations of RPE cells in the posterior eye are detached from Bruch's membrane, migrate and adhere onto the retinal vascular membrane, and then proliferate and transdifferentiate into the neural retina, while the other RPE cells remaining in the original RPE layer repair the RPE itself [142].

The problem of control over RPE differentiation is hence of major significance for both basic and applied research. A full understanding of the causes of phenotypic changes and control in the human RPE could provide ways to regulate pathological states, make effective tissue transplants, patching procedures, and even activation of neuronal properties for the

restoration of damaged retina [138, 143]. Several studies have linked many growth factors, extra cellular matrix (ECM) proteins and cell-cell interactions to both, the differentiation and dedifferentiation of RPE [138]. However, a full control and understanding of the external factors involved in the activation of signaling pathways for cell de- trans- differentiation has not yet been reached.

The culturing of human RPE cells provides the possibility to analyze in detail their morphology, functions, as well as molecular and genomic properties under normal and pathological conditions, which is hardly possible in-vivo. Similarly to RPE cells under pathological conditions, RPE cells cultured in-vitro as an adhesive monolayer gradually lose epithelial characteristics, including polarity and specific markers such as pigmentation; they also acquire migratory properties and mesenchyme cell-like features [144].

However, studies of RPE cells in-vitro have also some limitations related to genetic instability of continuous cell lines, with consequent variation in their properties between passages [145]. Furthermore, RPE cells are not uniform even in situ, forming a heterogeneous mosaic of similar but not identical cells [146].

Single-cell studies of RPE cells are hence of great interest to account for their intrinsic cell heterogeneity and could potentially provide a deeper understanding on their behavior. Cellular adhesion is key for RPE cell survival, avoiding death by anoikis or apoptosis [138]. We propose our fluorinated Pickering droplets as a suitable technological platform for single-cell encapsulation. This will provide: a rigid surface at the droplet interface (Si-NPs) for cell adhesion, isolation from cell-cell interactions, individualization of the cell micro-environment, and continuous visual monitoring of single-cells in culture conditions.

### 6.2.1 Single-cell incubation of RPE cells reveal its phenotypic heterogeneity

We used the microfluidic incubation model described in section 6.1 to monitor droplets containing RPE cells (RPE-1 type expressing actin-GFP).

Bright field (BF) and fluorescent images demonstrate cell adhesion at the droplet interface, as well as the intrinsic heterogeneity of the cell phenotype (Fig. 6.5).

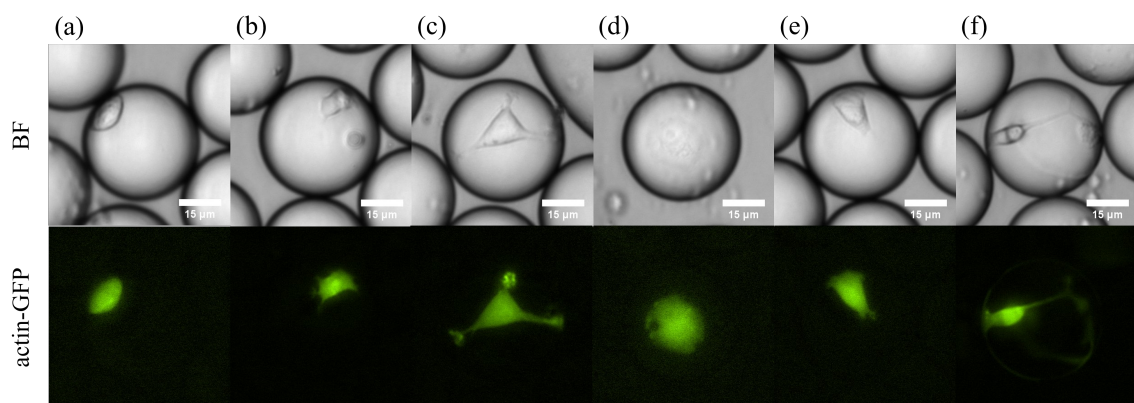


**Fig. 6.5** BF and green fluorescence pictures of different phenotype observations for the same cells encapsulated in Pickering droplets: (a-c) mesenchyme-like cells; (d) macrophage-like cell; and (e) epithelial-like and (f) neural-like polarized cells.

The images shown on Fig. 6.5 correspond to different droplets with identical composition and under the same incubation conditions. We observe mesenchyme-like cells of different sizes: non-polarized, contracted and clearly adhered to the droplet interface (Fig. 6.5a); spread with protruding filopodia filaments (Fig. 6.5b); and showing big focal adhesions at different points of the droplet interface (Fig. 6.5c). Additionally, we observe macrophage-like cells, with a rounded irregular shape (Fig. 6.5d); and polarized cells resembling the phenotype of a differentiated RPE cell (Fig. 6.5e) and of a neural-like cell (Fig. 6.5f).

RPE cells dedifferentiation and epithelial-mesenchymal transition (EMT) has been widely observed for RPE cells in-vitro [138]. EMT is initiated upon loss of cell-cell contact [147]. Isolating cells in droplets would hence promote dedifferentiation as evidenced in their expressed phenotype (Fig. 6.5)

Cell to cell heterogeneity as well as heterogeneity between multiple passages of the same cell populations has also been observed in culture conditions [145, 148]. Encapsulating RPE in droplets allow us to observe this heterogeneity independently of cell-cell contact.

Trans-differentiation of RPE cells into neural is of particular interest for restoration of damaged retina [144]. Salero *et al.* found evidence for multipotency of adult human RPE cells, they showed that depending on culture conditions, RPE cells can redifferentiate into stable RPE monolayers or transdifferentiate into neural or mesenchymal cells [149].

We found some cells with a phenotype resembling the polarized features of an epithelial (Fig. 6.5e) and of a neural (Fig. 6.5f) cell. However, protein markers for those specific cell differentiation states would be needed to confirm their expression within our cell line.

Nevertheless, our first observations confirmed the heterogeneous phenotypic expression of our RPE-1 cells, which is independent on the culture passage number, cell micro-environment, and cell-cell contact.

We also observed some markers characteristic of differentiated RPE cells: cell pigmentation (Fig. 6.6a), secretion (Fig. 6.6b), and phagocytic behavior (Fig. 6.6c).

The black pigmentation observed on the BF image on Fig. 6.6a indicates the presence of melanin granules, a marker of differentiated RPE, usually loss upon dedifferentiation [133]. Even though this cell has apparently loss polarity, additional visual evidence of EMT, such as cell migration (after 7 hours) is not observed.

Differentiated RPE cells are able to synthesize and secrete some components in a directional fashion; either from the apical surface towards the photoreceptors or from the basolateral surface towards the underlying choroid [138]. On Fig. 6.6b we observe the increasing polarization over time of a static cell. Apparently, the cell is also secreting a substance dyed with GFP, evidenced in the accumulation of fluorescence at the droplet interface, which reaches a complete surface coverage after nine hours of observation.

Differentiated RPE cells also carry out phagocytosis, which is an important feature for

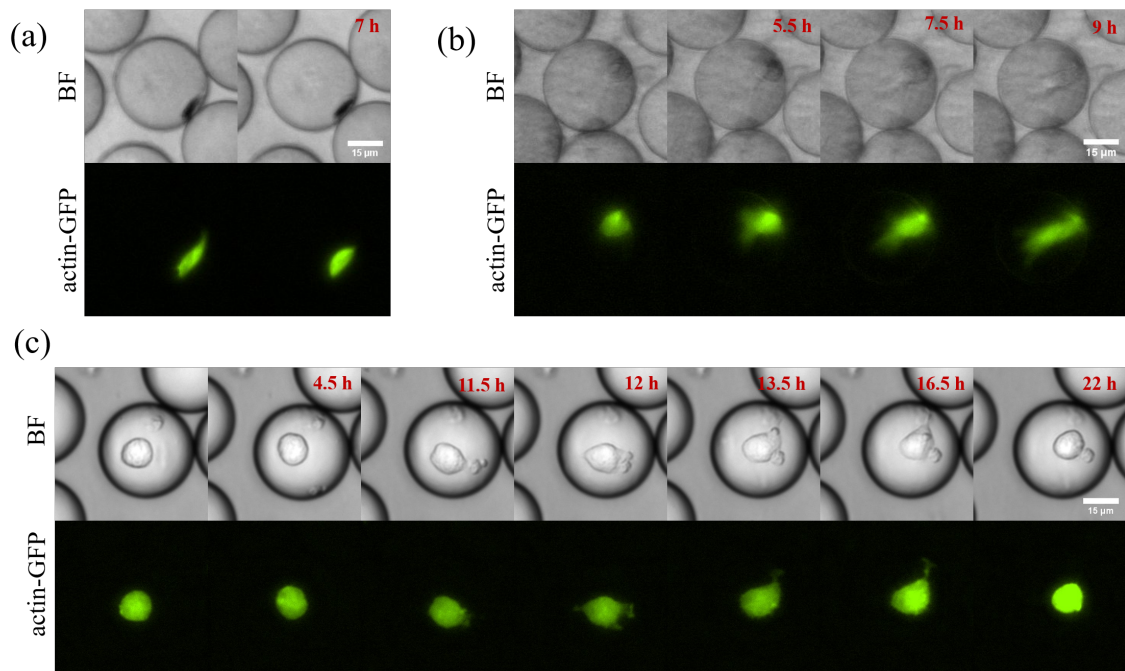


**Fig. 6.6** BF and green fluorescence time sequence of cells exhibiting RPE markers:(a) Pigmentation; (b) Polarization and secretion; and (c) Phagocytosis. The time frame is indicated in red with respect to the first image of the sequence.

photoreceptors survival [133]. On Fig. 6.6c we show a time sequence of a cell trapping an unidentified body (maybe another cell that underwent lysis) present in the droplet and consuming part of it. The cell interacts with the external element for five hours, and its fluorescence intensity increases during the following five and a half hours. However, given its rounded shape this cell most likely corresponds to a macrophage-like cell instead of a differentiated RPE.

The presence of pigmentation and polarized secretion nevertheless indicates that even after removing cell-cell contact, some of these cells preserved characteristics of a differentiated RPE cell.

Another interesting feature observed in a heterogeneous fashion was the presence of cell migration, some cells remained immobile during the monitored time (such as the ones shown on Fig. 6.6a and 6.6b). However, some cells exhibited two distinct types of cell migration: amoeboid migration (Fig. 6.7a) and mesenchymal migration (Fig. 6.7b).

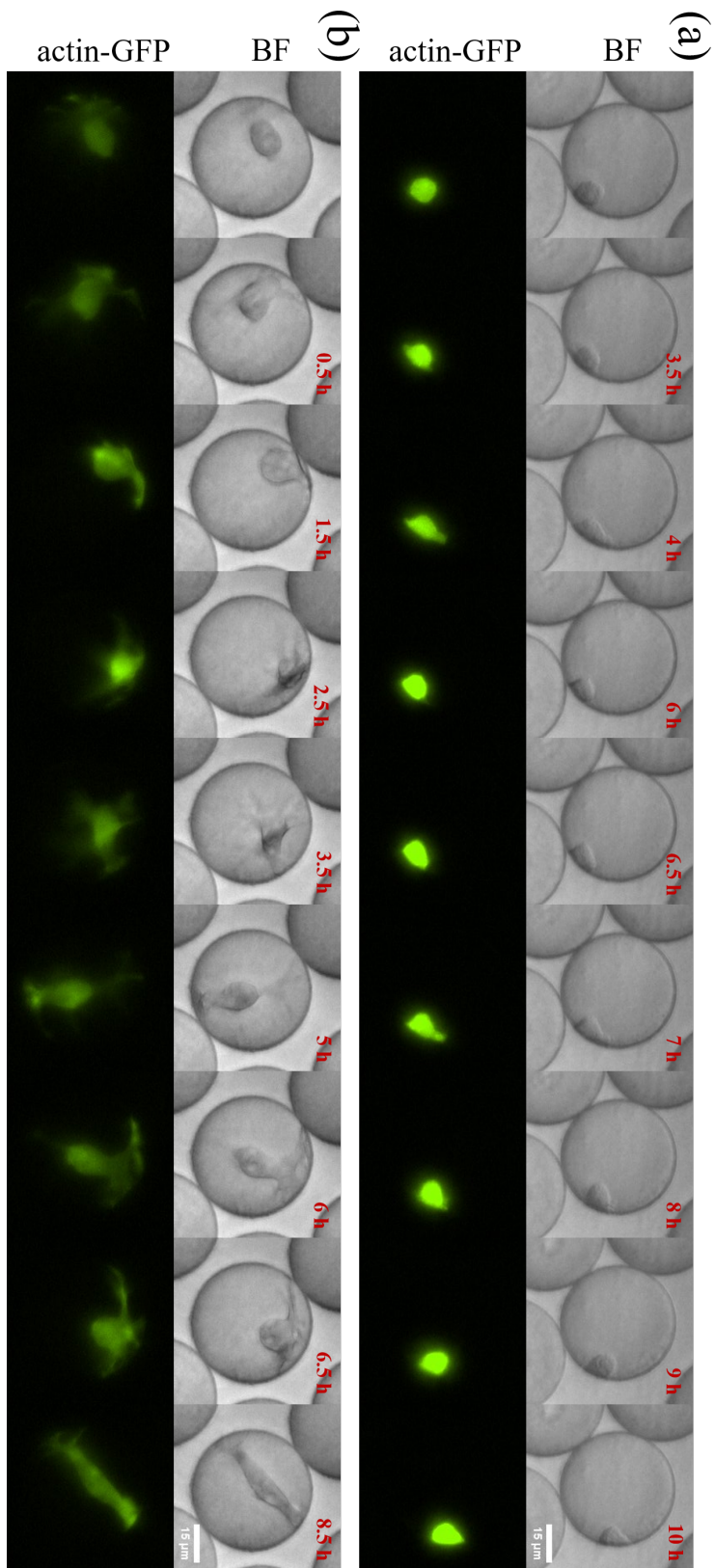


**Fig. 6.7** BF and green fluorescence time sequence of two migration modes: (a) Amoeboid migration; and (b) mesenchymal migration. Time reference with respect of the first image of the sequence in red.

Amoeboid migration is characterized by cells adopting round or irregular shapes while moving through cycles of expansion and contraction [150]. On Fig. 6.7a we show a time sequence of a cell migrating at the edge of the droplet interface in an amoeboid fashion. The cell contracts into a round shape, then a bleb-like protrusion is formed and the cell contracts again moving to a new position.

Mesenchymal migration is characterized by cells adopting an elongated, spindle-like shape and exerting traction on the ECM via focal adhesions associated with actin-rich protrusions [151]. On Fig. 6.7b we show a time sequence of a cell exhibiting a mesenchymal migration mode, where the cell moved by spreading long actin-rich filaments, which at times reached opposite sides of the droplet edge.

Cell micro-environment such as adhesiveness and level of confinement has been associated with mesenchymal-amoeboid transition [152]. However, the identical micro-environment provided for each cell by our Pickering droplets demonstrate that the presence of different migration mechanism is directly associated to the heterogeneous characteristics of our cell population.

### **6.2.2 Illustrative model of a study accounting for RPE cells heterogeneity**

We designed a simple experiment to explore our technological platform potential. With this aim we chose an ECM glycoprotein –fibronectin– which is also found in Bruch’s membrane [153]. We studied the effect of a small concentration of fibronectin on the RPE phenotypic expression.

From the six chambers available in our incubation device (Fig. 6.8a): two contained non-encapsulated cells in media, where cells were cultured as a reference directly on the PDMS surface; the other four were designated for our test samples, containing encapsulated cells in drops. Half of both, references and samples, were divided in two cases: without

added fibronectin (case A) and with added fibronectin (case B).

Cells were monitored in each chamber and BF and fluorescence images taken every thirty minutes. The fluorescence images were used to extract the contour of each individual cell per time frame (Fig. 6.8b). And values such as: area, mean grey value, position, aspect-ratio (AR) and circularity were extracted.

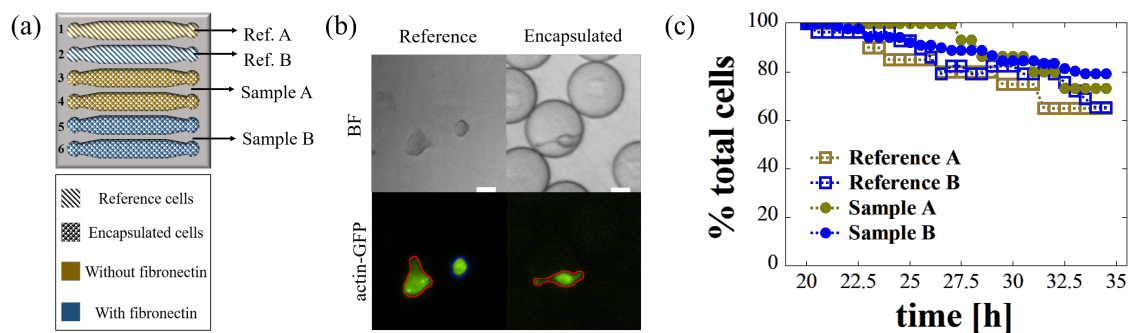


**Fig. 6.8** (a) Experimental conditions, encapsulated cells and references. (b) Example of cell contour determination based on actin-GFP image. (c) Viability test, comparison samples and references on cell survival over time.

We experienced difficulty on discriminating rounded contracted cells adhered to the droplet interface from floating or sedimented ones, in both, the encapsulated cells and the reference cases. We then started the monitoring time after twenty hours of droplet incubation, when non-adhered cells would have undergone apoptosis [133].

We monitored cell viability during fourteen and a half hours (6.8c). We observed a similar decrease of the percentage of living cells for all cases, with a slightly better viability for encapsulated cells. We did not observe an apparent influence of added fibronectin on cell viability.

Due to technical problems, we were unable to provide the required  $\text{CO}_2$  atmosphere to keep the media pH balanced during our culturing time. However, a similar viability between our encapsulated samples and the two references, indicates a good viability of cell culture in our Pickering system.

In order to account for cell phenotypic heterogeneity, we divided the cells in four groups:

Type 1 corresponded to rounded cells, with a phenotype resembling macrophages (Fig. 6.5d). Type 2 to Type 4, corresponded to mesenchyme-like cells: Type 2 were not very elongated, and included cells resembling an epithelial-like differentiation (Fig. 6.5a and 6.5e); Type 3 were more elongated, and included cells resembling a neural-like differentiation (Fig. 6.5f); and Type 4 were cells presenting multiple filopodia protrusions or focal adhesions (Fig. 6.5b and 6.5c).

Discrimination between types was done by setting a threshold of cell AR and circularity (Fig. 6.9): Type 1 were cells with an AR smaller than 1.5, and circularity larger than 0.76; Type 3 and 4 had a circularity smaller than 0.5, and AR larger (Type 3) or smaller (Type 4) than 2.5; Type 2 corresponded to all the cells that did not fit within those criteria.

In order to illustrate the phenotypic classification established by the set thresholds we constructed a map of AR vs Circularity using six example cells from both reference (Fig. 6.9a) and samples (Fig. 6.9b). We found there is no apparent difference between the diversity of phenotypes expressed for cells spread on the PDMS surface and on the droplets interface.

On both phenotypic maps (Fig. 6.9) cell shapes with the same color correspond to the same cell in different time frames. Some cells experienced very little variations, remaining within the same threshold type during the entire observation time; such as the orange, blue and grey colored examples on Fig. 6.9a, remaining as Type 1, Type 2, and Type 3 respectively. On the other hand, some cells widely varied their phenotype –due to filament protrusions and/or cell expansion and contraction– and exhibited phenotypes corresponding to different set thresholds; this is the case of the orange, black and yellow examples on Fig. 6.9b, which varied between Type 1 and 2, Type 1 and 3, and Type 2 and 4 respectively.

In order to account for these changes we measured two classes of cell type: one corresponding to the maximum type the cell exhibited during the monitored time, implying that a cell exhibiting a Type 4 phenotype would be counted as such even if this phenotype was present in just one time frame; and a second class corresponding to the median value of type

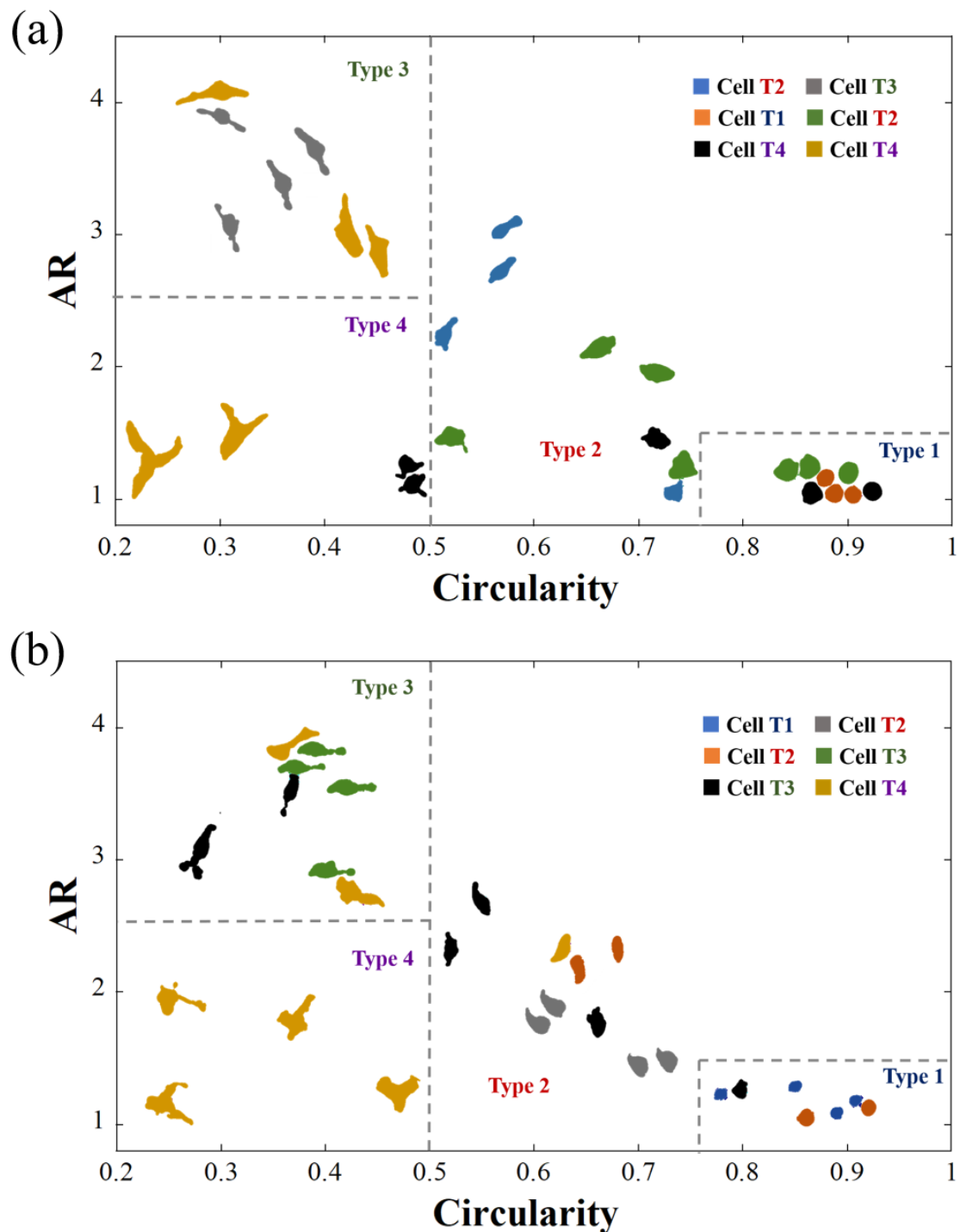


**Fig. 6.9** Six different cells are used as an example to show the phenotype classification set by AR and circularity thresholds, which divides the cell phenotype in four types. The color of the shape indicates the same cell in different time frames. The map is reproduced with examples from: (a) Reference, which are cells spread on PDMS; and (b) Samples, which are cells spread on the Pickering droplet interface.

manifested along the entire monitored time. For example, on Fig. 6.9b, the black colored cell would have a maximum type corresponding to 3 and a median type corresponding to 2.

On Fig. 6.10 we present the percentage distribution of cell types for the studied cases. Cell type is presented in three different forms: the median type, corresponding to the outer ring of the pie chart; the maximum type, corresponding to the inner ring of the pie chart; and the time dependent type, where the cell type was updated based on the maximum type exhibited by each individual cell so far on each time data point; this percentage is affected by cells moving up the cell type over time as well as dying cells which are excluded from the total population.

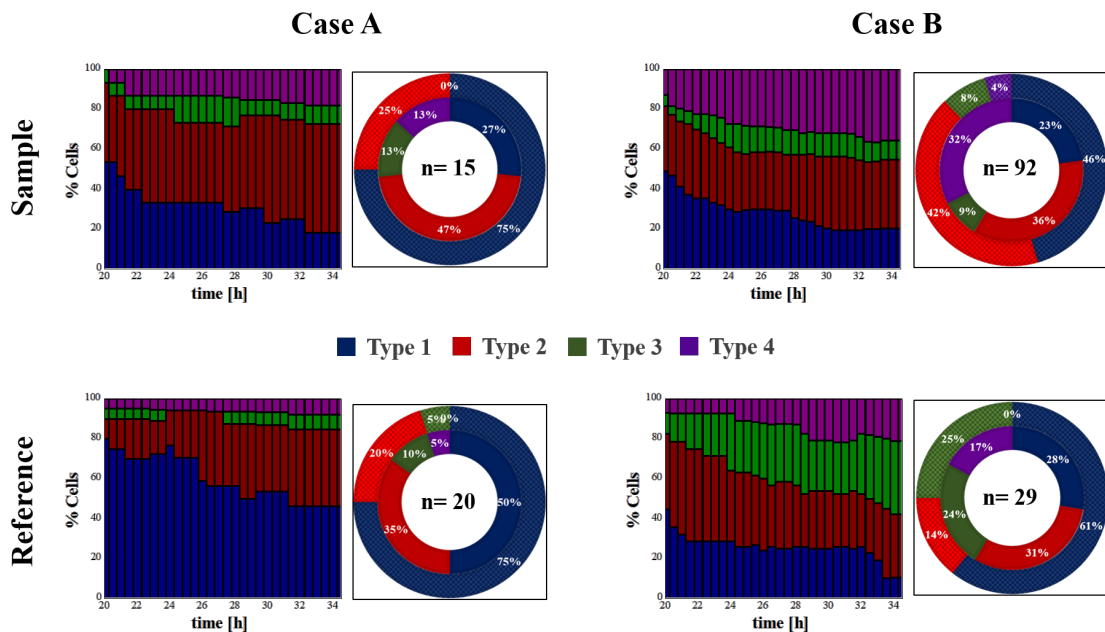


**Fig. 6.10** Cell type percentage distribution for non-encapsulated (reference) and encapsulated (sample) cells, and for the two cases of study: without fibronectin (A) and with fibronectin (B). Cell type is presented in three forms: median type and maximum type, corresponding to the outer and inner ring of the pie chart respectively; and time dependent type, which is updated as the maximum type taken by each individual cell at each time frame.

We observe a clear difference between case A and B: In case B, the proportion of Type 3 and Type 4 cells present in the population increases over time; on the other hand, in case A these same cell types remain approximately constant over time, representing a clear minority

of the population. Taking the maximum type value as reference this is: 15 % and 26 % of the population for the reference and sample in case A, versus 41 % of the population for both reference and sample in case B.

Cell phenotype 3 and 4 correspond to mesenchyme-like cells which form clear focal adhesion complexes with the substrate (PDMS or droplet interface). ECM components such as collagen and fibronectin stimulate integrin signaling and consequent formation of focal adhesion complexes [154]. Furthermore, fibronectin has also been linked to cell migration [155] and EMT [156]. Consequently, our results confirmed an influence of fibronectin on the expression of mesenchyme-like cells phenotype, which is independent on the cell microenvironment (PDMS substrate or nanoparticles interface).

We also observed that for both, case A and case B the proportion of cells expressing Type 4 phenotype with respect of Type 3 is larger for encapsulated cells. This result indicates that the droplet microenvironment might be promoting the formation of multiple focal adhesion complexes. This result could be related to a difference in substrate rigidity and/or to the confinement imposed by the droplet volume.

It is worth noting that cell phenotype identification required the dynamic observation of cells. Around five hours of monitoring was required to obtain a cell type distribution consistent in time.

In order to investigate characteristics that could provide additional information to identify the cell phenotype more directly, we measured the cells mean grey value (directly linked to fluorescence intensity of actin-GFP) and area along the monitored time. Then for both parameters, we calculated the average value in each population type (maximum type) per each data frame. Similar results were obtained for all samples (Fig. 6.11 shows data corresponding to Sample B).

The average area separated by maximum types show distinct curves, decreasing from population Type 4 to population Type 1. This result is not surprising, since the level of

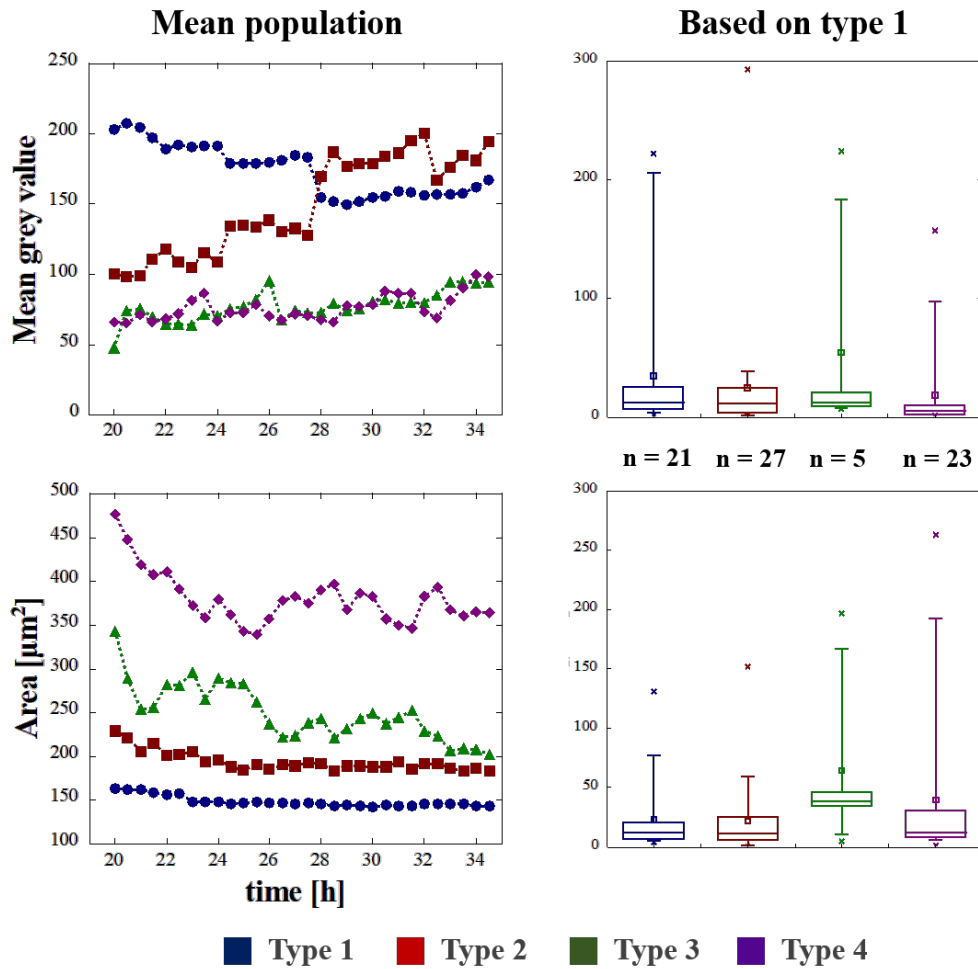


**Fig. 6.11** Cell mean fluorescence intensity and area calculated along the monitored time (right panel) and calculated based on Type 1 expression and independently of time (left panel). Data based on Sample B.

cell spreading on the surface decreases in the same direction. However, this criteria is not necessarily sufficient to determine the cell type independently of time. For example, an individual cell of population Type 4 could contract its membrane in a specific time frame, and even though the population average is not greatly affected, the cell identification for this frozen image would be erroneous.

To test this supposition we measured the population average (independent of time) and including only cells in specific time frames where they exhibited a contracted phenotype that classified as Type 1. We observed that the difference between individual cells from different populations cannot be distinguished based on cell area when said cells are contracted (Fig. 6.11 lower-right panel). Even though there is a great variability in cell sizes when contracted, this variability seems to be unrelated to the phenotypic expression the cell adopts afterwards.

The same result is obtained for actin-GFP: when contracted, an individual cell phenotype cannot be determined based on fluorescence intensity (Fig. 6.11 upper-right panel). This result implies that dynamic monitoring of an individual cell is required in order to determine its phenotypic expression by image analysis.

### **6.2.3 Conclusions**

Fluorinated Pickering emulsions serve as a viable platform for the culture and study of adherent cells. They provide an isolated microenvironment of great interest for single-cell studies.

RPE cells phenotypic heterogeneity at a cell to cell level for the same cell line was evidenced after single-cell encapsulation: phenotypes exhibiting RPE cells dedifferentiation and transdifferentiation were observed, as well as typical markers of differentiated RPE cells, such as pigmentation and polarized secretion. Additionally, different migration modes were observed, whose manifestation was independent of the cell microenvironment.

We demonstrated that Pickering encapsulation does not affect cell viability or phenotype

expression and confirmed the influence of fibronectin on increasing EMT within the cell population in the same degree for both: cells spreading on a 2D surface and on the Pickering droplet interface. This opens the potential for further studies –which could not be carry out without cell isolation– on a single-cell level, such as adding protein markers within the cell isolated microenvironment to identify particular phenotypes of interest and link it to the visual expression.

We demonstrated a simple method to visually discriminate between various cell phenotypes. However, more sophisticated methods –such as advanced cell classifiers based on machine learning algorithms– would be of benefit to identify phenotypic expressions of interest such as neural and differentiated RPE cells.

## 6.2.4 Materials and methods

### Cell culture

RPE-1 cells (transfected to express actin-GFP) were kindly provided by Prof. Martial Balland (MOTIV, LiPhy, Grenoble). RPE-1 cells were cultivated in Dulbecco's modified eagle GlutaMAX (DMEM/F-12 GlutaMAX) medium with foetal bovine serum (FBS, 10% v/v) in 10 ml flasks and are stored, protected form light, in an incubator at 37 °C (5% CO<sub>2</sub>)<sup>3</sup>.

The RPE-1 cells were prepared for subculture and microfluidic experiments during their exponential growing phase (Fig. 6.12). Briefly, the DMEM/F-12 GlutaMAX medium in the flask was extracted and discarded. Then, RPE-1 cells attached to the flask were gently washed with 3 ml solution of Dulbecco's phosphate buffered saline (D-PBS). The supernatant containing cellular debris was discarded and a 3 ml Trypsine-EDTA solution was added to detach the cells from the flask. The flask was stored in the incubator at 37 °C until all RPE-1 cells were observed in the supernatant phase (~3 min).

---

<sup>3</sup>Cell culture done by Dr. Mathias Girault

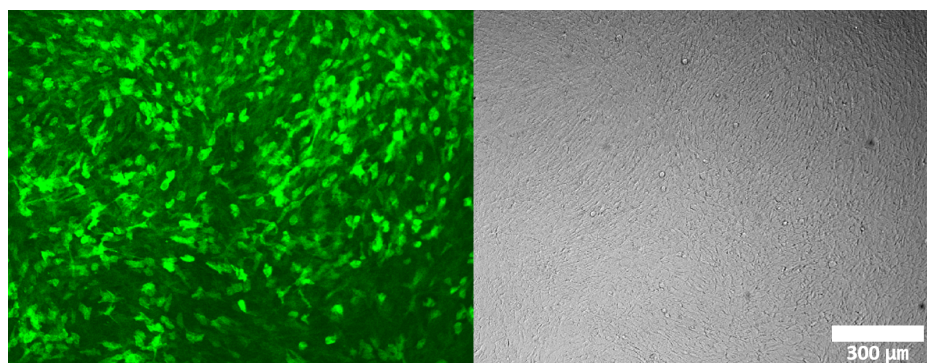


**Fig. 6.12** BF (right) and Fluorescence image (left) of RPE-1 cells after reaching high level of confluency on a culture flask

The supernatant consisting of RPE-1 cells and Trypsine-EDTA solution was added to 10 ml centrifuge tube which contained 7 ml of fresh DMEM/F-12 GlutaMAX FBS medium (37 °C). The sample was centrifuged at 2000 rpm during 3 min. Then, supernatant was discarded and 2 ml of fresh DMEM/F-12 GlutaMAX FBS medium (37 °C) was added to re-suspend cells.

The suspension of RPE-1 cells was directly used as mother solution for a new cell passage and for the microfluidic experiments: For the new cell passage, 100  $\mu\text{L}$  of mother solution was placed in a new flask with 10 ml of fresh DMEM/F-12 GlutaMAX FBS medium (37 °C) and stored in the incubator (37 °C, 5%  $\text{CO}_2$ ); for the microfluidic experiments, a syringe (1 ml) was filled with mother solution, connected to Peek tubing (0.75 mm inner diameter) and taken to the microfluidic station for immediate use.

Fibronectin (Superfibronectin from human plasma, S5171 SIGMA) was diluted with sterile PBS to a concentration of 5  $\mu\text{g}/\text{ml}$ . When applied (case B on Fig. 6.8a) 280  $\mu\text{L}$  was added to 1 ml of cell suspension for a final concentration of 1.4  $\mu\text{g}/\text{ml}$ .

### **Cell encapsulation, incubation and monitoring**

Cell encapsulation was done in a PDMS microfluidic device fabricated by standard soft lithography techniques [113]. The droplet production design was that described on chapter

5 (Fig. 6.13): it consisted on a co-flow of cells suspension in medium with a highly concentrated stream of fluorinated Si-NPs in HFE-7500 oil ( $c_p^* = 5$  mg/ml, local concentration before dilution); droplets were then produced when said stream met in a flow-focusing geometry a cross-flow of clean FC-40 oil.

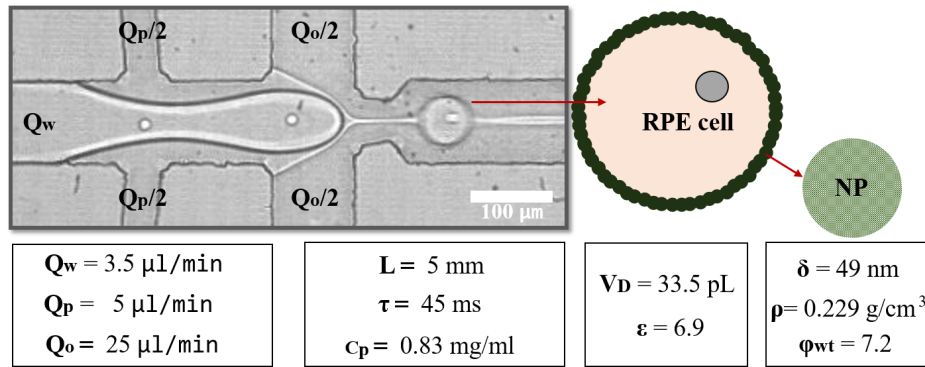


**Fig. 6.13** Cell encapsulation conditions: Flow-rates ( $Q_w$ ,  $Q_p$  and  $Q_o$ ); incubation length ( $L$ ), time ( $\tau$ ) and particle concentration ( $c_p$ ); droplet volume ( $V_D$ ) and particles in excess ( $\epsilon=6.9$ ); nanoparticles size ( $\delta$ ), density ( $\rho$ ) and degree of surface functionalization ( $\phi_{wt}$ ).

The flow-rates were controlled using syringe pumps (Nemesys, Cetoni) and for all the encapsulation experiments they were set as:  $3.5 \mu\text{L}/\text{min}$  for cells suspension flow-rate ( $Q_w$ );  $5 \mu\text{L}/\text{min}$  for fluorinated Si-NPs flow-rate ( $Q_p$ ); and  $25 \mu\text{L}/\text{min}$  for FC-40 oil flow-rate ( $Q_o$ ). This experimental conditions produced  $33.5 \text{ pL}$  droplets stabilized with around seven times the Si-NPs needed to form an hexagonal packing at the interface ( $\epsilon = 6.9$ ). Si-NPs were synthesized and functionalized as described on chapter 3, their size was  $49 \text{ nm}$  and their degree of surface functionalization ( $\phi_{wt}$ ) was  $7.2$ .

Droplets were stabilized in a channel of  $5 \text{ mm}$  before collection on a reservoir adapted from a plastic pipette tip (Fig. 6.3d). Re-injection of the emulsion in the incubation chambers (Fig. 6.1c) was done at a flow rate between  $20$  and  $40 \mu\text{L}/\text{min}$ . The device was placed inside a petri-dish along with wet filter paper to maintain humidity.

Droplet monitoring was done in an epifluorescence microscope integrated with an incubation chamber able to keep a stable temperature at  $37 \text{ }^\circ\text{C}$ . Due to technical problems we

were not able to provide a 5% CO<sub>2</sub> atmosphere inside the microscope chamber.

Bright field and fluorescence images were taken every 30 min with a Nikon camera and microscope objective of 20X (40X for figures 6.5 and 6.6c) using the image software NIS-Elements viewer.

### Image analysis

Images were pre-calibrated with acquisition software NIS-Elements viewer (microns/pixel) and then processed with Image-J software [114] as schematically shown on Fig. 6.14. Briefly, cell fluorescence images were converted into a binary image to extract the cell contour as region of interest (ROI). Then, with ROI and the fluorescence image (with subtracted background) several values were calculated: cell area, which was obtained in calibrated square microns ( $\mu\text{m}^2$ ); mean grey value, which is the sum of grey values in all the pixels within the ROI divided by the total number of pixels; aspect-ratio, which is the major axis divided by the minor axis of an ellipse fitting the ROI; and circularity, which is calculated as  $4\pi(\text{area})/(\text{perimeter})^2$  from ROI.

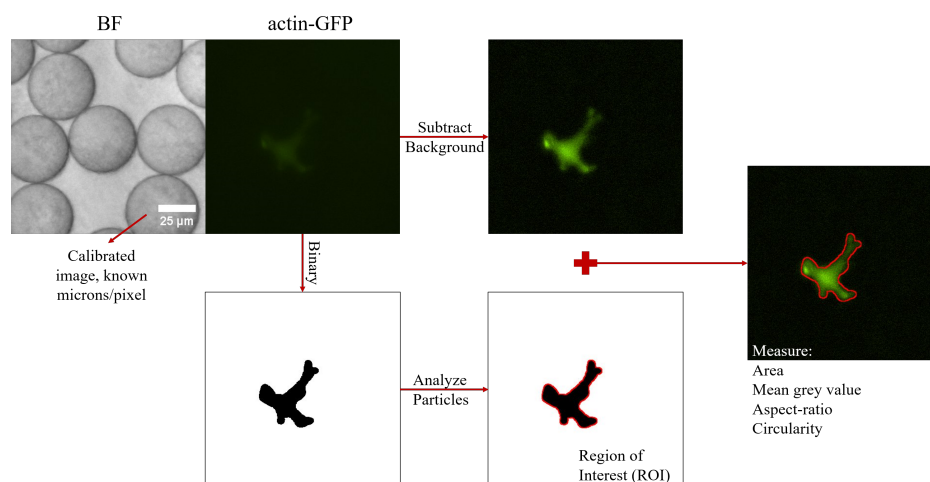


**Fig. 6.14** Image analysis steps: Fluorescence image made into binary and cell contour extracted (ROI); ROI used on fluorescence image (with background subtracted) to measure area, mean grey value, aspect-ratio and circularity.

The data obtained from every cell in each frame of time was finally organized and

processed with MATLAB to obtain the final results that were plot with qtiplot software.

## CHAPTER 6

**Summary**

- After integrating the knowledge gained on fluorinated Pickering emulsions and implementing technical adjustments for the proper design of an incubation device we managed to make stable Pickering drops at high production throughput, collect them in a reservoir, re-inject them in an incubation device and monitor them in a microscope without disruptions for more than 48 hours. We then applied this system for the study of an adherent cell model: Retinal Pigment Epithelium (RPE) cells.
  - We demonstrated the suitability of the engineered technological platform for the isolation, incubation and study of adherent cells.
  - We confirmed the phenotypic heterogeneity –on a cell to cell level– of RPE cells in culture.
  - We demonstrated the possibility to take into account this intrinsic heterogeneity in single-cell studies.
  - Finally, we confirmed the influence of the glycoprotein fibronectin on the stimulation of EMT within the cell population.

# Chapter 7

## General conclusions and outlook

Fluorinated silica nanoparticles are an attractive alternative to fluorinated surfactants for droplet-based microfluidics technology, opening possibilities for applications that to date had not been attainable with surfactant stabilized systems. These possibilities are a consequence of the intrinsic properties of Pickering emulsions, such as: the ability to deplete the continuous phase from particles while retaining droplet stability and the rigid substrate provided by the adsorbed particles at the droplet interface. These differences however also imply that new limitations and technical challenges are introduced when attempting to implement Pickering emulsions within a technology that has been developing for a decade along fluorinated surfactant stabilized emulsions.

In this thesis project we explore several of these limitations –such as the Pickering emulsions poor flowability and low production throughput– and we propose technical solutions that allow us to develop a suitable technological platform for the study of adherent cells.

This study helps to elucidate that rather than a substitute for fluorinated surfactants, fluorinated silica nanoparticles offer a great addition to the droplet-based microfluidics toolbox, increasing the already wide set of options available for lab-on-chip applications and with a great potential to keep expanding.

Each one of the addressed subjects on this thesis project opened additional lines of inquiry

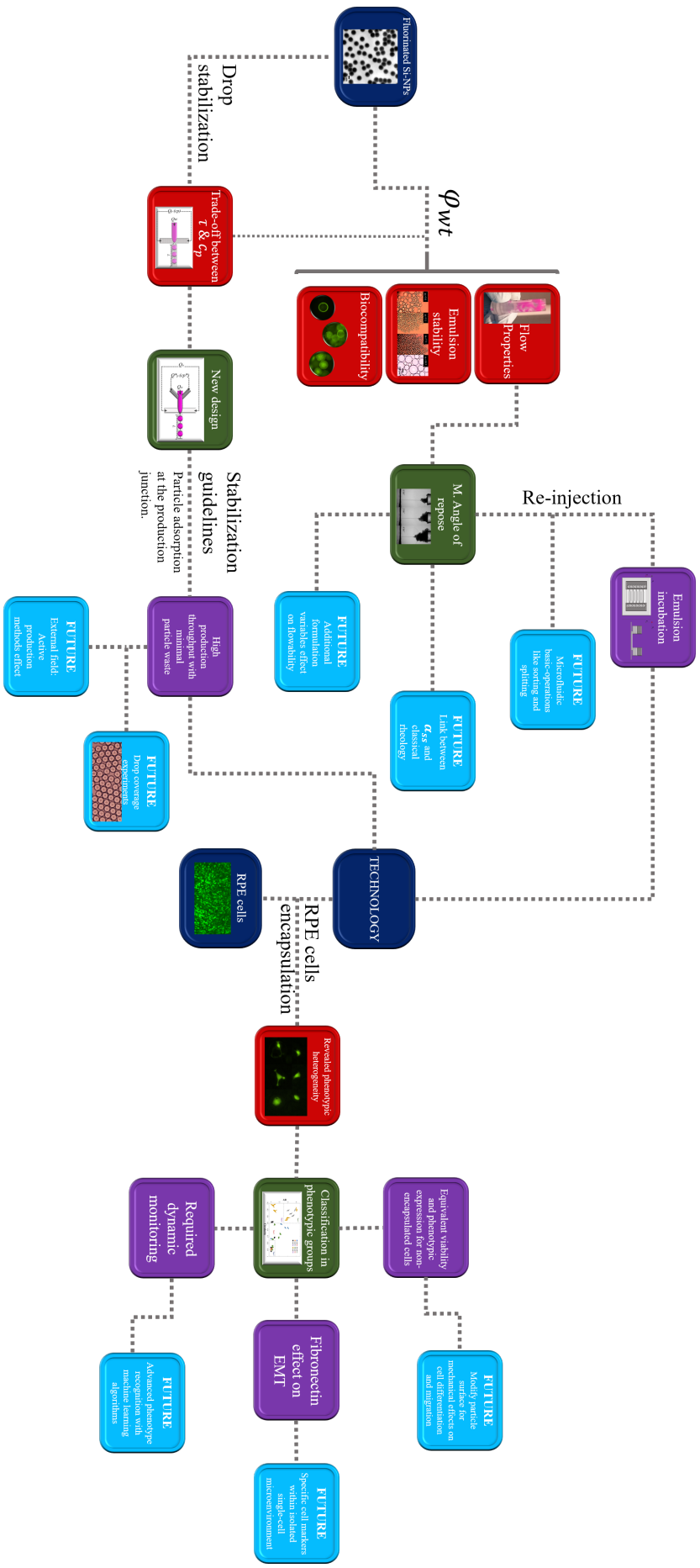


Fig. 7.1 Schematic representation of achievements and perspectives

---

and applications that could be followed further in future projects (Fig. 7.1):

The microfluidic version of the angle of repose test is a practical test to quantify different flow behaviors between formulation conditions. However, the study of additional formulation variables –such as salt content and droplet size– would be of interest to advance our understanding on the modulation of the droplet interfacial properties. Furthermore, additional analysis will be of interest to determine a quantitative link between the angle of repose method and classical rheological parameters.

The adequate formulation of fluorinated Pickering emulsions allow their re-injection in a new microfluidic device, we studied droplet incubation after re-injection in a customized incubation device. However, further studies on typical droplet-based microfluidic operations –such as sorting, splitting and mixing– will be of great interest for the further advancement of the technology.

The multi-parametric study made for fluorinated Pickering droplets stabilization, elucidated practical guidelines for the efficient stabilization of droplets in microfluidics, with high throughput and minimal particle waste. However, a quantitative analysis exploring the full capacity of this method –without the constrictions set to allow the comparison with the standard production method– integrated with experiments to verify the droplet coverage, will be of interest for a full optimization and control of the produced droplet properties. Furthermore, the effect of external fields –such as electric, thermal and mechanical– on particle adsorption during droplet production would be of great interest to further advance this technique.

The combination of the technological achievements, with an adherent cell model (RPE cells), allowed the verification of their phenotypic heterogeneity in a cell to cell level. We classified the cell phenotype using a simple model –based on cell shape parameters– which needs the dynamic observation of individual cells for the consistent classification. Future applications could involve advanced techniques for cell phenotype identification, such as

those based on machine learning algorithms.

We demonstrated that the cell viability and phenotypic expression variability is not affected by the cell encapsulation in droplets, and we verified the effect of the glycoprotein fibronectin on the stimulation of EMT. This result opens the door for future studies on both: the bio-chemical and the mechanical micro-environment effect on cell trans- differentiation.

The mechanical micro-environment could be modified by altering the droplet size and/or the surface chemistry of particles, for example: a batch of particles with grafted PEG molecules could be mixed –in different ratios– with standard particles, allowing the modulation of the adhesive properties of the droplets.

The isolated micro-environment provided by the Pickering droplet opens the possibility for the addition of bio-chemical protein markers –for accurate single cell identification– and several proteins and growth factors to advance the understanding of the external factors involved in the activation of signaling pathways for RPE cells de- trans- differentiation.

In general, this thesis project set the fundamental basis to continue the understanding of Pickering emulsion systems and the further adaptation to lab-on-chip technology. Additionally, it offers a panorama of the powerful application potential this technology has for the study of RPE cells and adherent cells in general.

# References

- [1] Shia-Yen Teh, Robert Lin, Lung-Hsin Hung, and Abraham P. Lee. Droplet microfluidics. *Lab Chip*, 8:198–220, 2008.
- [2] Oliver J. Dressler, Xavier Casadevall i Solvas, and Andrew J. deMello. Chemical and biological dynamics using droplet-based microfluidics. *Annual Review of Analytical Chemistry*, 10(1):1–24, 2017.
- [3] Ansgar Huebner, Sanjiv Sharma, Monpichar Srisa-Art, Florian Hollfelder, Joshua B. Edel, and Andrew J. deMello. Microdroplets: A sea of applications? *Lab Chip*, 8:1244–1254, 2008.
- [4] Helen Song, Delai L. Chen, and Rustem F. Ismagilov. Reactions in droplets in microfluidic channels. *Angewandte Chemie International Edition*, 45(44):7336–7356, 2006.
- [5] Isao Kobayashi, Kunihiro Uemura, and Mitsutoshi Nakajima. Formulation of monodisperse emulsions using submicron-channel arrays. *Colloids and Surfaces A: Physicochemical and Engineering Aspects*, 296(1):285 – 289, 2007.
- [6] Jung-uk Shim, Rohan T. Ranasinghe, Clive A. Smith, Shehu M. Ibrahim, Florian Hollfelder, Wilhelm T. S. Huck, David Klenerman, and Chris Abell. Ultrarapid generation of femtoliter microfluidic droplets for single-molecule-counting immunoassays. *ACS Nano*, 7(7):5955–5964, 2013.
- [7] Charles N. Baroud, Francois Gallaire, and Remi Dangla. Dynamics of microfluidic droplets. *Lab Chip*, 10:2032–2045, 2010.
- [8] P. B. Umbanhowar, V. Prasad, and D. A. Weitz. Monodisperse emulsion generation via drop break off in a coflowing stream. *Langmuir*, 16(2):347–351, 2000.
- [9] A. S. Utada, E. Lorenceau, D. R. Link, P. D. Kaplan, H. A. Stone, and D. A. Weitz. Monodisperse double emulsions generated from a microcapillary device. *Science*, 308(5721):537–541, 2005.
- [10] Sung-Wook Choi, Yu Zhang, and Younan Xia. Fabrication of microbeads with a controllable hollow interior and porous wall using a capillary fluidic device. *Advanced functional materials*, 19:2943–2949, 2009.
- [11] Luoran Shang, Fanfan Fu, Yao Cheng, Yunru Yu, Jie Wang, Zhongze Gu, and Yuanjin Zhao. Bioinspired multifunctional spindle-knotted microfibers from microfluidics. *Small*, 13(4):1600286–n/a, 2017.

- [12] Yuanjin Zhao, Luoran Shang, Yao Cheng, and Zhongze Gu. Spherical colloidal photonic crystals. *Accounts of Chemical Research*, 47(12):3632–3642, 2014.
- [13] Dhananjay Dendukuri and Patrick S. Doyle. The synthesis and assembly of polymeric microparticles using microfluidics. *Advanced Materials*, 21(41):4071–4086, 2009.
- [14] Jiashu Sun, Yunlei Xianyu, and Xingyu Jiang. Point-of-care biochemical assays using gold nanoparticle-implemented microfluidics. *Chem. Soc. Rev.*, 43:6239–6253, 2014.
- [15] Dan S. Tawfik and Andrew D. Griffiths. Man-made cell-like compartments for molecular evolution. *Nature Biotechnology*, 16, 1998.
- [16] Rhutesh K. Shah, Ho Cheung Shum, Amy C. Rowat, Daeyeon Lee, Jeremy J. Agresti, Andrew S. Utada, Liang-Yin Chu, Jin-Woong Kim, Alberto Fernandez-Nieves, Carlos J. Martinez, and David A. Weitz. Designer emulsions using microfluidics. *Materials Today*, 11(4):18 – 27, 2008.
- [17] Shin-Hyun Kim, Jae Won Shim, and Seung-Man Yang. Microfluidic multicolor encoding of microspheres with nanoscopic surface complexity for multiplex immunoassays. *Angewandte Chemie International Edition*, 50(5):1171–1174, 2011.
- [18] Pingan Zhu and Liqiu Wang. Passive and active droplet generation with microfluidics: a review. *Lab Chip*, 17:34–75, 2017.
- [19] Luoran Shang, Yao Cheng, and Yuanjin Zhao. Emerging droplet microfluidics. *Chemical Reviews*, 117(12):7964–8040, 2017.
- [20] Andrew S. Utada, Alberto Fernandez-Nieves, Howard A. Stone, and David A. Weitz. Dripping to jetting transitions in coflowing liquid streams. *Phys. Rev. Lett.*, 99:094502, Aug 2007.
- [21] J C McDonald, D C Duffy, J R Anderson, D T Chiu, H Wu, O J Schueller, and G M Whitesides. Fabrication of microfluidic systems in poly(dimethylsiloxane). *Electrophoresis*, 21(1):27–40, 2000.
- [22] Todd Thorsen, Richard W. Roberts, Frances H. Arnold, and Stephen R. Quake. Dynamic pattern formation in a vesicle-generating microfluidic device. *Phys. Rev. Lett.*, 86:4163–4166, Apr 2001.
- [23] Shelley L. Anna, Nathalie Bontoux, and Howard A. Stone. Formation of dispersions using “flow focusing” in microchannels. *Applied Physics Letters*, 82(3):364–366, 2003.
- [24] Arjen M. Pit, Michèl H. G. Duits, and Frieder Mugele. Droplet manipulations in two phase flow microfluidics. *Micromachines*, 6(11):1768–1793, 2015.
- [25] Rémi Dangla, Etienne Fradet, Yonatan Lopez, and Charles N Baroud. The physical mechanisms of step emulsification. *Journal of Physics D: Applied Physics*, 46(11):114003, 2013.
- [26] Muhsincan Sesen, Tuncay Alan, and Adrian Neild. Droplet control technologies for microfluidic high throughput screening ([small mu ]hts). *Lab Chip*, 17:2372–2394, 2017.

- 
- [27] Zhuang Zhi Chong, Say Hwa Tan, Alfonso M. Gañán-Calvo, Shu Beng Tor, Ngiap Hiang Loh, and Nam-Trung Nguyen. Active droplet generation in microfluidics. *Lab on a Chip*, 16(1):35–58, 2016.
- [28] Piotr Garstecki, Michael J. Fuerstman, Howard A. Stone, and George M. Whitesides. Formation of droplets and bubbles in a microfluidic t-junction-scaling and mechanism of break-up. *Lab Chip*, 6:437–446, 2006.
- [29] Carsten Cramer, Peter Fischer, and Erich J. Windhab. Drop formation in a co-flowing ambient fluid. *Chemical Engineering Science*, 59(15):3045 – 3058, 2004.
- [30] M. DE MENECH, P. GARSTECKI, F. JOUSSE, and H. A. STONE. Transition from squeezing to dripping in a microfluidic t-shaped junction. *Journal of Fluid Mechanics*, 595:141–161, 2008.
- [31] D. Funfschilling, H. Debas, H.-Z. Li, and T. G. Mason. Flow-field dynamics during droplet formation by dripping in hydrodynamic-focusing microfluidics. *Phys. Rev. E*, 80:015301, Jul 2009.
- [32] Thomas Cubaud and Thomas G. Mason. Capillary threads and viscous droplets in square microchannels. *Physics of Fluids*, 20(5):053302, may 2008.
- [33] Linas Mazutis and Andrew D. Griffiths. Preparation of monodisperse emulsions by hydrodynamic size fractionation. *Applied Physics Letters*, 95(20):204103, 2009.
- [34] Andrew C. Hatch, Apurva Patel, N. Reginald Beer, and Abraham P. Lee. Passive droplet sorting using viscoelastic flow focusing. *Lab Chip*, 13:1308–1315, 2013.
- [35] Keunho Ahn, Charles Kerbage, Tom P. Hunt, R. M. Westervelt, Darren R. Link, and D. A. Weitz. Dielectrophoretic manipulation of drops for high-speed microfluidic sorting devices. *Applied Physics Letters*, 88(2):024104, 2006.
- [36] Nicolas Bremond, Abdou R. Thiam, and Jérôme Bibette. Decompressing emulsion droplets favors coalescence. *Phys. Rev. Lett.*, 100:024501, Jan 2008.
- [37] Heng-Dong Xi, Hao Zheng, Wei Guo, Alfonso M. Gañán-Calvo, Ye Ai, Chia-Wen Tsao, Jun Zhou, Weihua Li, Yanyi Huang, Nam-Trung Nguyen, and Say Hwa Tan. Active droplet sorting in microfluidics: a review. *Lab on a Chip*, 17(5):751–771, 2017.
- [38] Jean-Christophe Baret, Oliver J. Miller, Valerie Taly, Michael Ryckelynck, Abdelslam El-Harrak, Lucas Frenz, Christian Rick, Michael L. Samuels, J. Brian Hutchison, Jeremy J. Agresti, Darren R. Link, David A. Weitz, and Andrew D. Griffiths. Fluorescence-activated droplet sorting (fads): efficient microfluidic cell sorting based on enzymatic activity. *Lab Chip*, 9:1850–1858, 2009.
- [39] Bruno Teste, Nicolas Jamond, Davide Ferraro, Jean-Louis Viovy, and Laurent Malaquin. Selective handling of droplets in a microfluidic device using magnetic rails. *Microfluidics and Nanofluidics*, 19(1):141–153, Jul 2015.
- [40] Charles N. Baroud, Jean-Pierre Delville, François Gallaire, and Régis Wunenburger. Thermocapillary valve for droplet production and sorting. *Phys. Rev. E*, 75:046302, Apr 2007.

- [41] Adam R. Abate, Jeremy J. Agresti, and David A. Weitz. Microfluidic sorting with high-speed single-layer membrane valves. *Applied Physics Letters*, 96(20):203509, 2010.
- [42] Thomas Franke, Adam R. Abate, David A. Weitz, and Achim Wixforth. Surface acoustic wave (saw) directed droplet flow in microfluidics for pdms devices. *Lab Chip*, 9:2625–2627, 2009.
- [43] Lung-Hsin Hung, Kyung M. Choi, Wei-Yu Tseng, Yung-Chieh Tan, Kenneth J. Shea, and Abraham Phillip Lee. Alternating droplet generation and controlled dynamic droplet fusion in microfluidic device for cds nanoparticle synthesis. *Lab Chip*, 6:174–178, 2006.
- [44] Luis M. Fidalgo, Chris Abell, and Wilhelm T. S. Huck. Surface-induced droplet fusion in microfluidic devices. *Lab Chip*, 7:984–986, 2007.
- [45] Ralf Seemann, Martin Brinkmann, Thomas Pfohl, and Stephan Herminghaus. Droplet based microfluidics. *Reports on Progress in Physics*, 75(1):016601, 2012.
- [46] Albert Liau, Rohit Karnik, Arun Majumdar, and Jamie H. Doudna Cate. Mixing crowded biological solutions in milliseconds. *Analytical Chemistry*, 77(23):7618–7625, 2005.
- [47] Kai-Yang Tung, Chih-Chieh Li, and Jing-Tang Yang. Mixing and hydrodynamic analysis of a droplet in a planar serpentine micromixer. *Microfluidics and Nanofluidics*, 7(4):545, Feb 2009.
- [48] Yung-Chieh Tan, Jeffrey S. Fisher, Alan I. Lee, Vittorio Cristini, and Abraham Phillip Lee. Design of microfluidic channel geometries for the control of droplet volume, chemical concentration, and sorting. *Lab Chip*, 4:292–298, 2004.
- [49] David N. Adamson, Debarshi Mustafi, John X. J. Zhang, Bo Zheng, and Rustem F. Ismagilov. Production of arrays of chemically distinct nanolitre plugs via repeated splitting in microfluidic devices. *Lab Chip*, 6:1178–1186, 2006.
- [50] D. R. Link, S. L. Anna, D. A. Weitz, and H. A. Stone. Geometrically mediated breakup of drops in microfluidic devices. *Phys. Rev. Lett.*, 92:054503, Feb 2004.
- [51] Ansgar Huebner, Dan Bratton, Graeme Whyte, Min Yang, Andrew J. deMello, Chris Abell, and Florian Hollfelder. Static microdroplet arrays: a microfluidic device for droplet trapping, incubation and release for enzymatic and cell-based assays. *Lab Chip*, 9:692–698, 2009.
- [52] Petra S. Dittrich, Michael Jahnz, and Petra Schwille. A new embedded process for compartmentalized cell-free protein expression and on-line detection in microfluidic devices. *ChemBioChem*, 6(5):811–814, 2005.
- [53] Fabienne Courtois, Luis F. Olguin, Graeme Whyte, Daniel Bratton, Wilhelm T. S. Huck, Chris Abell, and Florian Hollfelder. An integrated device for monitoring time-dependent in vitro expression from single genes in picolitre droplets. *ChemBioChem*, 9(3):439–446, 2008.

- [54] Andrew C. Hatch, Tathagata Ray, Kelly Lintecum, and Cody Youngbull. Continuous flow real-time pcr device using multi-channel fluorescence excitation and detection. *Lab Chip*, 14:562–568, 2014.
- [55] Haakan N. Joensson, Michael L. Samuels, Eric R. Brouzes, Martina Medkova, Mathias Uhlen, Eric R. Brouzes, Darren R. Link, and Helene Andersson-Svahn. Detection and analysis of low-abundance cell-surface biomarkers using enzymatic amplification in microfluidic droplets. *Angewandte Chemie International Edition*, 48(14):2518–2521, 2009.
- [56] Haakan N. Joensson and Helene Andersson Svahn. Droplet microfluidics a tool for single-cell analysis. *Angewandte Chemie International Edition*, 51(49):12176–12192, 2012.
- [57] David J. Collins, Adrian Neild, Andrew deMello, Ai-Qun Liu, and Ye Ai. The poisson distribution and beyond: methods for microfluidic droplet production and single cell encapsulation. *Lab Chip*, 15:3439–3459, 2015.
- [58] Jeonghun Nam, Hyunjung Lim, Choong Kim, Ji Yoon Kang, and Sehyun Shin. Density-dependent separation of encapsulated cells in a microfluidic channel by using a standing surface acoustic wave. *Biomicrofluidics*, 6(2):024120, 2012.
- [59] Sarah Koster, Francesco E. Angile, Honey Duan, Anton Agresti, Jeremy J. Winter, Christian Schmitz, Amy C. Rowat, Christoph A. Merten, Dario Pisignano, Andrew D. Griffiths, and David A. Weitz. Drop-based microfluidic devices for encapsulation of single cells. *Lab-Chip*, 8(7):1110–1115, 2008.
- [60] Evelien W. M. Kemna, Rogier M. Schoeman, Floor Wolbers, Istvan Vermes, David A. Weitz, and Albert van den Berg. High-yield cell ordering and deterministic cell-in-droplet encapsulation using dean flow in a curved microchannel. *Lab Chip*, 12:2881–2887, 2012.
- [61] Jenifer Clausell-Tormos, Diana Lieber, Jean-Christophe Baret, Abdeslam El-Harrak, Oliver J. Miller, Lucas Frenz, Joshua Blouwolff, Katherine J. Humphry, Sarah Köster, Honey Duan, Christian Holtze, David A. Weitz, Andrew D. Griffiths, and Christoph A. Merten. Droplet-based microfluidic platforms for the encapsulation and screening of mammalian cells and multicellular organisms. *Chemistry & Biology*, 15(5):427–437, may 2008.
- [62] Christian H. J. Schmitz, Amy C. Rowat, Sarah Koster, and David A. Weitz. Dropspots: a picoliter array in a microfluidic device. *Lab Chip*, 9:44–49, 2009.
- [63] James Q. Boedicker, Liang Li, Timothy R. Kline, and Rustem F. Ismagilov. Detecting bacteria and determining their susceptibility to antibiotics by stochastic confinement in nanoliter droplets using plug-based microfluidics. *Lab Chip*, 8:1265–1272, 2008.
- [64] Lucas Armbrrecht and Petra S. Dittrich. Recent advances in the analysis of single cells. *Analytical Chemistry*, 89(1):2–21, 2017.

- [65] Eric Brouzes, Martina Medkova, Neal Savenelli, Dave Marran, Mariusz Twardowski, J. Brian Hutchison, Jonathan M. Rothberg, Darren R. Link, Norbert Perrimon, and Michael L. Samuels. Droplet microfluidic technology for single-cell high-throughput screening. *Proceedings of the National Academy of Sciences*, 106(34):14195–14200, 2009.
- [66] Yusi Fu, Chunmei Li, Sijia Lu, Wenxiong Zhou, Fuchou Tang, X. Sunney Xie, and Yanyi Huang. Uniform and accurate single-cell sequencing based on emulsion whole-genome amplification. *Proceedings of the National Academy of Sciences*, 112(38):11923–11928, 2015.
- [67] D. Hummer, F. Kurth, N. Naredi-Rainer, and P. S. Dittrich. Single cells in confined volumes: microchambers and microdroplets. *Lab Chip*, 16:447–458, 2016.
- [68] Evan Z. Macosko, Anindita Basu, Rahul Satija, James Nemesh, Karthik Shekhar, Melissa Goldman, Itay Tirosh, Allison R. Bialas, Nolan Kamitaki, Emily M. Martersteck, John J. Trombetta, David A. Weitz, Joshua R. Sanes, Alex K. Shalek, Aviv Regev, and Steven A. McCarroll. Highly parallel genome-wide expression profiling of individual cells using nanoliter droplets. *Cell*, 161(5):1202–1214, 2015.
- [69] Aaron M. Streets, Xiannian Zhang, Chen Cao, Yuhong Pang, Xinglong Wu, Liang Xiong, Lu Yang, Yusi Fu, Liang Zhao, Fuchou Tang, and Yanyi Huang. Microfluidic single-cell whole-transcriptome sequencing. *Proceedings of the National Academy of Sciences*, 111(19):7048–7053, 2014.
- [70] Thomas C. Scanlon, Sarah M. Dostal, and Karl E. Griswold. A high-throughput screen for antibiotic drug discovery. *Biotechnology and Bioengineering*, 111(2):232–243, 2014.
- [71] Anastasia Zinchenko, Sean R. A. Devenish, Balint Kintses, Pierre-Yves Colin, Martin Fischlechner, and Florian Hollfelder. One in a million: Flow cytometric sorting of single cell-lysate assays in monodisperse picolitre double emulsion droplets for directed evolution. *Analytical Chemistry*, 86(5):2526–2533, 2014.
- [72] James Q. Boedicker, Meghan E. Vincent, and Rustem F. Ismagilov. Microfluidic confinement of single cells of bacteria in small volumes initiates high-density behavior of quorum sensing and growth and reveals its variability. *Angewandte Chemie International Edition*, 48(32):5908–5911, 2009.
- [73] Jean-Christophe Baret. Surfactants in droplet-based microfluidics. *Lab Chip*, 12:422–433, 2012.
- [74] C. Holtze, A. C. Rowat, J. J. Agresti, J. B. Hutchison, F. E. Angile, C. H. J. Schmitz, S. Koster, H. Duan, K. J. Humphry, R. A. Scanga, J. S. Johnson, D. Pisignano, and D. A. Weitz. Biocompatible surfactants for water-in-fluorocarbon emulsions. *Lab Chip*, 8:1632–1639, 2008.
- [75] Philipp Gruner, Birte Riechers, Laura Andreina Chacòn Orellana, Quentin Brosseau, Florine Maes, Thomas Beneyton, Deniz Pekin, and Jean-Christophe Baret. Stabilisers for water-in-fluorinated-oil dispersions: Key properties for microfluidic applications. *Current Opinion in Colloid & Interface Science*, 20(3):183 – 191, 2015.

- [76] Yunpeng Bai, Ximin He, Dingsheng Liu, Santoshkumar N. Patil, Dan Bratton, Ansgar Huebner, Florian Hollfelder, Chris Abell, and Wilhelm T. S. Huck. A double droplet trap system for studying mass transport across a droplet-droplet interface. *Lab Chip*, 10:1281–1285, 2010.
- [77] Jean G. Riess and Marie Pierre Krafft. Fluorinated materials for in vivo oxygen transport (blood substitutes), diagnosis and drug delivery. *Biomaterials*, 19(16):1529 – 1539, 1998.
- [78] Jessamine Ng Lee, Cheolmin Park, and George M. Whitesides. Solvent compatibility of poly(dimethylsiloxane)-based microfluidic devices. *Analytical Chemistry*, 75(23):6544–6554, 2003.
- [79] Fabienne Courtois, Luis F. Olguin, Graeme Whyte, Ashleigh B. Theberge, Wilhelm T. S. Huck, Florian Hollfelder, and Chris Abell. Controlling the retention of small molecules in emulsion microdroplets for use in cell-based assays. *Analytical Chemistry*, 81(8):3008–3016, 2009.
- [80] Alexander K. Price and Brian M. Paegel. Discovery in droplets. *Analytical Chemistry*, 88(1):339–353, 2016.
- [81] Yousr Skhiri, Philipp Gruner, Benoit Semin, Quentin Brosseau, Deniz Pekin, Linas Mazutis, Victoire Goust, Felix Kleinschmidt, Abdeslam El Harrak, J. Brian Hutchison, Estelle Mayot, Jean-Francois Bartolo, Andrew D. Griffiths, Valerie Taly, and Jean-Christophe Baret. Dynamics of molecular transport by surfactants in emulsions. *Soft Matter*, 8:10618–10627, 2012.
- [82] K. Short & P. Gruner, B. Riechers, B. Semin, J. Lim, A. Johnston and JC. Baret. 2016 Controlling molecular transport in minimal emulsions. *Nature Communications*, page 9, 2016.
- [83] Ming Pan, Liat Rosenfeld, Minkyu Kim, Manqi Xu, Edith Lin, Ratmir Derda, and Sindy K. Y. Tang. Fluorinated pickering emulsions impede interfacial transport and form rigid interface for the growth of anchorage-dependent cells. *ACS Applied Materials & Interfaces*, 6(23):21446–21453, 2014.
- [84] Ilia Platzman, Jan-Willi Janiesch, and Joachim Pius Spatz. Synthesis of nanostructured and biofunctionalized water-in-oil droplets as tools for homing t cells. *Journal of the American Chemical Society*, 135(9):3339–3342, 2013.
- [85] Ming Pan, Minkyu Kim, Lucas Blauch, and Sindy K. Y. Tang. Surface-functionalizable amphiphilic nanoparticles for pickering emulsions with designer fluid–fluid interfaces. *RSC Adv.*, 6(46):39926–39932, 2016.
- [86] Ya Gai, Minkyu Kim, Ming Pan, and Sindy K.Y. Tang. Amphiphilic nanoparticles suppress droplet break-up in a concentrated emulsion flowing through a narrow constriction. *Biomicrofluidics*, 11(3), 2017.
- [87] Werner Stöber, Arthur Fink, and Ernst Bohn. Controlled growth of monodisperse silica spheres in the micron size range. *Journal of Colloid and Interface Science*, 26(1):62–69, jan 1968.

- [88] Kurtis D. Hartlen, Aristidis P. T. Athanasopoulos, and Vladimir Kitaev. Facile preparation of highly monodisperse small silica spheres (15 to 200 nm) suitable for colloidal templating and formation of ordered arrays. *Langmuir*, 24(5):1714–1720, mar 2008.
- [89] N. N. Greenwood and A. Earnshaw. *Chemistry of the Elements*. Pergamon, 1984. pp. 393-99.
- [90] M. Szekeres, I. Dékány, and A. de Keizer. Adsorption of dodecyl pyridinium chloride on monodisperse porous silica. *Colloids and Surfaces A: Physicochemical and Engineering Aspects*, 141(3):327–336, nov 1998.
- [91] G. W. Sears. Determination of specific surface area of colloidal silica by titration with sodium hydroxide. *Analytical Chemistry*, 28(12):1981–1983, dec 1956.
- [92] Stephen Brunauer, P. H. Emmett, and Edward Teller. Adsorption of gases in multimolecular layers. *Journal of the American Chemical Society*, 60(2):309–319, feb 1938.
- [93] William C. Griffin. Classification of surface-active agents by hlb. *Journal of the society of cosmetic chemists*, 1(5):311–26, 1949.
- [94] Philip Finkle, Hal D. Draper, and Joel H. Hildebrand. THE THEORY OF EMULSIFICATION I. *Journal of the American Chemical Society*, 45(12):2780–2788, dec 1923.
- [95] B. P. Binks and S. O. Lumsdon. Influence of particle wettability on the type and stability of surfactant-free emulsions†. *Langmuir*, 16(23):8622–8631, nov 2000.
- [96] B. P. Binks and S. O. Lumsdon. Catastrophic phase inversion of water-in-oil emulsions stabilized by hydrophobic silica. *Langmuir*, 16(6):2539–2547, mar 2000.
- [97] Yves Chevalier and Marie-Alexandrine Bolzinger. Emulsions stabilized with solid nanoparticles: Pickering emulsions. *Colloids and Surfaces A: Physicochemical and Engineering Aspects*, 439:23–34, dec 2013.
- [98] Jean-Christophe Baret, Felix Kleinschmidt, Abdeslam El Harrak, and Andrew D. Griffiths. Kinetic aspects of emulsion stabilization by surfactants: A microfluidic analysis. *Langmuir*, 25(11):6088–6093, jun 2009.
- [99] Jing Shang and Xiaohu Gao. Nanoparticle counting: towards accurate determination of the molar concentration. *Chem. Soc. Rev.*, 43(21):7267–7278, aug 2014.
- [100] L A Chacon and J C Baret. Microfluidic angle of repose test for pickering emulsions. *Journal of Physics D: Applied Physics*, 50(39):39LT04, sep 2017.
- [101] Matthew N. Lee, Hubert K. Chan, and Ali Mohraz. Characteristics of pickering emulsion gels formed by droplet bridging. *Langmuir*, 28(6):3085–3091, nov 2011.
- [102] Véronique Schmitt, Mathieu Destribats, and Rénal Backov. Colloidal particles as liquid dispersion stabilizer: Pickering emulsions and materials thereof. *Comptes Rendus Physique*, 15(8-9):761–774, oct 2014.

- 
- [103] T. Mason, Martin-D. Lacasse, Gary Grest, Dov Levine, J. Bibette, and D. Weitz. Osmotic pressure and viscoelastic shear moduli of concentrated emulsions. *Physical Review E*, 56(3):3150–3166, sep 1997.
- [104] Rodrigo Emigdio Guerra. *Elasticity of compressed emulsions*. Harvard University, 2014.
- [105] S. Arditty, V. Schmitt, F. Lequeux, and F. Leal-Calderon. Interfacial properties in solid-stabilized emulsions. *The European Physical Journal B*, 44(3):381–393, apr 2005.
- [106] Siddhartha Gupta, William S. Wang, and Siva A. Vanapalli. Microfluidic viscometers for shear rheology of complex fluids and biofluids. *Biomicrofluidics*, 10(4):043402, jul 2016.
- [107] Steven D. Hudson, Prasad Sarangapani, Jai A. Pathak, and Kalman B. Migler. A microliter capillary rheometer for characterization of protein solutions. *Journal of Pharmaceutical Sciences*, 104(2):678–685, feb 2015.
- [108] Thomas J. Ober, Simon J. Haward, Christopher J. Pipe, Johannes Soulages, and Gareth H. McKinley. Microfluidic extensional rheometry using a hyperbolic contraction geometry. *Rheologica Acta*, 52(6):529–546, may 2013.
- [109] Lichao Pan and Paulo E. Arratia. A high-shear, low reynolds number microfluidic rheometer. *Microfluidics and Nanofluidics*, 14(5):885–894, dec 2012.
- [110] A Mehta and G C Barker. The dynamics of sand. *Reports on Progress in Physics*, 57(4):383–416, apr 1994.
- [111] Albert W. Alexander, Bodhisattwa Chaudhuri, AbdulMobeen Faqih, Fernando J. Muzzio, Clive Davies, and M. Silvina Tomassone. Avalanching flow of cohesive powders. *Powder Technology*, 164(1):13–21, may 2006.
- [112] G. Lumay, F. Boschini, K. Traina, S. Bontempi, J.-C. Remy, R. Cloots, and N. Vandewalle. Measuring the flowing properties of powders and grains. *Powder Technology*, 224:19–27, jul 2012.
- [113] Younan Xia and George M. Whitesides. Soft lithography. *Angewandte Chemie International Edition*, 37(5):550–575, mar 1998.
- [114] Johannes Schindelin, Ignacio Arganda-Carreras, Erwin Frise, Verena Kaynig, Mark Longair, Tobias Pietzsch, Stephan Preibisch, Curtis Rueden, Stephan Saalfeld, Benjamin Schmid, Jean-Yves Tinevez, Daniel James White, Volker Hartenstein, Kevin Eliceiri, Pavel Tomancak, and Albert Cardona. Fiji: an open-source platform for biological-image analysis. *Nature Methods*, 9(7):676–682, jul 2012.
- [115] Juntao Tang, Patrick James Quinlan, and Kam Chiu Tam. Stimuli-responsive pickering emulsions: recent advances and potential applications. *Soft Matter*, 11(18):3512–3529, 2015.

- [116] David J. French, Phil Taylor, Jeff Fowler, and Paul S. Clegg. Making and breaking bridges in a pickering emulsion. *Journal of Colloid and Interface Science*, 441:30–38, mar 2015.
- [117] M. E. Leunissen, A. van Blaaderen, A. D. Hollingsworth, M. T. Sullivan, and P. M. Chaikin. Electrostatics at the oil-water interface, stability, and order in emulsions and colloids. *Proceedings of the National Academy of Sciences*, 104(8):2585–2590, feb 2007.
- [118] Craig Priest, Mathew D. Reid, and Catherine P. Whitby. Formation and stability of nanoparticle-stabilised oil-in-water emulsions in a microfluidic chip. *Journal of Colloid and Interface Science*, 363(1):301–306, nov 2011.
- [119] Tobias Bollhorst, Kurosch Rezwan, and Michael Maas. Colloidal capsules: nano- and microcapsules with colloidal particle shells. *Chemical Society Reviews*, 46(8):2091–2126, 2017.
- [120] Anand Bala Subramaniam, Manouk Abkarian, and Howard A. Stone. Controlled assembly of jammed colloidal shells on fluid droplets. *Nature Materials*, 4(7):553–556, jun 2005.
- [121] Zhihong Nie, Jai Il Park, Wei Li, Stefan A. F. Bon, and Eugenia Kumacheva. An “inside-out” microfluidic approach to monodisperse emulsions stabilized by solid particles. *Journal of the American Chemical Society*, 130(49):16508–16509, dec 2008.
- [122] Omkar S. Deshmukh, Dirk van den Ende, Martien Cohen Stuart, Frieder Mugele, and Michel H.G. Duits. Hard and soft colloids at fluid interfaces: Adsorption, interactions, assembly & rheology. *Advances in Colloid and Interface Science*, 222:215–227, aug 2015.
- [123] H.A. Stone, A.D. Stroock, and A. Ajdari. ENGINEERING FLOWS IN SMALL DEVICES. *Annual Review of Fluid Mechanics*, 36(1):381–411, jan 2004.
- [124] David E. Tambe and Mukul M. Sharma. Factors controlling the stability of colloid-stabilized emulsions. *Journal of Colloid and Interface Science*, 157(1):244–253, apr 1993.
- [125] Thomas Krebs, Karin Schroën, and Remko Boom. Coalescence dynamics of surfactant-stabilized emulsions studied with microfluidics. *Soft Matter*, 8(41):10650, 2012.
- [126] Dongju Chen, Ruth Cardinaels, and Paula Moldenaers. Effect of confinement on droplet coalescence in shear flow. *Langmuir*, 25(22):12885–12893, nov 2009.
- [127] Pieter De Bruyn, Ruth Cardinaels, and Paula Moldenaers. The effect of geometrical confinement on coalescence efficiency of droplet pairs in shear flow. *Journal of Colloid and Interface Science*, 409:183–192, nov 2013.
- [128] Qianqian Zhou, Yue Sun, Shiting Yi, Kai Wang, and Guangsheng Luo. Investigation of droplet coalescence in nanoparticle suspensions by a microfluidic collision experiment. *Soft Matter*, 12(6):1674–1682, 2016.

- 
- [129] Sujit S. Datta, Ho Cheung Shum, and David A. Weitz. Controlled buckling and crumpling of nanoparticle-coated droplets. *Langmuir*, 26(24):18612–18616, dec 2010.
- [130] N. Tsapis, E. R. Dufresne, S. S. Sinha, C. S. Riera, J. W. Hutchinson, L. Mahadevan, and D. A. Weitz. Onset of buckling in drying droplets of colloidal suspensions. *Physical Review Letters*, 94(1), jan 2005.
- [131] Jiseok Lim, Ouriel Caen, Jérémy Vrignon, Manfred Konrad, Valérie Taly, and Jean-Christophe Baret. Parallelized ultra-high throughput microfluidic emulsifier for multiplex kinetic assays. *Biomicrofluidics*, 9(3):034101, may 2015.
- [132] Bo Zheng, Joshua D. Tice, L. Spencer Roach, and Rustem F. Ismagilov. A droplet-based, composite PDMS/glass capillary microfluidic system for evaluating protein crystallization conditions by microbatch and vapor-diffusion methods with on-chip x-ray diffraction. *Angewandte Chemie International Edition*, 43(19):2508–2511, may 2004.
- [133] Morten la Cour and Tongalp Tezel. The retinal pigment epithelium. In *Advances in Organ Biology*, pages 253–272. Elsevier, 2005.
- [134] Guillermo L. Lehmann, Ignacio Benedicto, Nancy J. Philp, and Enrique Rodriguez-Boulan. Plasma membrane protein polarity and trafficking in RPE cells: Past, present and future. *Experimental Eye Research*, 126:5–15, sep 2014.
- [135] D. Bok. The retinal pigment epithelium: a versatile partner in vision. *Journal of Cell Science*, 1993(Supplement 17):189–195, dec 1993.
- [136] Atsuhiko Kanda and Susumu Ishida. Roles of the retinal pigment epithelium in neuroprotection. In *Neuroprotection and Neuroregeneration for Retinal Diseases*, pages 227–238. Springer Japan, 2014.
- [137] J. Wayne Streilein, Naili Ma, Hartmut Wenkel, Tat Fong Ng, and Parisa Zamiri. Immunobiology and privilege of neuronal retina and pigment epithelium transplants. *Vision Research*, 42(4):487–495, feb 2002.
- [138] Carl Sheridan, Paul Hiscott, and Ian Grierson. Retinal pigment epithelium differentiation and dedifferentiation. In *Essentials in Ophthalmology*, pages 101–119. Springer-Verlag, 2006.
- [139] Sabine Fuhrmann, ChangJiang Zou, and Edward M. Levine. Retinal pigment epithelium development, plasticity, and tissue homeostasis. *Experimental Eye Research*, 123:141–150, jun 2014.
- [140] Chikafumi Chiba. The retinal pigment epithelium: An important player of retinal disorders and regeneration. *Experimental Eye Research*, 123:107–114, jun 2014.
- [141] Ian Grierson, Paul Hiscott, Penny Hogg, Helen Robey, Ank Mazure, and Genevieve Larkin. Development, repair and regeneration of the retinal pigment epithelium. *Eye*, 8(2):255–262, mar 1994.

- [142] Chika Yoshii, Yoko Ueda, Mitumasa Okamoto, and Masasuke Araki. Neural retinal regeneration in the anuran amphibian *xenopus laevis* post-metamorphosis: Transdifferentiation of retinal pigmented epithelium regenerates the neural retina. *Developmental Biology*, 303(1):45–56, mar 2007.
- [143] Katharina Lueck, Amanda-Jayne F. Carr, Dimitrios Stampoulis, Volker Gerke, Ursula Rescher, John Greenwood, and Stephen E. Moss. Regulation of retinal pigment epithelial cell phenotype by annexin a8. *Scientific Reports*, 7(1), jul 2017.
- [144] Alla V. Kuznetsova, Alexander M. Kurinov, and Maria A. Aleksandrova. Cell models to study regulation of cell transformation in pathologies of retinal pigment epithelium. *Journal of Ophthalmology*, 2014:1–18, 2014.
- [145] Hui Cai and Lucian V Del Priore. Gene expression profile of cultured adult compared to immortalized human retinal pigment epithelium. *Molecular vision*, 12:1–14, 2006.
- [146] A. V. Kuznetsova and M. A. Aleksandrova. Heterogeneity of retinal pigment epithelial cells from adult human eye in different culturing systems. *Bulletin of Experimental Biology and Medicine*, 162(4):569–577, feb 2017.
- [147] Shigeo Tamiya, LanHsin Liu, and Henry J. Kaplan. Epithelial-mesenchymal transition and proliferation of retinal pigment epithelial cells initiated upon loss of cell-cell contact. *Investigative Ophthalmology & Visual Science*, 51(5):2755, may 2010.
- [148] Rie Sonoï, Mee-Hae Kim, Kenta Yamada, and Masahiro Kino-oka. Phenotypic heterogeneity of human retinal pigment epithelial cells in passaged cell populations. *Journal of Bioscience and Bioengineering*, 124(2):227–233, aug 2017.
- [149] Enrique Salero, Timothy A. Blenkinsop, Barbara Corneo, Ashley Harris, David Rabin, Jeffrey H. Stern, and Sally Temple. Adult human RPE can be activated into a multipotent stem cell that produces mesenchymal derivatives. *Cell Stem Cell*, 10(1):88–95, jan 2012.
- [150] Tim Lämmermann and Michael Sixt. Mechanical modes of ‘amoeboid’ cell migration. *Current Opinion in Cell Biology*, 21(5):636–644, oct 2009.
- [151] Peter Friedl and Katarina Wolf. Plasticity of cell migration: a multiscale tuning model. *The Journal of Cell Biology*, 188(1):11–19, dec 2009.
- [152] Yan-Jun Liu, Maël Le Berre, Franziska Lautenschlaeger, Paolo Maiuri, Andrew Callan-Jones, Méline Heuzé, Tohru Takaki, Raphaël Voituriez, and Matthieu Piel. Confinement and low adhesion induce fast amoeboid migration of slow mesenchymal cells. *Cell*, 160(4):659–672, feb 2015.
- [153] Peter A Campochiaro, JA Jerdon, and Bert M Glaser. The extracellular matrix of human retinal pigment epithelial cells in vivo and its synthesis in vitro. *Investigative ophthalmology & visual science*, 27(11):1615–1621, 1986.
- [154] A. Huttenlocher and A. R. Horwitz. Integrins in cell migration. *Cold Spring Harbor Perspectives in Biology*, 3(9):a005074–a005074, sep 2011.

- [155] Grasieli de Oliveira Ramos, Lisiane Bernardi, Isabel Lauxen, Manoel Sant'Ana Filho, Alan Rick Horwitz, and Marcelo Lazzaron Lamers. Fibronectin modulates cell adhesion and signaling to promote single cell migration of highly invasive oral squamous cell carcinoma. *PLOS ONE*, 11(3):e0151338, mar 2016.
- [156] Cheng-Lin Li, Dan Yang, Xin Cao, Fan Wang, Duan-Yang Hong, Jing Wang, Xiang-Chun Shen, and Yan Chen. Fibronectin induces epithelial-mesenchymal transition in human breast cancer MCF-7 cells via activation of calpain. *Oncology Letters*, 13(5):3889–3895, mar 2017.



# Résumé

Les émulsions fluorées de Pickering sont étudiées et mises au point dans la technologie de microfluidique en gouttes pour des applications d'études sur des cellules adhérentes isolées. Les principaux résultats de ce projet sont : l'établissement d'un lien entre la couverture de surface des nanoparticules et la fluidité de l'émulsion de Pickering ; l'établissement des lignes directrices pour la stabilisation des gouttes avec un débit de production élevé et un minimum de déchets de particules ; et la mise en œuvre d'une plateforme technologique complète pour l'étude des cellules RPE, pour mesurer leur hétérogénéité phénotypique au niveau de la cellule individuelle.

**Mots-clé:** microfluidique de gouttes, émulsions fluorées de Pickering, fluidité, stabilisation, cellules adhérentes, cellules RPE, hétérogénéité phénotypique.

# Abstract

Fluorinated Pickering emulsions are studied and engineered within droplet-based microfluidics technology for adherent-cell studies applications. The main findings of this project include: linking the nanoparticles surface coverage to the bulk flowability of the Pickering emulsion; deriving guidelines for droplet stabilization with high production throughput and minimal particle waste; and implementing the full technological platform for the study of RPE cells, while unraveling their phenotypic heterogeneity at the single cell level.

**Keywords:** Droplet-based microfluidics, fluorinated Pickering emulsions, flowability, stabilization, encapsulation, adherent cells, RPE cells, phenotypic heterogeneity.